

Atomic layer deposition of noble metal nanoparticles

Citation for published version (APA):

Weber, M. J. (2014). *Atomic layer deposition of noble metal nanoparticles*. [Phd Thesis 1 (Research TU/e / Graduation TU/e), Applied Physics and Science Education]. Technische Universiteit Eindhoven.
<https://doi.org/10.6100/IR776263>

DOI:

[10.6100/IR776263](https://doi.org/10.6100/IR776263)

Document status and date:

Published: 01/01/2014

Document Version:

Publisher's PDF, also known as Version of Record (includes final page, issue and volume numbers)

Please check the document version of this publication:

- A submitted manuscript is the version of the article upon submission and before peer-review. There can be important differences between the submitted version and the official published version of record. People interested in the research are advised to contact the author for the final version of the publication, or visit the DOI to the publisher's website.
- The final author version and the galley proof are versions of the publication after peer review.
- The final published version features the final layout of the paper including the volume, issue and page numbers.

[Link to publication](#)

General rights

Copyright and moral rights for the publications made accessible in the public portal are retained by the authors and/or other copyright owners and it is a condition of accessing publications that users recognise and abide by the legal requirements associated with these rights.

- Users may download and print one copy of any publication from the public portal for the purpose of private study or research.
- You may not further distribute the material or use it for any profit-making activity or commercial gain
- You may freely distribute the URL identifying the publication in the public portal.

If the publication is distributed under the terms of Article 25fa of the Dutch Copyright Act, indicated by the "Taverne" license above, please follow below link for the End User Agreement:

www.tue.nl/taverne

Take down policy

If you believe that this document breaches copyright please contact us at:

openaccess@tue.nl

providing details and we will investigate your claim.

Atomic Layer Deposition of Noble Metal Nanoparticles

PROEFSCHRIFT

ter verkrijging van de graad van doctor aan de
Technische Universiteit Eindhoven, op gezag van de
rector magnificus prof.dr.ir. C.J. van Duijn, voor een
commissie aangewezen door het College voor
Promoties, in het openbaar te verdedigen
op donderdag 4 september 2014 om 16:00 uur

door

Matthieu Jacques Weber

geboren te Obernai, Frankrijk

Dit proefschrift is goedgekeurd door de promotoren en de samenstelling van de promotiecommissie is als volgt:

voorzitter:	prof.dr.ir. G. M. W. Kroesen
1 ^e promotor:	prof.dr.ir. W. M. M. Kessels
co-promotoren:	dr. A. A. Bol dr. M. A. Verheijen
leden:	prof.dr.ir. R. van de Krol (Technische Universität Berlin) prof. D. Cameron (Lappeenranta University of Technology) dr. ir. C. F. J. Flipse prof.dr. ir. E. J. M. Hensen

This research was financially supported by the European Community's Seventh Framework Programme (FP7/2007-2013) under grant agreement number ENHANCE-238409.



Printed and bound by Gildeprint, Enschede, The Netherlands.

The cover has been designed by Claire Douat, Penny Webb and I. The photos were taken in the Mangyshlak peninsula near Aktau, Kazakhstan (photograph: Richard “Mouser” Williams).

A catalogue record is available from the Eindhoven University of Technology Library
ISBN: 978-90-386-3658-0

Preface

This thesis deals with atomic layer deposition (ALD) of noble metals and with the development of a novel process for the synthesis of bimetallic core/shell nanoparticles entirely by ALD. The work was carried out in the research group “Plasma & Materials Processing” (PMP) at the Department of Applied Physics of the Eindhoven University of Technology. The group has extensive and valuable expertise in the field of ALD, including the areas of plasma-assisted ALD and ALD of noble metals. The research project was part of a Marie Curie (MC) Initial Training Network (ITN) and has received funding from the European Community's Seventh Framework Programme (FP7/2007-2013). The name of this MC program is ENHANCE, which stands for “European Research Training Network of New Materials: Innovative Concepts for their Fabrication, Integration and Characterisation”.

Matthieu Weber
Eindhoven, April 2014

CONTENTS

Chapter 1	Introduction	1
Chapter 2	Noble metal nanoparticles synthesis by atomic layer deposition: An overview.	15
Chapter 3	Preparation of noble metal nanoparticles by atomic layer deposition: preparation details, analysis, and underlying physical mechanisms	77
Chapter 4	Atomic Layer Deposition of High-Purity Palladium Films from Pd(hfac) ₂ and H ₂ and O ₂ Plasmas. M. J. Weber, A. J. M. Mackus, M. A. Verheijen, V. Longo, A. A. Bol, and W. M. M. Kessels. This work was presented at the American Vacuum Society (AVS) 59 th Symposium and Exhibition (Tampa, Florida, U.S.A., October 2012) and has published as <i>The Journal of Physical Chemistry C</i> , 2014, 118 (16), pp 8702–8711.	113
Chapter 5	Supported Core/Shell Bimetallic Nanoparticles Synthesis by Atomic Layer Deposition M. J. Weber, A. J. M. Mackus, M. A. Verheijen, C. van der Marel, and W. M. M. Kessels. This work was presented at the American Vacuum Society (AVS) 58 th Symposium and Exhibition (Nashville, Tennessee, U.S.A., October 2011) and at the 12 th International Conference on Atomic Layer Deposition Conference (Dresden, Germany, June 2012), and has been published as <i>Chemistry of Materials</i> , 2012, 24 (15), pp 2973–2977.	143
Chapter 6	Nanotailored Pd/Pt Core/Shell Nanoparticles prepared by Atomic Layer Deposition M. J. Weber, M. A. Verheijen, A. A. Bol, and W. M. M. Kessels. This work was presented at the American Vacuum Society (AVS) 60 th Symposium and Exhibition (Long Beach, California, U.S.A., October 2013) and will be submitted for publication in <i>Chemistry of Materials</i> .	159

Chapter 7	General conclusions and outlook	179
Summary		187
Acknowledgments		191
Curriculum vitae		195

Chapter 1

Introduction

1.1 Noble metals as catalysts

The metals considered as noble metals are silver, gold, and the platinum group metals ruthenium, rhodium, palladium, osmium, iridium and platinum. They are transition metals and are called “noble” because of their chemical stability. They have a positive standard reduction potential and most of them are highly resistant to oxidation.¹ The noble metals typically present excellent electrical and thermal conductivity.^{1,2} Ruthenium and osmium have the hexagonal close packed (hcp) crystal structure while rhodium, iridium, palladium, platinum, gold and silver normally have the face-centered cubic (fcc) structure.^{1,3} Due to their scarcity and high economic value, noble metals are also called precious metals.

Nanoparticles (NPs), *i.e.* particles with a diameter between 1 and 100 nm, have a very high surface-to-volume ratio, which makes them more attractive to use in catalysis when compared to bulk materials. NPs of noble metals have been used in heterogeneous catalysis for more than 50 years,^{4,5} and platinum and palladium are the most important noble metals for this purpose. They are typically used as NPs supported on oxide or carbon substrates in a typical range of 0.02-0.5 wt.% content.⁶⁻⁸ The intrinsic properties of noble metal NPs such as their catalytic activity depend strongly on their size, but also on their composition, structure, and on the substrate (e.g. oxides, porous carbon) which supports them. Thus, a continuing goal in catalysis research is to engineer the dimensions, the composition and structure of noble metal NPs in order to precisely tune their catalytic activity.

Precisely engineered NPs can be applied in real catalytic systems or serve as model catalysts for fundamental studies. The most important application fields of noble metals NPs are the chemical and oil-refining industries. They also find applications in automotive converters, and there is an increasing use of these metals for fuel cells applications as well.^{6,9-12} Micro fuel cells and micro reactors are small devices (see Figure 1.1) which benefit from the use of NPs of noble metals. Further miniaturization of these devices at the sub-micro or even at the nanoscale would open prospects for many new applications.

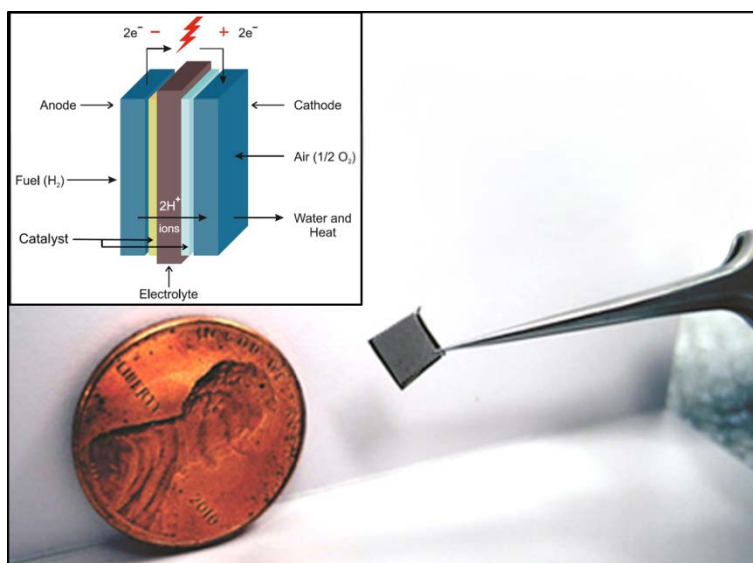


Figure 1.1. Picture of a micro fuel cell based on zirconium and platinum compounds. The comparison of the fuel cell and a penny illustrates how small these devices are (taken and adapted from Reference¹³). The inset at the upper left shows the basic operating principle of a fuel cell (taken and adapted from Reference¹⁴). The catalyst typically consists of noble metal NPs supported on carbon black.

Various conventional methods based on wet chemistry or vapor phase deposition exist for the preparation of noble metal NPs. However, to implement precisely engineered NPs in miniaturised devices by compatible processes, new nanoengineering routes must be explored. Atomic layer deposition (ALD), a well-established and scalable vapor phase technology for the deposition of thin films, offers many opportunities for nanoengineering also beyond the field of thin films. In the work described in this dissertation, this route was investigated and exploited for the synthesis of noble metal NPs.

1.2 Atomic Layer Deposition

Atomic layer deposition (ALD) is a vapor phase deposition technique enabling the synthesis of ultrathin films of inorganic materials, with a subnanometer thickness control.¹⁵ ALD can be used to coat demanding 3D substrates with a conformal and uniform layer of high quality material, a capability unique amongst thin film deposition techniques. Consequently, ALD-grown materials have a wide range of applications, from displays to microelectronics, and from nanocatalysts to photovoltaics.^{15,16} ALD research began in the 1960s and 1970s in

the former USSR and Finland, and the technique has been patented by T. Suntola in 1977.¹⁷ In the mid-1990s, the semiconductor industry became interested in ALD. This industry is the key-driver of the ALD field since then.¹⁸ It is noted that there was already interest in using ALD for catalysis applications in the mid-1990s.^{19,20}

ALD relies on the sequential use of self-terminating gas-solid reactions which sequentially take place in a cycle-wise fashion. A typical ALD cycle consists of alternate pulses of precursor and co-reactant gasses in the reactor chamber, separated by purge or pump steps. A precursor is typically an inorganic coordination compound, i.e., a metal center surrounded by chemical functional groups called ligands. To understand the concepts of the self-limiting surface reactions and how they result in uniform and conformal films, ALD of Al_2O_3 is discussed below. This process based on trimethylaluminum (TMA, $\text{Al}(\text{CH}_3)_3$) as precursor and water as co-reactant is chosen as an example because it can be considered as a typical and “close-to-ideal” ALD process.²¹ Figure 1.2 is a schematic representation of an ALD cycle of Al_2O_3 from a TMA/ H_2O process.

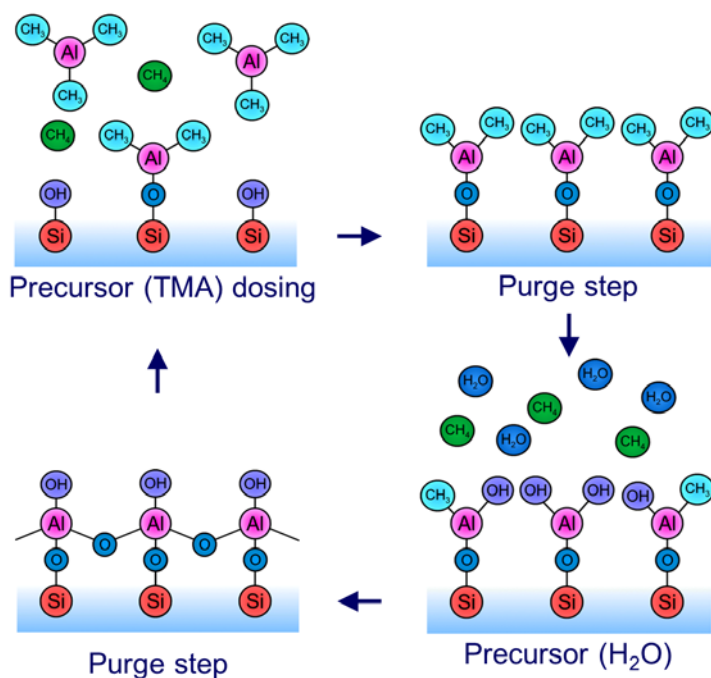


Figure 1.2. Schematic illustration of a typical ALD cycle of Al_2O_3 based on a TMA ($\text{Al}(\text{CH}_3)_3$) and H_2O process. The cycle is based on the alternate exposure of a surface to the precursor (TMA) and (c) the co-reactant (H_2O) gases separated by pump/purge steps.

An oxide surface is considered as a starting surface for the ALD process. Such surfaces are typically covered with hydroxyl (OH) surface groups. The first step in this ALD process is the exposure of the substrate to $\text{Al}(\text{CH}_3)_3$ precursor molecules that adsorb at the surface in a reaction with the OH groups. The reactions between the hydroxyl groups and the TMA precursor molecules taking place result in the formation of surface O-Al bonds and the release of CH_4 as a reaction product. The precursor molecules are volatile and reactive towards the surface groups, thus these reactions take place at the whole substrate surface, independently of the substrate geometry. Ideally, the surface becomes entirely terminated with $-\text{CH}_3$ groups, which hinder the adsorption of more precursor molecules and ensure the self-limiting nature of this first half-cycle. Subsequently, the reactor chamber is purged or pumped in order to remove the excess of precursor and the reaction products. The second half-cycle begins with the introduction of the co-reactant, in this case H_2O . The $-\text{CH}_3$ terminated surface reacts with the H_2O molecules. This results in the formation of new hydroxyl groups at the surface and CH_4 as a reaction product. This reaction removes all $-\text{CH}_3$ molecules and is self-limiting as well. The last step of the process is again a purge or pumping step to remove the excess of water and reaction products. These four steps are referred to as an “ALD cycle”, and result in the deposition of a submonolayer of Al_2O_3 , typically of a thickness of 0.1 nm. The surface is again terminated with -OH groups after one full cycle, and the process can therefore be repeated. This can be done until the desired thickness is obtained. The details of this ALD of Al_2O_3 have been discussed extensively by Puurunen *et al.*²¹

A large set of technologically important materials can be prepared by ALD.²² The most common materials deposited by this technique are binary compounds such as metal oxides, but more advanced ALD processes allow for the preparation of single-element films as well as ternary or quaternary compounds. Current metal precursors are almost exclusively inorganic coordination compounds. As the interactions between precursor and co-reactant molecules can be complex, the choice of the co-reactant is of great importance. The co-reactant typically involves small molecules, as a gas or a vapor (e.g. H_2O), and the surface reactions are thermally driven. The method is therefore also referred as thermal ALD. In plasma-assisted ALD, the surface is exposed to species generated by a plasma during the co-reactant step. The high reactivity of the plasma species typically allows for more freedom in processing conditions and lower deposition temperatures. Evidently, each precursor or co-reactant in an ALD cycle has a profound impact on the chemistry of the process.

Many ALD surface chemistries can be applied, depending on the material to be deposited and the process used. The reaction mechanisms of ALD of Pt or

Pd are quite different from the “close-to-ideal” Al_2O_3 case. One difference is that in metal ALD, the deposition of a metallic material containing one single element needs to be achieved. This can be accomplished if the co-reactant enables the removal of the organic ligands (of the adsorbed metallic precursor) without being incorporated in the film. For this purpose, the chemistries applied can for example be based on combustion chemistry, hydrogen reduction or fluorosilane elimination. The precise understanding of the underlying surface reactions and chemical mechanisms taking place during ALD is challenging but crucial for the optimization of the process. For more details on the reaction mechanisms of noble metal ALD processes, the reader is referred to references^{23–25} and to the Chapter 4 of this thesis.

In most ALD processes, like those of metal oxides such as Al_2O_3 , the growth of a uniform film on a substrate starts already after the first few cycles. If the appropriate surface species are present at the starting surface for the precursors to react with, the nucleation of the film and subsequent continuous growth is rather straightforward. In the ALD of noble metals, the start of the film growth on certain substrates is more difficult. In general, a nucleation delay is observed before the formation of a film. Because of the difference in surface energies between the metal and the substrate, ALD of noble metals usually initiates with the formation of isolated islands at the surface.²⁶ This lack of uniform nucleation can be exploited to produce supported NPs. These NPs grow with increasing number of cycles, coalesce and finally form a closed film on which the ALD growth continues at a constant rate. Figure 1.3 illustrates this process for Pt ALD.

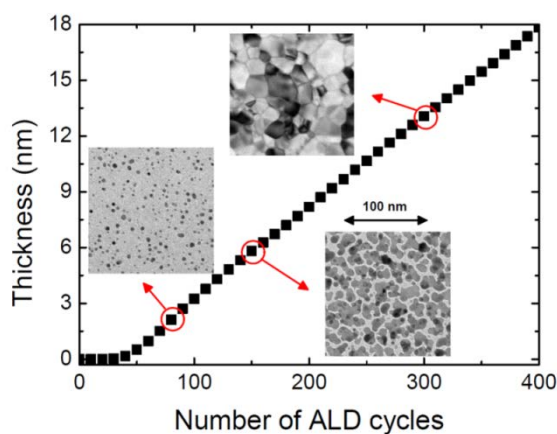


Figure 1.3. Thickness as a function of the number of ALD cycles as measured by *in situ* spectroscopic ellipsometry (SE). The bright field transmission electron microscopy (TEM) images in the figure illustrate that Pt ALD nucleation evolves from island growth, via island coalescence, to a continuous film after closure. Taken from Reference.²⁷

The design of an experimental reactor is relatively easy due to the self-limiting nature of ALD. A typical experimental ALD reactor basically consists of a (heated) vessel to which a pumping system and a gas dosing system are connected through gate valves. A plasma source can be connected to the chamber as well. A schematic overview of the home-built ALD reactor used in this work is given in Figure 1.4.

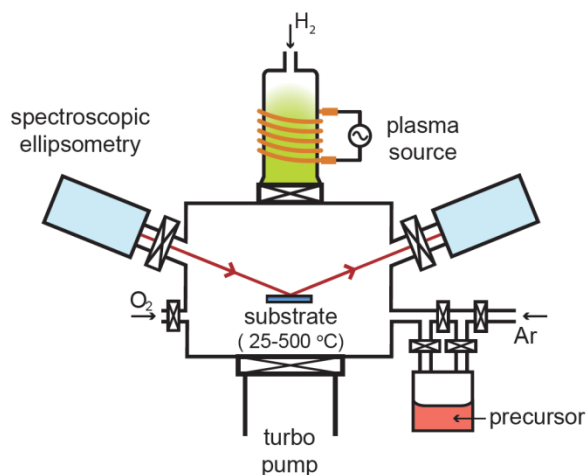


Figure 1.4. Schematic representation of the thermal and plasma ALD reactor used in this work. The main components - the plasma source, pump, and precursor dosing system - as well as the *in-situ* spectroscopic ellipsometry (used for process characterization) are indicated. Ar is used as a carrier gas for the precursor delivery.

1.3 Aim of the research and research project

The research project described in this dissertation is entitled “Atomic Layer Deposition of Noble Metal Nanoparticles”. The main overall aim of this doctoral work is to explore the nanoengineering capabilities of ALD in order to achieve the controlled synthesis of high purity Pd and Pt NPs with tuneable properties. The in-depth understanding of the reaction mechanisms taking place during noble metal ALD nucleation and growth represents an equally important aim of this project. As mentioned earlier, NPs prepared by ALD may find their applications in the deposition of model catalysts, and could as well play an important role in the miniaturization of emerging devices such as micro fuel cells or microreactors in general.

ALD is explored as a new route for the preparation of noble metal NPs. The physical and chemical processes taking place during ALD under steady-state

growth conditions and during the nucleation phase are different. In this research project, the noble metals Pd and Pt have been deposited by ALD on Al_2O_3 substrates. Although the formation of NPs during the nucleation stage of ALD was reported several times by others, the NPs properties were often not described in detail and appeared challenging to control. Therefore the following research questions were addressed in this work: *Which opportunities does ALD offer for the preparation of noble metal NPs? What are the properties of supported Pd and Pt NPs prepared by ALD in terms of size distribution and surface density? What are the mechanisms behind the formation of NPs?* To obtain the properties of the NPs, TEM studies were carried out. The physical and chemical mechanisms underlying the formation of Pd and Pt NPs prepared by ALD were illustrated on the basis of these TEM studies, but also knowledge from surface science and catalysis reports was employed. These new insights into the mechanisms taking place during Pd and Pt ALD nucleation are also valuable for the understanding of the ALD nucleation stage of other platinum group metals.

For the development of pure NPs of noble metals, it is essential to develop robust ALD processes. For this purpose, a profound understanding of the chemistry taking place during ALD is required, and the material properties resulting from the process have to fit the requirements of the application. The reaction mechanisms taking place during Pt ALD process have already been investigated in detail by our group and by others.^{28,29} Therefore, in this work, the research questions were then focused on Pd ALD: *Which surface reactions occur on a Pd surface during Pd ALD? How can the process be tuned to allow for the preparation of a high purity material? What are the nucleation mechanisms of Pd ALD and does the process actually enable the preparation of supported NPs? To what extent do the material properties depend on the process temperature?* To develop and optimize this process, the material properties of the Pd thin films resulting from the process were determined, and the reaction mechanisms taking place during Pd ALD were investigated. In addition, the formation of NPs during the nucleation stage and the temperature dependence of the process were explored for this Pd ALD process as well.

From detailed understanding of the chemistry of noble metal ALD processes and their nucleation mechanisms an idea for an innovative approach for the synthesis of controllable and tuneable bimetallic core/shell structured NPs was developed. Consequently, the work focused on the following research questions: *Is it possible to synthesize bimetallic core/shell structured NPs entirely by ALD, and can the core and the shell dimensions be tailored at the subnanoscale?* To synthesize bimetallic and core/shell NPs entirely by ALD, an innovative process was developed. Its applicability to different metals and its flexibility for the

core/shell arrangement was investigated as well. The requirements for the preparation of core/shell NPs using exclusively ALD were identified as well.

The research project was carried out in the Plasma and Materials Processing (PMP) group at the Eindhoven University of Technology (TU/e) in the Netherlands. The facilities used for this project include the PMP laboratory (also known as the “Ries van de Sande laboratory”), the “Nanolab@TUe” cleanroom facility at the Department of Applied Physics (TU/e), and the Philips Innovation Services laboratory (TEM facility, High Tech Campus, Eindhoven). The experience and expertise on ALD processing present in the PMP group was very valuable for the research carried out in this doctoral work. The group has a background in the science and technology of plasma and materials processing, a research area which encompasses the fields of plasma science, surface science, and materials science. In the last decade, the group has obtained extensive and valuable expertise in the field of ALD, including the areas of plasma-assisted ALD and ALD of noble metals.

The project was part of a Marie Curie (MC) Initial Training Network (ITN) and has received funding from the European Community's Seventh Framework Programme (FP7/2007-2013) under grant agreement number ENHANCE-238409. The name of this MC program is ENHANCE, which stands for “European Research Training Network of New Materials: Innovative Concepts for their Fabrication, Integration and Characterisation”. This scientific research programme is mainly focused on the multi-disciplinary field of thin film vapor deposition process technologies of new materials.

1.4 Outline of thesis

To address the aforementioned research questions, ALD of noble metal NPs will be discussed in Chapters 2 to 6. Part of these individual chapters have been or will be submitted for publication as separate articles in peer-reviewed scientific journals. The chapters are not ordered chronologically and there is some overlap in contents between separate chapters to make them readable independently. Chapter 7 presents the general conclusions and an outlook to future studies. The chapters describing the outcome of this project can be separated in the four next sections.

Status of ALD as a route for the preparation of nanocatalysts: The preparation of noble metal NPs by ALD represents a promising new route, which is extensively evaluated in Chapter 2. The basics of heterogeneous catalysis and the required properties of NPs are introduced. Then, the different synthesis (chemi-

cal and gas phase) techniques of NPs are presented. The third part of this survey presents an overview of the achievements so far with respect to the preparation of noble metal NPs carried out by ALD.

Characterization of the NPs prepared by ALD: Chapter 3 aims to give experimental details of our Pd and Pt ALD processes to the reader, and describes the main physical properties of Pd and Pt NPs supported on Al₂O₃ and how these properties were extracted from experiments. The NPs were imaged using TEM, and the basics of this characterization technique are also given. Chapter 3 aims also to present and discuss the main processes taking place during metal ALD nucleation, such as island growth and surface diffusion mechanisms.

Development of an ALD process for high purity Pd: Chapter 4 deals with the development of a robust ALD process enabling the synthesis of pure Pd NPs and thin films. This process allows the deposition of high quality Pd material at low temperature and our studies bring an in-depth understanding of the reaction mechanisms taking place during Pd ALD. This study also reveals the importance of the surface reactions for the final material properties. This work has been published in *The Journal of Physical Chemistry C*, 2014, 118 (16), pp 8702–8711.

Synthesis of tuneable bimetallic core/shell NPs: Chapter 5 deals with the development of a proof-of-concept method enabling the synthesis of bimetallic core/shell structured NPs entirely by ALD. This work has been published in *Chemistry of Materials*, 2012, 24 (15), pp 2973–2977. Chapter 6 extends the understanding of the shell growth processes and demonstrates the possibilities for subnanotailoring of both the core and the shell dimensions. This chapter also gives the conditions for the preparation of core/shell NPs entirely by ALD. This work will be submitted for publication in *Chemistry of Materials*.

References

- (1) *CRC Handbook of Chemistry and Physics*; Lide, D. R., Ed.; 82nd ed.; CRC Press: Boca Raton, FL, 2001.
- (2) In *Gmelin Handbook of Inorganic Chemistry*; Springer-Verlag: New York, 1986; p. 43.
- (3) *International Centre for Diffraction Data (ICDD)*; Pennsylvania, PA, 1997.
- (4) Pachón, L. D.; Rothenberg, G. *Appl. Organomet. Chem.* **2008**, 22, 288–299.
- (5) Bell, A. T. *Science* **2003**, 299, 1688–91.

- (6) Hagelucken, C. *Hydrocarb. Eng.* **2003**, 8, 48–53.
- (7) *Materials flow of platinum group metals*; GFMS.; Oiko-Institut Umicore: London, 2005; p. 228.
- (8) Cheong, S.; Watt, J. D.; Tilley, R. D. *Nanoscale* **2010**, 2, 2045–53.
- (9) Shao, M.; Peles, A.; Shoemaker, K. *Nano Lett.* **2011**, 11, 3714–3719.
- (10) Raimondi, F.; Scherer, G. G.; Kötz, R.; Wokaun, A. *Angew. Chem. Int. Ed. Engl.* **2005**, 44, 2190–209.
- (11) Osaka, T.; Iida, H.; Tominaka, S.; Hachisu, T. *Isr. J. Chem.* **2008**, 48, 333–347.
- (12) Jayashree, R. S.; Spendelow, J. S.; Yeom, J.; Rastogi, C.; Shannon, M. A.; Kenis, P. J. A. *Electrochim. Acta* **2005**, 50, 4674–4682.
- (13) Gershon, E. Micro fuel cells made of glass: Power for your iPad?
<http://phys.org/news/2012-11-micro-fuel-cells-glass-power.html>.
- (14) Energy, U. S. D. of Hydrogen Fuel Cell Engines and Related Technologies Course Manual. Module 4: Fuel Cell technology
http://www1.eere.energy.gov/hydrogenandfuelcells/tech_validation/pdfs/fcm04r0.pdf.
- (15) Leskelä, M.; Ritala, M. *Angew. Chem. Int. Ed. Engl.* **2003**, 42, 5548–54.
- (16) Elam, J. W.; Dasgupta, N. P.; Prinz, F. B. *MRS Bull.* **2011**, 36, 899–906.
- (17) Suntola, T.; Antson, J. Method for producing compound thin films. U.S. Patent 4,058,430, 1977.
- (18) International Technology Roadmap for Semiconductors <http://www.itrs.net>.
- (19) Lakomaa, E. *Appl. Surf. Sci.* **1994**, 75, 185.
- (20) Lindblad, M.; Peter, L.; Suntola, T. *Catal. Letters* **1994**, 27, 323–336.
- (21) Puurunen, R. L. *J. Appl. Phys.* **2005**, 97, 121301.
- (22) Miikkulainen, V.; Leskela, M.; Ritala, M.; Puurunen, R. L. *J. Appl. Phys.* **2013**, 113, 021301.

- (23) George, S. M. *Chem. Rev.* **2010**, *110*, 111–31.
- (24) Häimäläinen, J.; Ritala, M.; Leskela, M. *Chem. Mater.* **2014**, *26*, 786–801.
- (25) Elliott, S. D. *Langmuir* **2010**, *26*, 9179–82.
- (26) Campbell, C. T. *Surf. Sci. Rep.* **1997**, *27*, 1–111.
- (27) Mackus, A. J. M.; Verheijen, M. A.; Leick, N.; Bol, A. A.; Kessels, W. M. M. *Chem. Mater.* **2013**, *25*, 1905–1911.
- (28) Kessels, W. M. M.; Knoops, H. C. M.; Dielissen, S. A. F.; Mackus, A. J. M.; van de Sanden, M. C. M. *Appl. Phys. Lett.* **2009**, *95*, 013114.
- (29) Mackus, A. J. M.; Leick, N.; Baker, L.; Kessels, W. M. M. *Chem. Mater.* **2012**, *24*, 1752–1761.

Chapter 2

Noble metal nanoparticles synthesis by ALD: An overview

2.1 Introduction

Noble metal nanoparticles (NPs) are focus of interest in research because they have a wide range of potential applications, such as magnetic recording,¹ biomedicine,² plasmonics,³ water purification⁴ and heterogeneous catalysis.⁵⁻⁸ Heterogeneous catalysis is by far the main application of noble metal NPs. In this case, the NPs are used as catalysts for numerous applications, from oil refinery to fuel cells, and from gas sensing to automobile catalytic converters. Heterogeneous catalysis, which enhances chemical reactions between species in different phases, is in fact one of the most important technologies existing in our modern society. Approximately 90% of all chemicals or materials are produced using catalysis at one stage or another. Therefore much of the food we eat, the medicine we take, the clothes we wear, the fuels that transport us are produced by heterogeneously catalysed reactions.

Many approaches exist for the preparation of noble metal NPs. A promising new route for the synthesis of supported noble metal NPs is atomic layer deposition (ALD). ALD, a scalable technique mainly used for the deposition of conformal thin films, can in fact also be used as a robust method for the synthesis of NPs that can be used as nanocatalysts. ALD allows for NPs synthesis with high surface density on various challenging substrates. Furthermore, because the material is deposited in a layer-by-layer fashion, this deposition technique enables the deposition of NPs with a growth control at the atomic level.

This chapter is divided in three main parts. In the first part, an introduction to heterogeneous catalysis will be given. The main properties of the noble metal catalysts will be addressed, as well as the potential effects of their size, shape and composition on their catalytic activity. Subsequently, the deactivation processes that could occur to these supported NPs will be briefly described. In a second part, the different “conventional” techniques used to synthesize supported metallic NPs will be presented. The different routes presented form a relatively extensive but non exhaustive list, which shows the impressive diversity of possible ways to synthesize metal NPs. Furthermore, it illustrates the efforts of the scientific community in this field of research. The third part presents an overview of the depositions of noble metal NPs carried out by ALD. Based on the literature data, an overview of the results already obtained will be given, categorized by material. The achievements of the scientific community in this young field are impressive, and some examples will be described in order to show the potential of ALD.

2.2 Basics of heterogeneous catalysts systems

2.2.1 Introduction to heterogeneous catalysts

A catalyst is a material that increases the rate of a chemical reaction without being consumed in the process. In heterogeneous catalysis, the catalyst and reactant are in different phases. Heterogeneous catalysts are commonly solid-phase materials which enhance chemical reactions between gaseous or liquid phase species. One famous and widespread application of catalysis is the reduction of polluting car emissions (automobile catalytic converter) using solid catalysts in contact with the gas phase exhaust.^{5,6}

In general, heterogeneous catalysts consist of three distinct and complementary components: the support, the active component and the promoter.

The most commonly used support materials are high melting point oxides such as Al_2O_3 , SiO_2 , aluminosilicates (zeolites) and carbon based materials.^{7,9} In fact, an important factor affecting metal catalysts is their relative lack of thermal stability, which results in materials having a lower specific surface area due to sintering. Thus, the metallic “active” phase is “supported” on a thermally strong support phase such as alumina or silica. All of these supports can be produced with a very high surface area (up to $200 \text{ m}^2 \text{ g}^{-1}$) and they can maintain their morphology even in harsh conditions. The high surface area support has three main functions. First, it ensures large catalyst surface area per unit weight and unit volume of catalyst. It provides anchorage for the active sites, and finally, it should prevent sintering of the active material. It has to be noted that the support material can have a strong influence on certain catalytic reactions, especially when considering nanometer sized particles. On these small particles, spillover of material from support, charge transfer to/from the substrate or edge effects can be very important.^{5,6} The catalytic behavior can be optimized if the NPs are deposited on well-chosen support materials. Oxide surfaces are often chosen for this purpose because the electronic states of clusters or NPs (important for their catalytic properties) lie within the bandgap of many oxide materials.¹⁰ The nature of the support also affects the nanocatalysts activity. For example, Pd and Pt NPs become electron-deficient on acidic supports and electron-excessive on alkaline supports. The electron deficiency of NPs is explained by the withdrawal of their electron density by acidic centers of the support. This effect typically increases the catalytic activity of the NPs. For example, the enhanced electron-deficiency of Pd and Pt NPs enhances the

hydrogenation of aromatic compounds, and the most active catalysts reside on the surface of an acidic support such as alumina.¹¹

The active component is the portion of the catalyst that mediates the primary chemical reaction. The active component can be the support itself, or another material (such as a noble metal) which is added to the support.

Promoters are the third component, and their addition often increases a certain aspect of the catalyst system (e.g. activity, stability, etc.). For example, the addition of rare earth metal to zeolite supports increases their thermal stability.⁸ The most common use of a promoter is to prevent the formation of coke (residue of hydrocarbons) on both the support and the active component.⁹

In this thesis, the focus is on the synthesis of the active component (noble metal), which will be referred with the general term catalyst. Metals represent one main group of catalysts (active components), which are usually deposited onto a support. Only the d-electron transition metals are able to perform catalytic functions. These include Fe, Co, Ni, Cu, Ru, Rh, Pd, Ag, Re, Os, Ir, Pt and Au.^{7,8,12} Among them, the noble metals (Ru, Rh, Pd, Ag, Os, Ir, Pt and Au), due to their “bond-breaking abilities”, are the most widely used in catalysis. According to the Encyclopaedia Britannica Online, “the chemical behaviour of these metals is paradoxical in that they are highly resistant to attack by most chemical reagents yet, employed as catalysts, readily accelerate or control the rate of many oxidation, reduction, and hydrogenation reactions.”¹³ These noble metals used in catalysis can be classified by their bond-breaking abilities, as shown in Figure 2.1. Note that each metal has the capacity to break specific chemicals bonds.

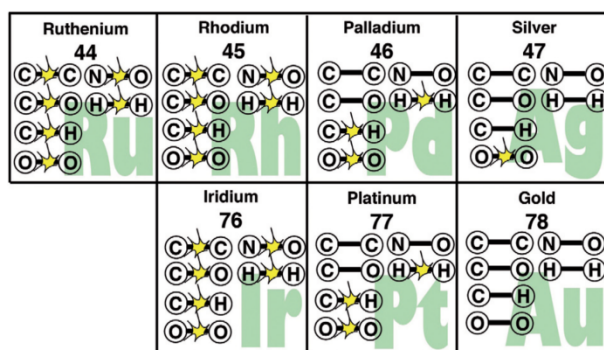


Figure 2.1. The precious metals used in catalysis can be "ranked" by their bond-breaking abilities. The capacity of each metal to break specific chemical bonds is indicated. The ability of clean gold to activate O-O bonds is a subject of current debate, particularly for gold nanoparticles (taken from Reference¹⁴).

2.2.2 The catalytic cycle

The progress of heterogeneous catalytic reactions can be summarized into at least five distinct steps (see Figure 2.2):

- (i) Diffusion of the reactants to the catalyst,
- (ii) Adsorption of reactants at the surface,
- (iii) Diffusion, reaction, chemical changes at the surface,
- (iv) Decomposition/reaction of the adsorbed complex,
- (v) Desorption and diffusion of the reaction products from the catalyst.

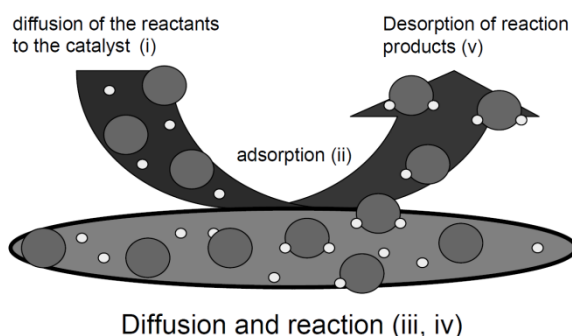
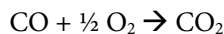


Figure 2.2. Main steps taking place during heterogeneous catalytic reactions. (taken from Reference¹⁵)

For example, during the CO oxidation on a metal surface, the first step is the diffusion of the O₂ and CO molecules through the gas phase to the metal surface where the molecules may bond (adsorption). Surface diffusion and dissociation of the molecule into atoms may then occur. In this example, O₂ dissociates but not CO which bond strength is too high. The next step is a surface reaction where oxygen atoms react with the CO to form the adsorbed product CO₂. This surface reaction step is commonly the rate determining step in a catalytic reaction. Finally, the product desorption occurs, where the bond between the surface and the product is broken, and the CO₂ enters the gas phase.⁶ The overall equation of this simple catalytic reaction is



2.3 Noble metal catalyst properties

2.3.1 Catalyst properties

Three catalyst properties are essential: activity, selectivity and lifetime. Whereas the activity represents the speed at which the chemical reaction takes place, the selectivity reflects the ability of the catalyst to convert the reactant along one specific chemical pathway. The catalyst lifetime is basically the time over which the activity and selectivity are maintained.

2.3.1.1 Activity

The activity of a catalyst is obviously essential to be of any use.

Generally, the rate of a catalytic reaction, that demonstrates the activity of the catalyst, can be expressed as the product of the rate coefficient and a pressure/concentration dependent term (of the reactant). The activity of a catalyst is related to the rate of consumption of reactant.

$$R = K \cdot P_i$$

K , apparent rate coefficient

P_i , Partial pressure of reactant i

The rate coefficient K can typically be represented by the Arrhenius equation:

$$K = A e^{-E_a/k_B T}$$

A is a temperature-independent pre-exponential factor, k_B the Boltzmann constant, T is the temperature and E_a is the activation energy of the catalytic reaction.

Usually, for convenience, the term turnover frequency or turnover number is used to define the activity of a catalyst. The turnover frequency (often designated TOF) is simply the number of times n that the overall catalytic reaction in question takes place per catalytic site/area per unit time for a fixed set of reaction conditions (temperature, pressure or concentration, reactant ratio, extent of reaction).

$$\text{TOF} = \left(\frac{\text{number of molecules of a given product}}{\text{number of active sites or active area}} \right) / \text{time}$$

As shown by the TOF, the activity of a catalyst can be defined as the rate of consumption of reactant, but the activity to a precise product can also be specified.

2.3.1.2 Selectivity

Selectivity reflects the catalyst ability to direct the conversion of the reactant(s) along one specific pathway. Good selectivity is therefore very important for the formation of the desired product and minimum production of undesired by-products. Catalyst selectivity is also vital to reduce consumption of raw materials and to prevent separation problems of products consisting of a mixture of compounds.

2.3.1.3 Lifetime

The catalyst lifetime can be defined as the time over which the catalyst activity and selectivity are maintained. Obviously this should be as long as possible in most cases.^{16,17} Catalyst decay is actually unavoidable, at least after a certain time, and a common industrial practice is to compensate for the decrease of activity by increasing the reactor temperature. There are three main mechanisms for the deactivation of a catalyst: poisoning, fouling and sintering (see section 2.3.3 for more details).

2.3.2 Nanocatalysts morphology/composition effects

The origin of the NPs catalytic performance is linked to their physical and chemical properties, which can depend on their morphology. Both the catalytic activity and selectivity of noble metal NPs can be highly dependent not only on the size and composition,¹⁸ but also on the shape and the nature of their surface structures.^{10,11,19-22} Therefore, research has focused on improving the nanocatalyst performance by controlling size, composition and shape.²²⁻²⁵ The exact relationship between the NPs morphology and their catalytic performance is usually dependent on which surface reaction needs to be catalyzed.²⁶

Catalytic reactions happen only on the catalyst surface. Therefore, the catalyst surface should be as large as possible, but moreover, the surface must be accessible to the reactants. A high density of NPs is typically the requirement, and the number of NPs can be even further increased when deposited in 3D structured high aspect ratio substrates. Generally, particles in the nanometer size range have the highest activity per material volume, because of the higher surface area exposed to the reactants (high surface-to-volume ratio).

The optimal NPs size varies depending on the specific chemical reaction one wants to catalyze.^{10,27,28} This is illustrated for Pd and Pt below.

Small Pd nanoparticles (0.2–0.4 nm) comprising 3–6 metal atoms are virtually inactive in most reactions. The NP diameter below which the catalytic activity starts to drop is dependent on the nature of the support, but is typically around 1 nm.¹¹ Some catalytic reactions proceed with high efficiency on small NPs (1–3 nm) whereas larger NPs (5–10 nm) are required for other reactions.¹¹ Pd NPs with a size of 3 nm have a doubled specific catalytic activity in ethylene hydrogenation compared to NPs of 1 nm. Chen et al. demonstrated that the intrinsic TOF per surface Pd atom for benzyl alcohol conversion showed a maximum at a NPs size of 3.6–4.3 nm²⁹ (see Figure 2.3a). Stakheev *et al.* studied the specific catalytic behavior of supported palladium nanoparticles in terms of both the size of the particles and their interaction with the support, and they found that a precise particle size range would be optimal for a specific chemical reaction as illustrated in Figure 2.3b.¹¹

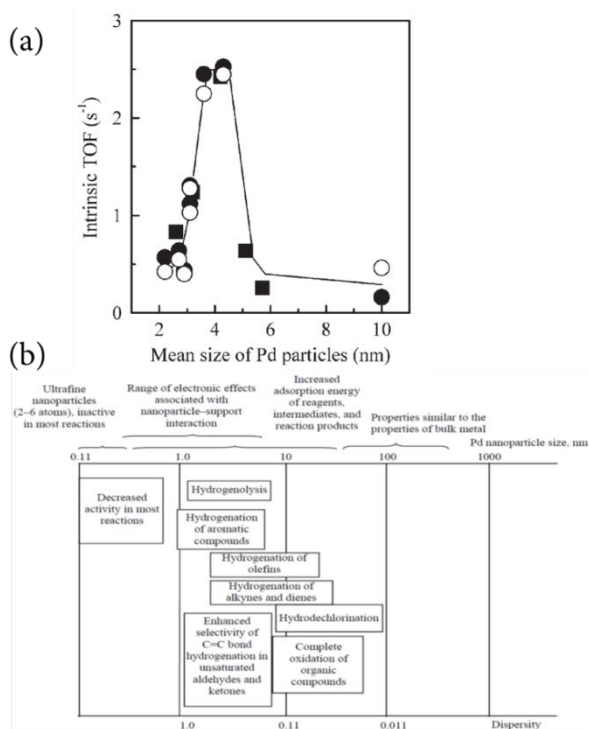


Figure 2.3. (a) Dependence of the intrinsic turnover frequency on the mean size of Pd particles in the aerobic oxidation of benzyl alcohol (taken from Reference²⁹) (b) Size ranges of Pd NPs optimal for different catalytic reactions (taken from Reference¹¹).

It is important to note that many reactions are considered structurally insensitive and are only dependent on surface area, which means that larger NPs will have a larger activity if they present a larger surface area.¹¹ For example, for CO oxidation catalyzed by Pd NPs, it has been found that the initial energy of adsorption (which can be seen as a measure for the catalytic activity) is increased with increasing particle size, when going from 2 nm Pd NPs to 8 nm NPs.²⁸ For olefin hydrogenation, the Pd NP activity increases 2–3 times as the NP size is changed from 1 to 10 nm.³⁰

Platinum small clusters and larger NPs can both present very high catalytic activities. For example, clusters of 8–10 Pt atoms supported on Al₂O₃ are extremely efficient for the dehydrogenation of propane.³¹ The size effect in the reaction of methane oxidation on the Pt NPs supported on Al₂O₃ showed the maximum specific activity for nanocatalysts in the range of 2 nm (see Figure 2.4). Smaller and bigger NPs led to considerably poorer results for this methane oxidation reaction.³²

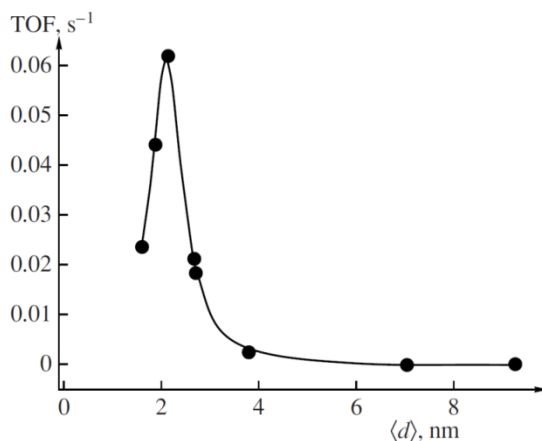


Figure 2.4. Size effect in the reaction of methane oxidation on Al₂O₃ supported Pt NPs catalysts (taken from Reference³²).

Concerning the oxygen reduction reaction, the maximal catalytic activity has been found for Pt NPs presenting a diameter of 2.2 nm.¹⁸ The activity, but also the catalytic selectivity can present a strong dependence on Pt NPs diameter. For example, the selectivity to cinnamyl alcohol as a product varied from 83% to 98% (at 50% conversion) as the NPs size was increased from 1.3 to 5 nm.²⁰

Since the NPs properties can depend on their dimensions, the synthesis of uniformly sized NPs is very important. The control of the NPs size is therefore critical and has been the focus of intense research.³³

The control of the NPs shape and crystallography is very challenging, but the catalytic activity can also depend on these factors.³⁴ The ability to control the NPs shape that terminates with the desired crystallographic plane is therefore highly desired. The information obtained from the literature concerning the best crystallinity for catalysis is however sometimes contradictory. Nanocrystals with open surface structures are usually superior in catalytic activity over the ones presenting closely packed surface atoms.^{9,19} However, it has been found that Pd NPs supported on alumina are more efficient for selective butadiene hydrogenation to butene when they exhibit a high fraction of (111) facets.²² Also, it is believed that Pt (111) surfaces are catalytically more active.³⁵ Being face-centered cubic (fcc) crystals, Pt and Pd can present a variety of geometrical shapes at the nanoscale (the most stable and often observed structures are cuboctahedron, icosahedron and decahedron).^{36,37}

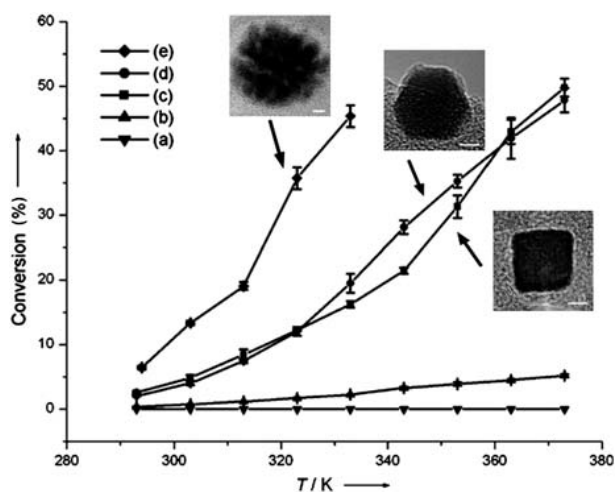


Figure 2.5. Comparison of catalytic activity for ethylene hydrogenation when using platinum (a) cuboctahedra of 9.1 nm, (b) cubes of 9.4 nm, (c) cubes of 13.4 nm, (d) cuboctahedra of 12.6 nm, and (e) porous nanoparticles of 19.3 nm. Nanoparticles of (a and b) were stabilized by PVP and (c–e) by TTAB. No treatment was performed to remove the stabilising agents (Reproduced from *Angew. Chem., Int. Ed.*, 2006, 45, 7824).

The properties of metallic nanocatalysts can be modified by mixing in another metallic component. Generally, alloying can have a wide variety of effects on the material properties, determined both by the distribution of the

atoms of both metals and by its chemical properties. The resulting alloyed nanomaterial usually shows a combination of the properties associated with the different metals. There is often an enhancement in specific physical and chemical properties, due to different effects.³⁸ There are three main effects that may improve the catalytic activity of bimetallic NPs in comparison to monometallic ones: ensemble, ligand and geometric effects.

Ensemble effects appear due to small groups (ensemble) of similar surface atoms that take on distinct functionalities, for example they promote different elementary reaction steps.³⁹

Ligand effects are due to the interactions between the two metals, resulting in electronic charge transfer between the atoms that affect their electronic band structure, thus possibly enhance the catalytic activity.⁴⁰

Geometric effects are linked to the atomic arrangement of surface atoms, often resulting in greater NP catalytic activity, and this is often linked to the so-called lattice strain. The lattice strain often induces an increase of the reactivity of the surface atoms with lattice expansion.^{41,42}

Due to the aforementioned ligand and geometric effects, bimetallic NPs, in particular core/shell structured nanomaterials, often present enhanced catalytic activity as compared to their monometallic counterparts. Thus, a key-challenge in catalysis research is the engineering of the composition and structure of noble metal nanomaterials, in order to precisely tune their catalytic activity. In addition, the ability to place an expensive and scarce noble metal as a shell around a less expensive core material is economically attractive. Therefore, evidently, the synthesis of noble metals core/shell nanoparticles became an increasingly important research topic over the years.^{25,43-50}

2.3.3 Catalysts deactivation processes

Any process which decreases the intrinsic activity or selectivity of a catalyst can be referred as deactivation. The understanding of the causes for deactivation of catalytic NPs is very relevant for the catalysts control. There are three main mechanisms for the deactivation of a catalyst: poisoning, fouling and sintering.

The poisoning mechanism is the catalyst deactivation due to the decrease in number of active sites via the strong chemisorption of some impurities, substances usually contained in the reaction mixture. In other words, poisoning is caused by the adsorption or reaction of poisonous precursors on or with the catalyst surface.

Fouling is a phenomenon where the reactants and products of the reaction cause the deactivation, due to their accumulation on the surface of the

catalyst. The decreased activity with time is referred as fouling if it is caused by an unfavourable interaction with the reactants or products. “Coke” formation can coincide with the fouling phenomenon. The term “Coke” originates from the name of the residue created during the cracking of hydrocarbons in the oil-gas refinery, which can also cause deactivation.

The third mechanism is sintering. The term “sintering”, when used for supported metallic catalysts, refers to the loss of catalytic metal sites due to the agglomeration of the metal particles. Sintering occurs via two main mechanisms: a) Ostwald ripening, where atoms from the smaller catalyst NPs move to other, bigger NPs by surface or gas phase diffusion, and b) particle migration (and subsequent coalescence), where the whole NPs diffuse over the support until they collide and coalesce.^{51–53} This mechanism is also referred as the “Smoluchowski ripening”.^{54,55} The atmosphere/environment to which the catalyst is exposed (oxidizing, reducing or inert) has a strong effect on sintering and atomic migration.^{51,56} Recently, Yu *et al.* visualized, by means of an electron tomography method, the electrochemical aging of Pt-Co fuel cell nanocatalysts supported on carbon (see Figure 2.6).⁵⁷ They deduced from this NPs tracking that the majority of sintering events in this system were caused by particle migration and coalescence.

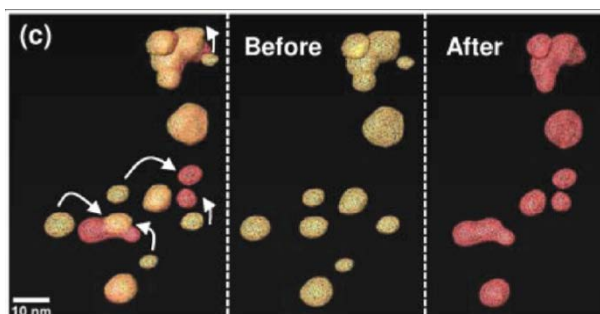


Figure 2.6. Pt-Co nanocatalyst NPs migration and coalescence after electrochemical aging on a fuel cell carbon support (taken from Reference⁵⁷).

To limit the sintering effect, the metallic NPs can be encapsulated with a (ultra) thin layer. For example, Pt NPs have been encapsulated in ceria⁵⁸ using a microemulsion technique and Pd NPs in alumina⁵⁹ prepared by ALD, while retaining their catalytic activity. This approach will be addressed in more detail later in this chapter (see Section 2.5.2.3).

A fourth additional deactivation process is the potential metal leaching (metal dissolution in liquid) taking place in certain reactions such as the

olefination of halides (Heck reaction), one major reaction heterogeneously catalyzed by Pd NPs on oxides or C supports.^{60–63}

In addition to the aforementioned deactivation processes, which affect mono- and bimetallic NPs, particular issues may concern multimetallic and structured (e.g. core/shell) NPs. The durability of these particular nanomaterials, in terms of activity and selectivity, may severely decay if they are subject of dealloying or restructuring. The structure and composition of core/shell NPs may undergo changes during their catalytic life. Inaba *et al.* found that the size of the core in Pd/Au and Pt/Pd core/shell NPs, as well as the dissolution of the shell material within the core (restructuring) are important degradation

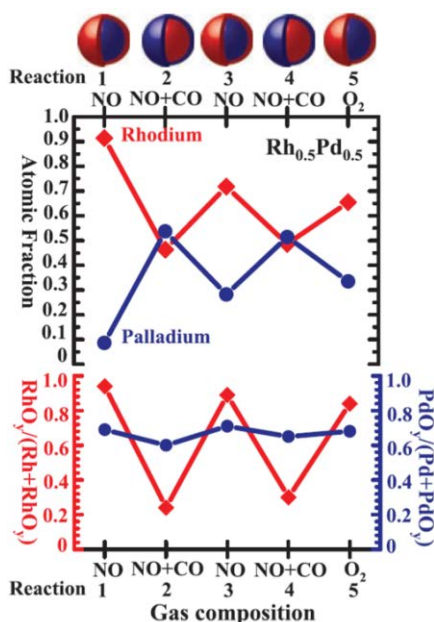


Figure 2.7. (Top) Evolution of Rh ($\text{Rh}^0 + \text{Rh}^{2y+}$) and Pd ($\text{Pd}^0 + \text{Pd}^{2y+}$) atomic fractions in the $\text{Rh}_{0.5}\text{Pd}_{0.5}$ NPs at 300°C under oxidizing conditions (100 mTorr NO or O_2) and catalytic conditions (100 mTorr NO and 100 mTorr CO) denoted in the x axis.

(Bottom) Evolution of the fraction of the oxidized Rh (left y axis) and Pd atoms (right y axis) in the examined region under the same reaction conditions as the top part of the figure. All atomic fractions in this figure were obtained with an X-ray energy of 645 eV for Rh3d and Pd3d, which generates photoelectrons with a MFP of ~ 0.7 nm. Schematic diagrams above the top of the figure show the reversible segregation of Rh and Pd under alternating oxidizing and catalytic conditions. The data points for reactions 1, 3, and 5 have an associated error of ± 0.03 ; for reactions 2 and 4, the error bar is ± 0.02 . (taken from Reference⁵⁶).

mechanisms.⁶⁴ Tao *et al.* demonstrated that Rh/Pd and Pt/Pd core/shell NPs undergo structural and chemical variations in response to different environments (oxidising, reducing) and catalytic reactions (Figure 2.7).⁵⁶ Under certain chemical conditions, the segregation (dealloying) effect of bimetallic catalysts can be controlled and used to synthesize core/shell nanomaterials, as shown by Oezaslan *et al.*⁶⁵ Guisbiers *et al.* have calculated that at a temperature of approximately 1100K, a spherical alloyed Pt-Pd NP of 4 nm will be the subject of Pd surface segregation, and the catalytic activity of core/shell NP (segregated) will be increased in comparison to the “randomly” mixed alloyed Pt-Pd NP.³⁷ Barcaro *et al.* performed DFT calculations showing that segregation in alloyed Pt-Pd NP can yield a novel multishell chemical ordering pattern, in which each shell is a patchwork of islands of atoms of the two elements.⁶⁶

2.4 “Conventional” synthesis techniques

A large variety of both chemical and gas phase methods have been developed for the preparation of noble metals NPs. The description of these routes can be classified in two parts. First the methods for preparing NPs suspensions will be described, and secondly the methods to synthesize supported NPs (on structured surfaces) will be presented. The aim of the next sections is to illustrate the diversity of routes enabling the synthesis of metallic NPs and not to present an exhaustive list. For more detailed information about these various synthesis techniques, the reader is referred to the books and review papers given in references.^{33,38,67–71}

2.4.1 Methods for preparing metal NPs suspensions

Of the many routes that have been explored to prepare noble metals NPs suspensions, the most widely used techniques are solution-phase colloidal chemistry methods, which have shown to be very powerful and versatile routes to prepare nanocatalysts. In short, these general routes to prepare noble metals NPs such as Pd and Pt involve the reduction or the thermal decomposition of the metal precursor in the presence of a surfactant or stabilizer. By varying the process parameters (temperature, pH, type of chemicals used, etc.), the size and shape of transition metals NPs (such as Pd⁷² and Pt⁷³) can be controlled.^{34,70,72}

The reduction method typically makes use of a chemical reducing agent, electrochemistry, or an organic phase in order to reduce the transition metal salt precursors.^{33,74} The reduction of metallic salts by a chemical reducing agent (such as hydrazine or borohydride) has been widely applied for the synthesis of

mono and bi-metallic nanoparticles.^{33,75-78} The electrochemical pathway eliminates the contamination problems resulting from chemical reducing agents, and allows for the NPs size selectivity by tuning the current density. The third pathway is the metal salts reduction in organic phase. In fact, using a single phase or a phase transfer technique, organic soluble reductants such as hydrides or alcohols have been used to synthesize many metallic NPs.³³

The thermal decomposition method is based on the rapid injection of the organometallic precursors in a hot solvent in the presence of surfactants. The monodispersity of the synthesized NPs and their dispersion ability in organic solvents makes this technique very attractive.

Independent of the type of reduction, the control of the NPs size and dispersion can be achieved by the separation of nucleation and growth. Furthermore, as “naked” NPs are not stable in solution, the use of stabilizing agents is also often required. Many approaches exist to satisfy these needs, in particular to stabilize the NPs. The metal NPs can be encapsulated by dendrimers,⁷⁹ stabilized by micelles,⁸⁰ polymers or surfactants.³³ Ionic liquids are also of interest, since they can act both as stabilizers and solvents.⁸¹ For example, a common method uses the inner core of reverse micelles as a nanoreactor⁸² where the size of the NPs is limited by the inner volume of this “nano-pool” where the nucleation began. The NPs must then be extracted from the micellar media and removed as a powder. This approach has been used for the synthesis of various nanomaterials⁸³ including Pt⁸⁴ and Pt/Pd⁸⁵ NPs. If the method used to synthesize NPs is the organic phase reduction, the NPs must also be stabilized. In this case a capping agent is typically used. The single-phase synthesis method is an approach in which all the chemicals (metal precursor(s), reducing agent, capping agent) are dispersed in the same solvent. This technique has been used for the synthesis of both mono and bi-metallic NPs.⁸⁶ Noble metal NPs can also be prepared by a two-phase synthesis (or the phase-transfer method), which involves the transfer of the metal ion from a polar to a non-polar phase.⁸⁷ The NPs size is controlled by a capping agent and by the reaction conditions at the interface. This method enables the production of large amount of metallic NPs with narrow size distribution, but the NPs composition control remains challenging. This phase-transfer method is therefore a good route for the synthesis of monometallic NPs, but is not so well adapted for nanoalloys synthesis.^{67,88,89}

These soft-chemistry approaches (or colloidal chemistry) - based on metal salts reduction (or co-reduction in case of nanoalloys synthesis) and thermal decomposition - are the most commonly used.^{33,88} In general, core/shell structured noble metal NPs are prepared by using successive sequential

reductions.^{48,90} Other wet-chemistry routes, mostly based on organometallic chemistry, have been used to create mono- and bi-metallic NPs, some of them enable the control of the nanostructure,^{25,44,47,91,92} but such synthesis procedures are more complex.^{67,88}

Although good progress has been achieved in the wet chemistry synthesis field, at the amazing point where the size, the composition and the shape of NPs can be controlled,^{25,33,34,46,73–75,92,93} several issues remain before practical application can be achieved. Synthesis needs to be scaled up with high yield for economical relevance and this is a great engineering challenge, especially for the complex synthetic procedures that allow for a total control of the NPs properties. Furthermore, chemical contaminants may stay at the surface of the synthesized catalysts, and the post-cleaning procedure may be difficult. Also, there is a big issue concerning the collection of the NPs while preventing aggregation. To avoid the need to collect the NPs after their synthesis, one solution is to directly prepare them on their support. In addition, immobilizing the catalysts on solid (oxide) supports can reduce the leaching from the NPs.

2.4.2 Methods for preparing supported metal NPs

2.4.2.1 Chemical routes

A method commonly used is the dispersion of a pre-synthesized material (oxide or metal catalyst) on a substrate. This is to coat specific substrates, such as the ones used in micro-reactors for example.⁹⁴ Figure 2.8 illustrates such a procedure, where presynthesized NPs are coated over a substrate. The immobilization of NPs (created in solution) on solid supports, for example Pd NPs stabilized in micelles immobilized on alumina, have been successfully used for hydrogenation purposes. However, the supported catalysts showed desorption of some micelles during its catalytic use.⁸⁰

Other routes exist to produce supported metallic catalysts, and almost all these other chemical methods can be classified in one of the following categories: Impregnation, deposition/precipitation, or ion exchange.⁹⁶

The impregnation technique consists of the precipitation of a soluble catalytic precursor on a substrate. A preformed support phase is impregnated with the solution containing the metallic catalytic precursor, and the subsequent processing (e.g. annealing) and reduction result in supported metal crystallites.

Deposition/precipitation is based on the precipitation of a catalyst precursor and a suspended support precursor. Both the support and the catalytic precursors are precipitated from aqueous salts solution. The subsequent

processing and reduction result in the metal crystallites separated by the support phases. It is a common preparation technique because it results in high loadings.^{17,96}

Ion exchange makes use of the replacement of charges at the substrate surface by ionic metal precursor molecules and a subsequent calcination in order to deposit small metal NPs.⁷¹

The sol-gel technology is another technique applied for the synthesis of supported NPs. It is similar to the deposition/precipitation approach because it is based on a solution or colloidal dispersion of chemical precursors. The ageing time of this solution (from a few minutes to several weeks) allows for its gelification. This technique can enable the synthesis of a supported active oxide layer or oxide supported noble metal NPs, such as alumina supported Rh or Pt

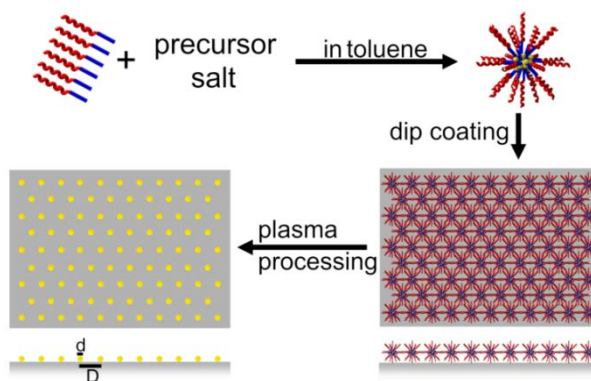


Figure 2.8. Preparation scheme of metal NPs (Fe, Co and Pt) by a reverse micelle technique. PS-*b*-P2VP or PS-*b*-P4VP is dispersed in anhydrous toluene. After adding a metal precursor salt and continuous stirring for about one week, reverse micelles are homogeneously loaded with the precursor material. By dip coating a hexagonal arrangement of loaded micelles can be obtained. This micelle monolayer is exposed successively to oxygen and hydrogen plasmas for (i) removal of the polymer and particle nucleation and (ii) the reduction of the metal oxide particles, respectively (taken from Reference⁹⁵).

NPs.⁹⁴ These sol-gels (solution phase) are in most cases deposited by washcoating on specific supports.⁹⁷

These last techniques are also based on wet chemistry, and the removal of potential chemical contaminants can potentially be challenging, especially if the deposition is done in a high-aspect ratio substrate or porous material, which is often the case.^{69,71,96} It has to be noted that the pretreatment of the substrate is also gaining more and more importance. Different methods are used, such as

anodic, thermal or chemical oxidation, which allows for a better impregnation of the catalyst precursor by forming an oxide layer or by creating anchoring sites.⁹⁴

2.4.2.2 Gas phase routes

Gas phase techniques, categorized in either physical vapour deposition (PVD) or chemical vapour deposition (CVD) techniques, have also been investigated for the synthesis of supported metallic NPs. The major advantage of gas phase methods is the possibility to produce a large quantity of directly supported NPs, and therefore upscaling of the process is easier than with the wet-chemistry techniques. The NPs size control, however, is more difficult.

Physical vapour deposition (PVD) routes require a vacuum environment. The main PVD techniques allowing for the synthesis of mono and bi-metallic nanoparticles are vapour flow condensation, molecular beam epitaxy (MBE), low energy cluster beam deposition (LECBD), spark discharge generation, ion sputtering, and pulsed laser deposition (PLD).⁶⁷

Vapour flow condensation is probably the most logical route to produce metal NPs. The process consists in heating a solid metal to evaporate it in a background gas under high vacuum conditions, and the metal vapour is then condensed on the substrate by adding a colder gas. The size distribution of metal NPs produced using this route can be tuned by adjusting the flow and the gas mixing.^{98,99}

MBE is based on the slow sublimation of the material itself under ultra high vacuum conditions. A mechanical shutter controls the time of the metal evaporation. The sublimated atoms do not interact with each other or with the vacuum chamber gases until they reach the wafer substrate (because of the long mean free path of the atoms). The advantage of this method is the resulting high purity and the possibility to make nanoalloys¹⁰⁰ by simply co-sublimating different materials on the same substrate. The NPs size is depending on the substrate temperature and the deposition time. Superfine crystalline nanostructures can be obtained by this technique, but the throughput is limited.¹⁰¹

LECBD is the NPs production by gas phase condensation, which requires the control of the vapour pressure of the evaporants and their velocity. However, it is very attractive, because it allows for the deposition of unstable metallic alloyed NPs with a very narrow size distribution.^{67,102}

Spark discharge generation enables the vaporization of a metal by charging electrodes made of the metal until the breakdown voltage. NPs are then

formed in the arc (spark) between the electrodes in a reproducible but quantity limited way.¹⁰³

Sputtering a metal with inert ions is another way to vaporize it, and the deposition of catalytic materials on various substrates can thus be achieved by this method.¹⁰⁴ Many metallic NPs can be produced using magnetron sputtering but the deposition of (very) small NPs (< 8 nm) is challenging.¹⁰⁵ This method has been used to coat microreactor substrates with Pt.¹⁰⁴

PLD, also called laser ablation, makes use of a short and energetic laser pulse to shoot on a target which results in a plasma whose species condense at the substrate (facing the target). The advantage of this technique is its versatility and the possibility to evaporate almost every material, including oxides, noble metals¹⁰⁶ and nanoalloys.¹⁰⁷

The limitations shared by these PVD techniques are the requirement of the high temperature (for the volatilization of the elements to deposit) and the expensive high vacuum equipment needed.

Chemical Vapour deposition (CVD), which does not require a high vacuum nor extremely high temperatures, has also been investigated for NPs deposition and led to successful deposition of various nanomaterials.¹⁰⁸ CVD has the advantage to use highly volatile compounds (metallorganic precursors) in the gas phase, which chemisorb, react and/or decompose at the substrate surface to produce the desired material.⁷⁰ The absence of liquid solvent facilitates the inclusion of NPs within porous materials, and there is no post treatment needed for the removal of potential chemical contaminants.⁷¹

2.5 ALD as a new route for nanocatalyst synthesis

2.5.1 Introduction to NP preparation by ALD

A promising new route for the synthesis of nanocatalysts is atomic layer deposition (ALD). ALD is basically a chemical vapor deposition (CVD) method in which the deposition process is generally split up into two self-limiting half-reactions. In CVD, the precursors reactants are led into the reactor simultaneously whereas in ALD, they are introduced in the reactor in alternate pulses. The ALD reactor is purged and/or pumped down between the two self-limiting steps, in order to remove the excess precursor or reactant molecules and the reaction products from the reactor. ALD enables the deposition of (ultra)thin films of various materials, including oxides, nitrides and metals. Plasma species can be employed as reactants, and so-called plasma-assisted ALD allows for more freedom in processing conditions, and for a wider range of

material properties compared to conventional thermal ALD.¹⁰⁹ ALD has the ability to control film growth at the atomic level, since the material is deposited in a layer-by-layer fashion.¹¹⁰ The main advantages of ALD can therefore be summarized as excellent uniformity, high conformality, and precise growth control. These characteristics can be attributed to the self-limiting nature of the ALD process.

A variety of metals, such as Cu,¹¹¹ W,¹¹² Mo,¹¹³ and noble metals such as Pd,¹¹⁴ Pt,¹¹⁵ Ru¹¹⁶ have been deposited by ALD. In this overview, we chose to focus on the NPs of noble metals. In case of noble metal ALD on oxides, the nucleation often begins with the formation of islands that increase in size cycle after cycle, and eventually they coalesce to form a continuous film.¹¹³ The elements considered as being noble metals, in order of increasing atomic number, are Ru, Rh, Pd, Ag, Os, Ir, Pt and Au. All these elements have been deposited by ALD, and the island-growth behavior is very likely to take place for all these noble metals when deposited on oxides supports. The TEM images presented in Figure 2.9 show the result of various numbers of cycles of ALD of Pt on Al₂O₃ and illustrate nicely the nucleation during ALD of metals. The metal NPs deposited are highly dispersed. For example, Pt and Pd NPs deposited on alumina nucleate with a typical and maximal density in the order of 10¹² NPs/cm².^{49,117}

The growth mechanism includes the adsorption of precursor molecules at the substrate surface followed by the diffusion of metal adatoms to form clusters or to join growing NPs. The formation of these nanosized islands is mainly due to the difference in surface energies between the substrate and the material deposited. The formation of NPs by ALD is presented in more details in the Chapter 3 of this thesis.

This noble metal ALD nucleation behavior has been investigated for the synthesis of supported NPs on various substrates. Both monometallic and bimetallic NPs have been deposited by this method.

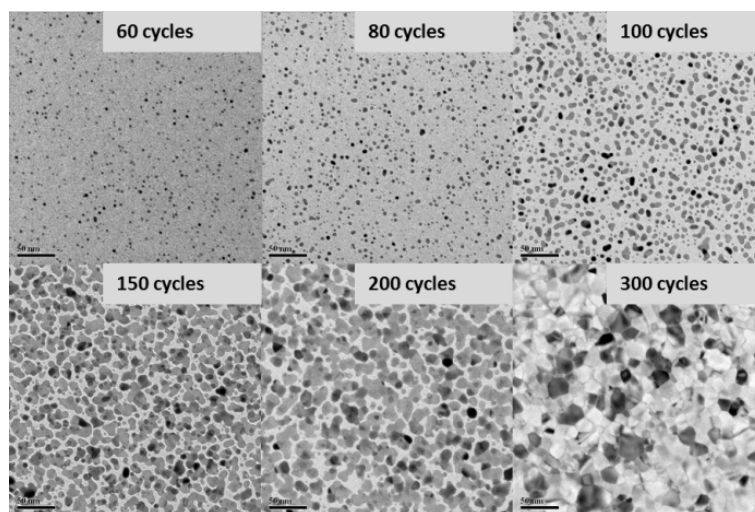


Figure 2.9. Nucleation and growth of nanoparticles by ALD of platinum presented as a function of the number of cycles (indicated in the upper right corner of each image). The substrates used were Al_2O_3 covered Si_3N_4 TEM windows. The scale bar is 50 nm.

2.5.2. Overview of noble metal NPs synthesized by ALD:

The noble metal NPs prepared by ALD are briefly summarized by material (monometallic Ru, Pd, Ag, Ir, Pt and bimetallic NPs) in the Tables 2.1 to 2.6 presented in this chapter. Note that the list of abbreviations and acronyms is given on the last page of this Chapter. The tables refer only to journal papers where NPs have been imaged or studied otherwise. In some cases the NPs were observed in a film growth study, not with the purpose of preparing NPs. The processes used and relevant observations are indicated in the tables. Some cases will be illustrated and explained in more detail below. This extensive list shows the amount of work carried out in this field, and demonstrates that ALD preparation of catalysts is of considerable interest.

2.5.2.1. Ruthenium

Ruthenium is a low resistivity metal, whose properties are of interest for many applications in semiconductor technologies such as electrode material for dynamic random access memory (DRAM) and ferroelectric random access memory (FRAM) devices.¹¹⁸ Due to its bond breaking abilities, Ru can also be used as heterogeneous catalyst, for example for dehydrogenation reactions of ammonia borane.¹¹⁹

Table 2.1: Overview of literature reports of Ruthenium NPs prepared by ALD.

Precursor	ALD process Co-reactant	Substrates	Objectives and remarks	References
DER	O ₂	Pristine nanoporous template ¹²⁰	Film growth	120
Ru(Cp) ₂	O ₂	SiO ₂ , Al ₂ O ₃	Comparison of high density of NPs	121
DER	O ₂	Si, SiO ₂ , TiO ₂ , and TiN	Film growth	122
Ru(EtCp) ₂	NH ₃ plasma	SiO ₂	High density of NPs and application in capacitors	123
C ₁₆ H ₂₂ Ru	O ₂	SiO ₂	NPs coalesce after only 10 cycles	124
Ru(Cp) ₂	Air	carbon and silica aerogels	Deposition on high aspect ratio substrates	125
Ru(EtCp) ₂		anodized aluminum oxide (AAO) template	High density of NPs on 3D substrate	126
Ru(EtCp) ₂	NH ₃ plasma	TiN	Film growth	119
Ru(EtCp) ₂	O ₂	Al ₂ O ₃	Control of the size and density	128
Ru(EtCp) ₂	NH ₃ plasma and O ₂ gas	SiO ₂	Control of the size and density	129
Ru(Cp) ₂	O ₂	Al ₂ O ₃	Application in capacitors	130

Ru(EtCp) ₂	O ₂	Al ₂ O ₃	Application in capacitors	131
Ru(^t Bu-Me-amd) ₂ (CO) ₂	NH ₃	Al ₂ O ₃	High density of NPs and application in capacitors	132
Ru(DMPD) ₂	O ₂	SiO ₂	NP crystal structure and growth	133

When “film growth” is mentioned in the “objectives and remarks” column, NPs resulting from island growth have been observed but the focus of the work was on the film growth and the material properties associated.

2.5.2.2 Rhodium

Rh is an efficient catalyst and has been exploited for hydrocarbon conversion reactions¹³⁴ and applications in automobile catalytic converters.¹³⁵ However, concerning ALD, only thin film samples have been prepared so far.^{136,137}

2.5.2.3 Palladium

The noble metal palladium can be applied as seed layer material for electroplating in integrated circuit interconnects,¹³⁸ and it is also object of great interest in catalysis,¹³⁹ as well as in hydrogen sensing¹⁴⁰ and storage.^{141,142} Palladium exhibits a high catalytic activity for hydrocarbon oxidation.^{7,12,143} Pd has a better catalytic activity for aromatic hydrocarbons combustion than Pt.⁷ Both metals (Pd and Pt) having such a high catalytic activity, they can be used at very low loadings (approximately 0.02-0.5 wt.%) in catalytic combustion applications.⁷ Therefore, NPs of Pd (and Pt) have been widely studied for many catalytic applications including hydrogenation reactions, carbon-carbon bond formation, and oxidation and reduction reactions in fuel cells.^{24,61,62,68,144}

Table 2.2: Overview of literature reports of Palladium NPs prepared by ALD.

Precursor	ALD process Co-reactant	Substrates	Objectives and remarks	References
Pd(hfac) ₂	H ₂	W	Film growth	145
	H ₂ plasma	Si, W	Film growth	146
	H ₂ plasma	Al ₂ O ₃	Film growth	49
	HCHO	Al ₂ O ₃	Film growth	114
	HCHO	ZnO, Al ₂ O ₃	Methanol decomposition catalyst	147
	HCHO/ TMA/H ₂ O	TiO ₂ or Al ₂ O ₃ coated silica gel	ABC-type ALD process for highly dispersed, uniform and ultrafine NPs	148
	TMA/ HCHO	Al ₂ O ₃ coated ZrO ₂ NPs	Enhanced NPs nucleation	149
	HCHO	Al ₂ O ₃ coated ZrO ₂ NPs	Surface chemistry study	150
	HCHO/ TMA/H ₂ O	Al ₂ O ₃	Detailed study of the ABC-type ALD	151
	HCHO	Al ₂ O ₃	Methanol decomposition catalyst	152
	HCHO	Al ₂ O ₃	Glucose oxidation catalyst, deposition in fluidized bed reactor	153
	HCHO	Al ₂ O ₃	Alumina over- coating of NPs	154

	HCHO	Al ₂ O ₃	Alumina over-coating of NPs, methanol decomposition catalyst	155
Pd(hfac) ₂	Air	Porous C powder	Ethanol and isopropanol oxidation catalyst	156
	HCHO, H ₂	Al ₂ O ₃ , ZrO ₂ , TiO ₂	Film growth	157
	HCHO	Porous C	Li-O ₂ battery cell catalyst	158
	HCHO	TiO ₂	Nucleation study	159

When “film growth” is mentioned in the “objectives and remarks” column, NPs resulting from island growth have been observed but the focus of the work was on the film growth and the material properties associated.

As is clear from the table, Pd NPs synthesized by ALD have been tested in different catalytic reactions: they have been successfully used in ethanol, isopropanol¹⁵⁶ and glucose oxidation¹⁵³ reactions, as well as for methanol decomposition.^{152,155}

Rikinen *et al.* deposited Pd NPs by ALD on a porous carbon support for fuel cell applications. In this case, the NPs activity has been tested for ethanol and isopropanol oxidation and compared to a commercial catalyst. The results obtained indicated that the ALD catalysts provide a similar mass activity with a lower loading than current commercial fuel cell catalysts.¹⁵⁶ Direct alcohol fuel cells represent a very promising energy source for low power portable devices.

Liang *et al.* used ALD to produce Pd/Al₂O₃ catalysts. The depositions were carried out at 200°C in a fluidized bed reactor. When compared to a commercial Pd/alumina catalyst, the ALD Pd/alumina presented a greater active metal surface area, and they had comparable activities for glucose oxidation to gluconic acid in aqueous solution.¹⁵³

Feng *et al.* deposited Pd NPs by ALD on alumina coated silica gel. Samples with various sizes of NPs (from 0.8 to 2.2nm) were obtained and their catalytic activities were compared for methanol decomposition. The ALD Pd

NPs presented a higher activity than those of catalysts containing larger Pd particles synthesized by “traditional” methods such as impregnation or sol-gel.¹⁵²

Furthermore, some process modifications can increase the possibilities offered by ALD. For example, the deposition of highly dispersed and ultrafine (< 1 nm) metallic NPs is possible using the so-called ABC-type ALD.¹⁴⁸ With this technique illustrated in Figure 2.10, metal NPs with protective ligands and the support material are deposited sequentially. The final step is the removal of the protective ligands by calcination and/or reduction to activate the metal NPs. This process has been used for the deposition of highly uniform ultra-fine supported Pd nanoparticles on high surface area supports. Further details can be found in the References.^{148,151}

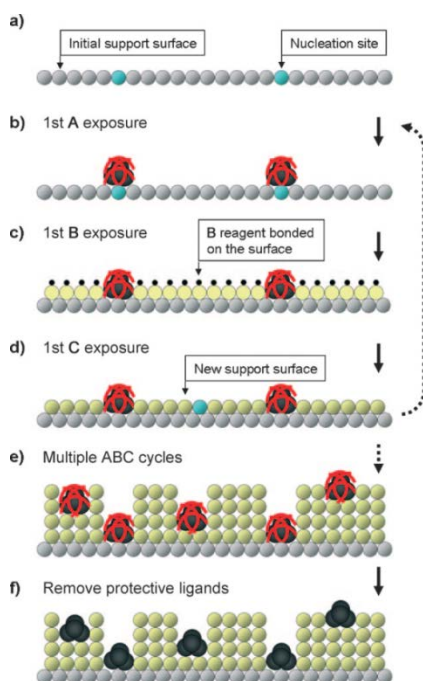


Figure 2.10. A schematic representation of one particular configuration for an ABC-type ALD process: a) Initial support with nucleation sites. b) A volatile metal precursor A is introduced to the surface to form metal nanoparticles with a part of the ligands retained. c) The first reagent B is introduced to the surface. d) The second reagent C is introduced to the surface to react with B and form a new support surface. e) New support and metal NPs protected by ligands are formed on the initial support surface after multiple ABC cycles. f) The protective ligands are removed to activate the metal NPs (taken from Reference¹⁴⁸).

As described earlier, supported catalysts can be the subject of deactivation with ageing. A major issue is the fact that many supported NPs are susceptible to sintering during aging and during their use in catalytic reactions. An innovative ALD process has been developed by Argonne National Laboratory group in order to overcome the sintering issue. After the deposition of metallic NPs (Pd in this case), an ALD layer of alumina was used as a protective layer to inhibit the sintering. It has been shown that up to a certain over-coat thickness (using 15 cycles with $\text{Al}(\text{CH}_3)_3$ and H_2O), the alumina protective layer preserved the catalytic activity while preventing NPs sintering up to 500°C (see Figure 2.11).^{59,154,155,160}

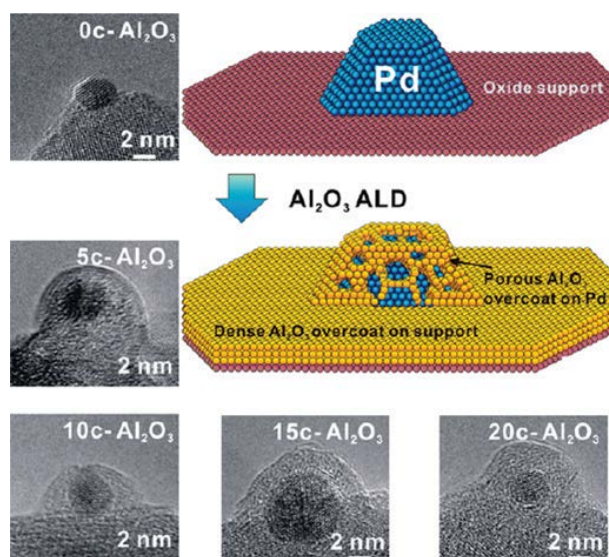


Figure 2.11. TEM images of alumina supported Pd catalysts with different numbers of Al_2O_3 ALD overcoating cycles (taken from Reference¹⁵⁴).

When these alumina-covered Pd catalysts were tested in oxidative dehydrogenation of ethane to ethylene at 650°C , it has been found that the overcoating effectively reduced the catalyst deactivation by coking and sintering.⁵⁹ It has to be noted that a chemical technique (a modified Stober method) has been used in an earlier work to coat supported Pt NPs with a porous silica layer in order to make them sintering resistant.¹⁶¹

2.5.2.4 Silver

Silver has the highest electrical conductivity of any metals. Silver catalysts are very efficient and they are used industrially in the oxidation of methanol to formaldehyde and in the epoxidation of ethylene.⁵

Table 2.3: Overview of literature reports of Silver NPs prepared by ALD.

Precursor	ALD process Co-reactant	Substrates	Objectives and remarks	References
Ag(fod)(PEt ₃)	H ₂ plasma	Si	Film growth, plasmonics	162
Ag(fod)(PEt ₃)	H ₂ plasma	Si	Film growth	163
(hfac)Ag(1,5-COD)	Propanol	Glass, SiN, porous C	Nucleation study, application in plasmonics	164
Ag(O ₂ C ^t Bu)(PEt ₃)	H radicals	Si, glass	Film growth	165
Ag(fod)(PEt ₃)	H ₂ plasma	Si	Film growth, application in plasmonics	162
Ag(fod)(PEt ₃)	H ₂ plasma	Si	Film growth	163

When “film growth” is mentioned in the “objectives and remarks” column, NPs resulting from island growth have been observed but the focus of the work was on the film growth and the material properties associated.

2.5.2.5 Osmium

Os metal is usually alloyed with other noble metals for use in electrical contacts,¹⁶⁶ but can also be used in catalysis.¹⁶⁷ Recently, Osmium NPs and thin films synthesis has been achieved on alumina, using an ALD process based on Os(Cp)₂ and O₂ gas.¹⁶⁷ The typical island growth has been observed for Os ALD during the nucleation phase but the focus of the paper was on film growth.¹⁶⁷ To our knowledge this is the only report on ALD of Os so far.

2.5.2.6 Iridium

Iridium, like other noble metals, is a potential electrode material in DRAMs and in FRAMs.¹⁶⁸ Since it has good bond-breaking abilities, Ir can also be used as catalyst material.¹⁶⁹ For example, Yinghuai *et al.* used dispersed Ir NPs for the catalytic borylation of alkanes and arenes to form boric acids, which have applications in pharmaceutical chemistry and organic synthesis.¹⁷⁰

Table 2.4: Overview of literature reports of Iridium NPs prepared by ALD.

Precursor	ALD process Co-reactant	Substrates	Objectives and remarks	References
Ir(EtCp)(COD)	O ₂	Si	Film growth, barrier layer	168
Ir(acac) ₃	O ₃ /H ₂	Al ₂ O ₃ , SiO ₂ , glass	Film growth	171
Ir(acac) ₃	O ₂	Al ₂ O ₃ and TiO ₂ covered cellulose	Photocatalyst of methylene blue	172
Ir(acac) ₃	Air	Zeolite	Catalyst in decalin ring opening	173
(MeCp)Ir(CHD)	O ₂	Al ₂ O ₃	Film growth	174
Ir(acac) ₃	Air calcination	Al ₂ O ₃ , SiO ₂	Toluene hydrogenation catalyst	169
Ir(acac) ₃ , Ir(thd)(COD)	Air calcination	Al ₂ O ₃ , SiO ₂ , zeolite	Catalyst preparation	175

When “film growth” is mentioned in the “objectives and remarks” column, NPs resulting from island growth have been observed but the focus of the work was on the film growth and the material properties associated.

As can be seen in the table, Iridium catalysts have been synthesized by ALD and tested in different reactions. An interesting example is described by Vuori *et al.* Zeolite, a typical support for metal catalysts, has been used as a substrate for the deposition of Ir NPs by ALD. A reference catalyst was prepared by wet impregnation on the same support and the catalysts were compared in

the decalin ring opening reaction. ALD Ir catalysts have been found to be clearly more active and selective than wet impregnated ones.¹⁷³

2.5.2.7 Platinum

Platinum is the most widely used catalyst, because its high catalytic activity for hydrocarbon oxidation, which is attributed to their activation of O-O, C-H and O-H bonds.^{7,12,143} Pt combusts more efficiently straight-chain hydrocarbons than Pd, and can be used at very low loadings (approximately 0.02-0.5 wt.%) in catalytic combustion applications.⁷ Pt NPs are often used as model catalysts and have been widely studied for many catalytic applications including hydrogenation reactions, carbon-carbon bond formation, and oxidation and reduction reactions in fuel cells.^{24,61,62,68,144}

Table 2.5: Overview of literature reports of Platinum NPs prepared by ALD.

Precursor	ALD process Co-reactant	Substrates	Objectives and remarks	References
MeCpPtMe ₃	H ₂	Al ₂ O ₃ , TiO ₂ , SrTiO ₃	Water gas shift reaction catalysis	176
	O ₂	Ta ₂ O ₅ and TiO ₂ nanotubes	Conformality of ALD	177
	O ₂	C aerogels	CO-oxidation catalysis	178
	O ₂	C cloth and CNTs	Application in fuel cell	179
	O ₂	SrTiO ₃ nanocubes	Control of NPs growth	180
	O ₂	SrTiO ₃	Nucleation study	181
	O ₂	Silica gel	CO-oxidation catalysis	182
	O ₂	Ag, Pd, Ru, Au	Application in fuel cell	183

	O ₂	SiO ₂	Charge storage memory	184
	O ₂	TiO ₂ powder	Photocatalysts	185
	O ₂	SnO ₂ nanowires	Gas and photon sensing	186
	Air calcination	SiO ₂	Cinnamaldehyde hydrogenation catalysis	187
	O ₂	Nanoporous Al ₂ O ₃ template	Nucleation study	188
	O ₂ plasma	Al ₂ O ₃	Nucleation study and enhancement	189
	O ₂	SrTiO ₃	Nucleation study and control	190
MeCpPtMe ₃	O ₂	Al ₂ O ₃ , ZrO ₂ , TiO ₂	Film growth	157
	O ₂	TiO ₂ nanotubes	Film growth in nanostructures	191
	O ₂	SiO ₂	Nucleation control using SAMs	192
	O ₂	TiO ₂	Catalysts model for DFT calculations	193
	O ₂	STO nanocuboids	Propane oxidation catalysis	194
	O ₂	CNTs	Application in micro fuel cells	195
	O ₃	TiO ₂ NPs	Upscaling	196
	O ₂	Al ₂ O ₃	Non-volatile memory applications	117

	O ₂	Al ₂ O ₃	Influence of oxygen exposure	197
	air	Si nanowires	Solar hydrogen generation	198
	air	TiSi ₂ nanonets	Oxygen reduction catalyst	35
	air	TiO ₂ nanowires	Photocathode catalyst	199
	O ₂	Multiwalled CNTs	hydrogenation of xylose to xylitol	200
MeCpPtMe ₃	O ₂	graphene	Methanol oxidation catalyst	201
	O ₂	Al ₂ O ₃	Application in nonvolatile memory	117
	O ₂	ZnO nanorods	Methanol oxidation catalyst	202
	O ₂	Yttria-Stabilized Zirconia	Nucleation study	203
	O ₂	ZnO	O ₂ and CO sensing	204

When “film growth” is mentioned in the “objectives and remarks” column, NPs resulting from island growth have been observed but the focus of the work was on the film growth and the material properties associated.

As can be seen in the table, Platinum prepared by ALD has been the subject of intense research. The ability of ALD to allow deposition on 3D substrates is often exploited for catalytic purposes. Setthapun *et al.* used ALD to deposit Pt NPs on high surface area Al₂O₃, TiO₂ and STO supports, and they showed that these catalysts produced by ALD had identical water gas shift reaction rates and reaction kinetics to those reported in literature.¹⁷⁶ Liu *et al.* deposited Pt NPs on carbon cloths and CNTs for application in proton-exchange membrane fuel cells, and they demonstrated that Pt nanocatalysts

supported on CNTs have a higher utilization efficiency than commercial electrodes.¹⁷⁹ The potential of Pt ALD for catalysts synthesis has also recently been proven by Goulas *et al.*, who deposited Pt nanoclusters with a narrow size distribution on TiO₂ NPs, in a fluidized bed reactor at atmospheric pressure.¹⁹⁶ The aim was to demonstrate the possibility to make an efficient use of the expensive Pt precursor and to show the viability of upscaling of the technique.

2.5.2.8 Gold

Gold has also become the focus of interest as a catalyst, since gold NPs on oxides can be used as effective catalysts for CO oxidation at low temperatures.²⁰⁵ To our knowledge, Au ALD is still in its infancy. However, some preliminary work on plasma-enhanced ALD of Gold has been reported by S. T. Barry *et al.*²⁰⁶

2.5.2.9 Bimetallic nanoparticles synthesis by ALD

The synthesis of bimetallic NPs can be achieved by alternating two different metal ALD processes. The research on the synthesis of bimetallic NPs by ALD is only in its early stages, but the work carried out shows promising results.

Table 2.6: Overview of literature reports of bimetallic NPs prepared by ALD.

Precursor	ALD process Co-reactant	Substrates	Objectives and remarks	References
Cu(thd) ₂ and Pd(thd) ₂	Air	SiO ₂ , Al ₂ O ₃	Alloyed Cu-Pd NPs synthesis	207
Ru(DER) and MeCpPtMe ₃	O ₂	Al ₂ O ₃ NPs	Alloyed Ru-Pt NPs for methanol decomposition*	208
Pt(acac) ₂ and Co(acac) ₃	-	Carbon black	Methanol oxidation and oxygen reduction	209
MeCpPtMe ₃ and Ru(EtCp) ₂	O ₂	CNTs	CO oxidation and methanol oxidation	210
MeCpPtMe ₃ and Ru(EtCp) ₂	O ₂	CNTs	CO oxidation and methanol oxidation	211

MeCpPtMe ₃	O ₂	Si nanowires	Core/shell Pt/Ag NPs synthesis for SERS application. Only cores were prepared by ALD	212
MeCpPtMe ₃	O ₂	WC particles	Core/shell WC/Pt NPs synthesis for hydrogen conversion catalysis. Only shells were prepared by ALD	213
Pd(hfac) ₂ and MeCpPtMe ₃	H ₂ plasma and O ₂	Al ₂ O ₃	Synthesis of Pd/Pt and Pt/Pd Core/shell NPs entirely by ALD	49
Pd(hfac) ₂ and MeCpPtMe ₃	Formalin and O ₂	Al ₂ O ₃ and TiO ₂ covered silica particles	Synthesis of Pt/Pd Core/shell NPs for propane dehydrogenation	50
Pd(hfac) ₂ , Ru(EtCp) ₂ and MeCpPtMe ₃	Formalin, H ₂ , O ₃ , O ₂	Al ₂ O ₃ , ZrO ₂ , TiO ₂	Synthesis of Core/shell NPs with combinations of the metals Pd, Pt and Ru entirely by ALD	214

By applying Ru(DER)/O₂ cycles for Ru and the Pt(MeCp)Me₃/O₂ cycles for Pt, Christensen *et al.* deposited Ru-Pt nanocatalysts on spherical alumina supports. By adjusting the ratio between the two metal ALD processes, the precise control of Ru/Pt ratio in the deposits could be achieved (see figure 2.12).

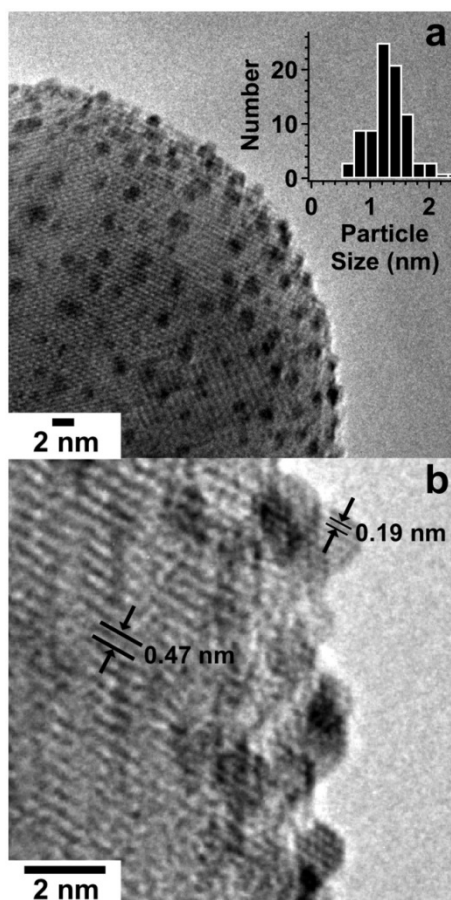


Figure 2.12. TEM images of ALD Ru-Pt NPs on Al_2O_3 . (a) ALD metal nanoparticles decorate the alumina sphere. The histogram gives the nanoparticle size distribution measured from TEM where the mean particle diameter is 1.2 nm with a distribution width of 0.3 nm. (b) High-resolution TEM image showing lattice fringes for the Al_2O_3 and the Ru-Pt nanoparticles. (taken from Reference²⁰⁸).

The synthesis of supported bimetallic core/shell nanoparticles entirely by ALD is also feasible. Two properties of ALD of noble metals, namely the Volmer-Weber growth and surface-selectivity, have been exploited to decouple primary island growth from subsequent selective shell growth. This concept has been applied to synthesize highly dispersed core/shell NPs with all the combinations of the metals Pd, Pt and Ru (as shown in Figure 2.13, see chapter 5 and 6 of this thesis for more details).^{49,214}

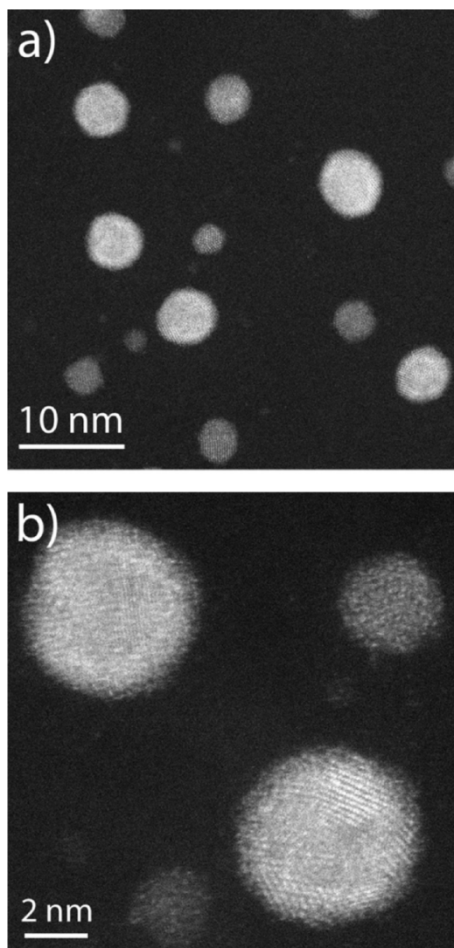


Figure 2.13. High magnification HAADF-STEM images of Pd/Pt core/shell NPs synthesized by ALD. In (a), the core/shell structure is visible on most of the particles. Contrast differences result from the atomic number (Z) difference between Pd and Pt. In (b), the HAADF-STEM high resolution image displays lattice fringes of the Pt shells. The substrates used were 3 nm Al_2O_3 ALD covered Si_3N_4 TEM windows (taken from Reference⁴⁹).

2.5.3. Other benefits of ALD for catalyst preparation:

Apart from the direct preparation of metallic NPs, there are additional benefits of ALD that can be used for the preparation of catalyst. As mentioned in section 2.5.1, ALD yields excellent uniformity, high conformality, and precise growth control. The control of the NPs properties, in terms of size, spatial density or

composition, as well as the ability to deposit them on various supports are key elements for the preparation of catalyst materials and can be achieved by ALD.

The size of noble metal NPs can be more or less controlled by varying the deposition parameters (such as the number of ALD cycles applied), and process modifications enable a better control of the NPs spatial density. For example, Lee *et al.* used self-assembled monolayers pre-adsorbed on a substrate as a template to control Pt ALD nucleation.¹⁹² A two-step ALD process, by varying the pulsing time and carrier flow, was proposed by Lee *et al.* to modulate both the size and the density of Ru NPs.¹²⁸ By including TMA/water cycles in the first cycles of a Pd ALD process, Lu and Stair presented an innovative way to synthesize ultrafine Pd NPs with a high dispersion.¹⁴⁸ As seen in Section 2.5.2.9, the composition and structure of metallic NPs can also be controlled by ALD.

Furthermore, ALD process parameters can be modified in order to allow for the selective growth on particular materials. For example, selective ALD growth of Pt from MeCpPtMe₃ can be obtained when using a low O₂ partial pressure during the O₂ pulse. This has already been used for nanopatterning applications^{215,216} and for synthesis of core/shell NPs.⁴⁹

Because the properties of the NPs are key elements for their catalytic activity, their stability and lifetime can be highly important. After the deposition of the metallic NPs, an ALD (ultra) thin layer of alumina can be deposited as a protective layer in order to inhibit sintering of the NPs. It has been shown that up to a certain over-coat thickness, this protective layer preserved the catalytic activity while preventing NPs sintering up to 500°C.^{59,154,155}

Another important property of catalysts is their selectivity towards certain molecules. The reactant selectivity of a catalyst can be enhanced by synthesizing a defined pore structure on a mesostructured oxide. Recently, a new ALD route has been found for the synthesis of highly selective catalyst system based on nanostructured oxide supports. This new technique has been used to create layers of ~0.5 nm alumina with 'nanocavities' (<2 nm in diameter) on a TiO₂ photocatalyst, as illustrated in Figure 2.14.

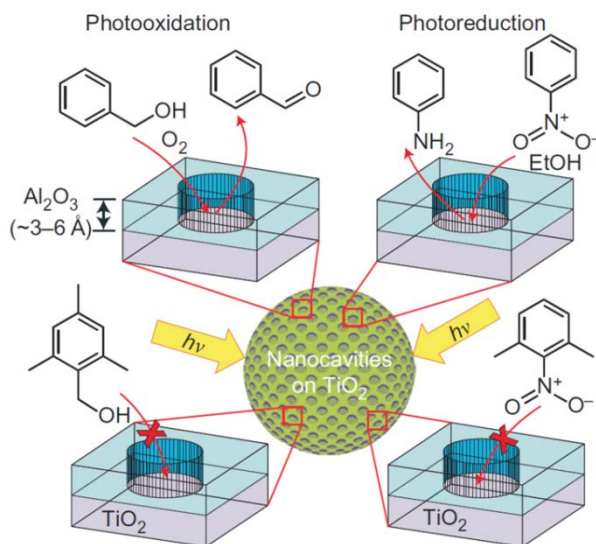


Figure 2.14. Selective photocatalytic oxidation and reduction of mixtures are carried out over templated nanocavities (taken from Reference²¹⁷).

The additional layers resulted in selectivity (up to 9:1) towards less hindered reactants in otherwise unselective, competitive photocatalytic oxidations and transfer hydrogenations.²¹⁷ These new inventive routes, recently developed for the improvement of catalytic systems, demonstrate how the field of catalysis can benefit from nanoengineering by ALD.

In addition, the key merit of ALD to enable deposition of films and NPs on very high aspect ratio substrates is particularly relevant for the field of catalyst synthesis. ALD can in fact be used to prepare a chosen support material, and to deposit NPs on challenging catalyst supports such as nanowires²¹⁸ or nano/micro spheres.²⁰⁸

Figure 2.15 aims to summarize the possibilities offered by ALD for the synthesis of NPs, considering the control of the NPs properties as well as the ability to deposit them on various supports. The ability to deposit NPs with different properties, such as alloyed or core/shell structured for example is shown. The possibility to prepare these NPs directly on challenging supports such as graphene or nanowires is also depicted.

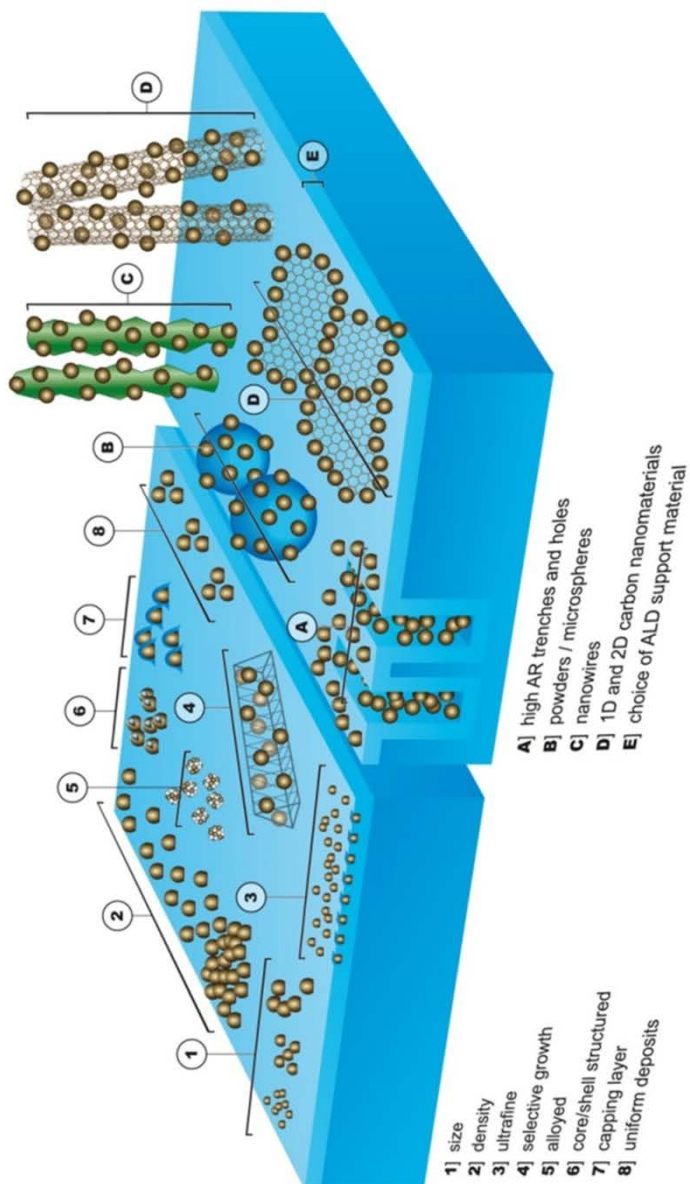


Figure 2.15. Schematic representation of the various possibilities that ALD offers for the synthesis of NPs. The left part shows the ability to precisely control of the NPs properties and the right part the ability to deposit them on various support materials and structures.

2.5.4 Outlook: ALD as a realistic new route for nanocatalysts synthesis?

ALD, a technique allowing for the deposition of high quality materials, with high uniformity, precise growth control, and excellent conformality, is currently used for the most challenging thin-film deposition applications. For example, in the semiconductor industry, this technique is applied for the preparation of the gate oxide in sub 45 nm processors and for the preparation of the dielectric layer in trench capacitors in DRAM manufacturing. The semiconductor industry is currently the main driver for ALD.^{219,220}

In the catalysis industry, the synthesis of heterogeneous catalytic systems, and noble metal NPs in general, is carried out using the more “conventional” routes described previously (in Section 2.4.2). These techniques, being mature and relatively cheap, have however their limitations. The preparation of NPs suspension by wet chemistry, which allows for nanostructured NPs with precise monodispersity, has two main drawbacks: the need of a post treatment to eliminate the potential chemical contaminants, and the challenging collection of the NPs after synthesis without aggregation of the NPs. The chemical routes allowing for the preparation of supported NPs such as impregnation, deposition/precipitation or ion exchange share the same first drawback, which is the need to eliminate the potential chemical contaminants. This removal of contaminants can be challenging, especially if the preparation is taking place in high aspect ratio substrates. The sol-gel technique commonly used to simultaneously deposit the oxide and the metal NPs is not very efficient, because some noble metal included deeply in the oxide cannot interact with the surface reactants such that some scarce metal is wasted. The gas phase techniques allowing for a direct synthesis of supported NPs have the advantage of large throughput, but the NPs size and dispersity control is limited.

As discussed earlier, the possibilities offered by the nanoengineering by ALD could provide great advantages to the catalysis industry. As described previously, ALD can be used to synthesize monometallic, alloyed or even core/shell structured NPs. These NPs can be deposited on various and challenging substrates. ALD has also capabilities to stabilize the NPs to make them sintering resistant, or even to modify the substrate itself to tune the catalyst selectivity. These few examples show the benefits of ALD for catalysis research, and it is likely that many more ALD processes will be developed in the future to continue improving catalytic systems. Obviously, ALD can and is also used as a

route to create model catalysts for fundamental studies, as shown in different examples in the tables presented in Section 2.5.2.

However, ALD also presents serious limitations and issues before it can be applied to the synthesis of industrial heterogeneous catalytic systems. The costs associated with this vacuum based high technology technique seem to be the first limitation. The capital and running costs are extensive, especially also considering the high costs of the noble metal ALD precursors. The second drawback is the design of the ALD reactors, which is typically adapted for research purposes but not for the high throughputs required in industry. One other issue concerning the synthesis of metallic NPs by ALD is the control of the temperature and the conditioning of the reactor walls. In fact, the ALD nucleation is highly dependent on the temperature and on the conditioning, and the size of the NPs can vary if a temperature gradient exists over the (3D) substrate. Finally, the last drawback is that ALD is not a proven technology yet in the field of catalysts synthesis, and therefore no industrial experience exists, as compared with the more conventional synthesis methods.

These limitations can partially be solved by the reactor designs. A proper reactor design could enable for a good temperature control, which would allow for the ALD deposition on multiple and larger substrates. Novel ALD reactor designs are being developed in order to increase the deposition throughput and to extend the ALD possibilities. For example, rotary reactors have been developed for the conformal ALD on particles and powders.²²¹ Another interesting and currently used reactor design is the so-called fluidized bed reactor, that enables the production of conformal and uniform nanocoatings or metal NPs on the surface of dry individual particles in the reactor.^{153,222–224} Figure 2.16 illustrates the rotary and fluidized bed reactor designs. These reactors offer the possibility to directly synthesize catalytic systems that consist of ALD-oxide coated nano or micro-spheres, with highly dispersed ALD-metal NPs covering them.

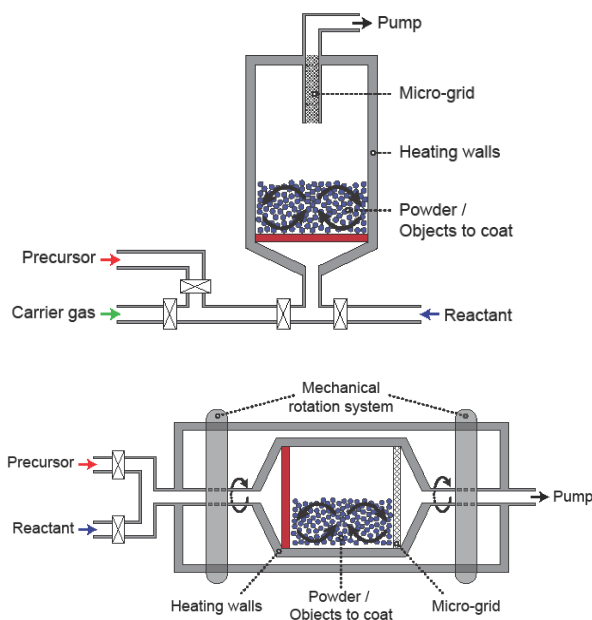


Figure 2.16. Schematic diagram of the ALD fluidized bed reactor (top) and a rotary reactor (bottom).

These fluidized bed ALD reactors have been developed in order to enable ALD to be carried out on microsphere substrates and to make better use of expensive precursors. Goulas *et al.* recently used an ALD fluidized bed reactor at atmospheric pressure to deposit Pt NPs, and they were able to utilize the Pt precursor with 95% efficiency.¹⁹⁶ This demonstrates the potential scalability of ALD for nanocatalysts synthesis. We expect the extensive capital and running costs of ALD systems to be considerably reduced in case of an expanding industrial use.

Due to these “economy of scale” reasons, the first applications would probably be “niche-applications” with “high end” value. The NPs prepared by ALD could be used for heterogeneous catalysis (molecules conversion, sensing,..) and integrated in micro/nano devices such as micro-fuel cells^{179,183,195,225} or microreactors^{94,226–228} in general.

Micro-fuel cells are a particular type of microreactors, attracting a lot of interest due to their potential in powering small autonomous devices.²²⁹ Micro fuel cells require the use of catalytically efficient noble metal NPs for the fuel (e.g. methanol) conversion. ALD has been explored by different research groups

as a way to deposit noble metal nanocatalysts on challenging substrates (e.g. carbon nanotubes) for this purpose.^{178,179,183,195,210,211,225}

Microreactors are particular type of devices, realized as miniaturized continuous flow systems (see Figure 2.17) with typical channel widths of 10 to 500 microns. The advantages of reactor downscaling are to carry out chemical reactions in unusual process regimes or under isothermal conditions, with an enhanced process control and better heat management. Microreactors are typically built up from several hundreds of individual reactor plates or channels on which catalytic coating is applied, and their performance highly depends on the uniformity of this catalytic coating.^{227,228,230,231}

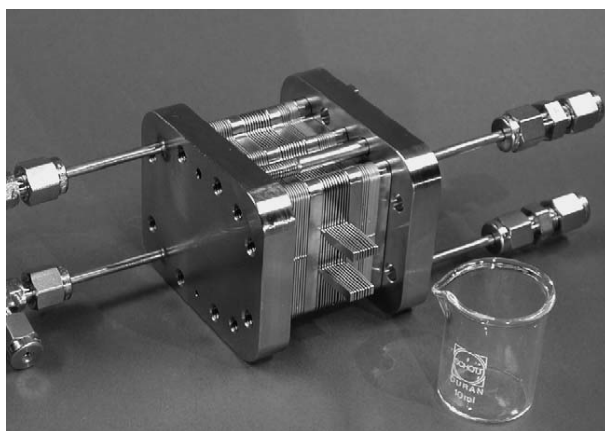


Figure 2.17. Microstructured integrated prototype of reactor used for selective oxidation and heat exchange purposes (Taken from Reference²³²).

Usually, the catalytic system is a nano-porous catalyst. A common commercial catalyst, such as a mixture of alumina/metal NPs in a sol-gel solution phase, is often deposited in the channels by washcoating followed by calcination. The average thickness of washcoats is a few dozens of microns, and these structures present a very high nano-porosity (pores size around 10-30 nm) with metal NPs of 1-10 nm.²³² The catalyst can also be deposited by a two-step process, washcoating and calcination for the oxide such as Al_2O_3 and subsequent wet impregnation for the metal (Cr, Pt, Rh...),^{228,232,233}

The potential of ALD could be to deposit the metal NPs on the nanoporous alumina washcoat, since the volatility of the precursors would allow for this penetration into the microreactor microchannels and washcoat nanopores. Another opportunity for ALD would be to fill the microstructured

channels of reactors with the microspheres supported ALD catalysts, offering a large catalyst surface area.

Up to now, ALD is still in its infancy concerning its application in microreactor technology. A molybdenum microreactor has been used in the frame of zeolite process optimization. In this work, ALD of Al_2O_3 and TiO_2 has been successfully used to coat the molybdenum plates in order to protect them from oxidation at reaction conditions.²³¹ Another study, aiming at the dehydrogenation of isobutene in a microreactor, made use of ALD to add catalytically active chromia on the alumina support, using chromia acetylacetonate precursor. In this study, a chromia/alumina powder catalyst was also prepared by ALD.²²⁶ The study demonstrated the catalyst good molecular selectivity, even at low conversion, and ALD was proven to be a reliable method for adding catalyst material in microreactor channels.²²⁶

To summarize, with the advancement of ALD reactor design, there might be real and viable possibilities for ALD prepared metal NPs to be applied in catalysis. With the continuous downscaling of electronics and portable devices in general, we believe the downscaling of the integrated powering or sensing devices could greatly benefit from ALD prepared metal NPs, in a similar way as the downscaling of transistor technology benefited from metal oxide ALD in the very recent past.

List of abbreviations and acronyms

acac = acetylacetonate
ALD = Atomic Layer Deposition
amd = acetamidinato
CHD = cyclohexadiene
CNT = carbon nanotube
COD = 1,5-cyclooctadiene
Cp = cyclopentadienyl
CVD = chemical vapour deposition
DER=2,4-(dimethylpentadienyl)(ethylcyclopentadienyl)Ru
DFT = Density functional theory
DRAM = dynamic random access memory
Et = Ethyl
fcc = face-centered cubic
fod = 2,2-dimethyl-6,6,7, 7,8,8,8-heptafluorooctade-3,5-dionato
FRAM = ferroelectric random access memory
HAADF = High angle annular dark field
hfac = hexafluoroacetylacetonate
LECBD = low energy cluster beam deposition
MBE = molecular beam epitaxy
Me = methyl
MFP = Mean free path
MOSFET = metal-oxide-semiconductor field effect transistor
NP = Nanoparticle
O₂C^tBu = 2,2-dimethylpropionato
PEt₃= triethylphosphine
PLD = pulsed laser deposition
PS-*b*-P2VP = polystyrene-block-poly(2-vinylpyridine)
PVD = physical vapour deposition
SAM = Self-assembled monolayers
SERS = Surface enhanced Raman spectroscopy
(S)TEM = (Scanning) Transmission Electron Microscopy
TMA = Tri methyl aluminum
TOF = turnover frequency

References

- (1) Osaka, T.; Iida, H.; Tominaka, S.; Hachisu, T. *Isr. J. Chem.* **2008**, *48*, 333–347.
- (2) Tartaj, P.; Morales, P.; Veintemillas-verdaguer, S.; Gonz, T. *J. Phys. D. Appl. Phys.* **2003**, *182*, 182–197.
- (3) Scholl, J. A.; Koh, A. L.; Dionne, J. A. *Nature* **2012**, *483*, 421–7.
- (4) Pradeep, T. *Thin Solid Films* **2009**, *517*, 6441–6478.
- (5) Thomas, J. M.; Thomas, W. J. *Principles and practice of heterogeneous catalysis*; VCH: Weinheim, 1997; p. 669.
- (6) Bowker, M. *The Basis and Applications of Heterogeneous Catalysis*; Oxford University Press Inc.: New York, U.S.A., 1998; p. 96.
- (7) Prasad, R.; Kennedy, L. A.; Ruckenstein, E. *Catal. Rev. - Sci. Eng.* **1984**, *26*.
- (8) Richardson, J. T. *Principles of Catalyst Development*; Plenum: New York, U.S.A., 1989; p. 288.
- (9) Bauer, J. E.; Ocelli, M. L.; Wiuiams, P. M.; Mccaslin, P. C. *Mar. Chem.* **1993**, *41*, 75–89.
- (10) Heiz, U.; Bullock, E. L. *J. Mater. Chem.* **2004**, *14*, 564.
- (11) Stakheev, A. Y.; Mashkovskii, I. S.; Baeva, G. N.; Telegina, N. S. *Russ. J. Gen. Chem.* **2010**, *80*, 618–629.
- (12) Bond, G. C. *Catalysis by Metals*; Academic press: New York, U.S.A., 1962; p. 519 pp.
- (13) Encyclopaedia Britannica Online **2012**.
- (14) Freyschlag, C. G.; Madix, R. J. *Mater. Today* **2011**, *14*, 134–142.
- (15) Hodar, F. J. M. *Heterogeneous catalysis (I)*; Camerino, Italy, 2009.
- (16) Twigg, M. V. *Catalyst Handbook*; 2nd ed.; Manson: London, 1996; p. 608 pp.
- (17) Spencer, M. S.; Twigg, M. V. *Annu. Rev. Mater. Res.* **2005**, *35*, 427–464.

- (18) Shao, M.; Peles, A.; Shoemaker, K. *Nano Lett.* **2011**, *11*, 3714–3719.
- (19) Li, Y.; Somorjai, G. A. *Nano Lett.* **2010**, *10*, 2289–95.
- (20) Rioux, R. M.; Song, H.; Grass, M.; Habas, S.; Niesz, K.; Hoefelmeyer, J. D.; Yang, P.; Somorjai, G. A. *Top. Catal.* **2006**, *39*, 167–174.
- (21) Grass, M. E.; Joo, S. H.; Zhang, Y.; Somorjai, G. A. *J. Phys. Chem. C* **2009**, *113*, 8616–8623.
- (22) Piccolo, L.; Valcarcel, A.; Bausach, M.; Thomazeau, C.; Uzio, D.; Berhault, G. *Phys. Chem. Chem. Phys.* **2008**, *10*, 5504–6.
- (23) Bell, A. T. *Science* **2003**, *299*, 1688–91.
- (24) Yudanov, I. V.; Genest, A.; Schauer mann, S.; Freund, H.-J.; Rösch, N. *Nano Lett.* **2012**, *12*, 2134–9.
- (25) Serpell, C. J.; Cookson, J.; Ozkaya, D.; Beer, P. D. *Nat. Chem.* **2011**, *3*, 478–83.
- (26) Cuenya, B. R. *Thin Solid Films* **2010**, *518*, 3127–3150.
- (27) Astruc, D. *Nanoparticles and Catalysis*; Wiley-VCH Verlag GmbH: Weinheim, Germany, 2008.
- (28) Schauer mann, S.; Nilius, N.; Shaikhutdinov, S.; Freund, H.-J. *Acc. Chem. Res.* **2013**, *46*, 1673–1681.
- (29) Chen, J.; Zhang, Q.; Wang, Y.; Wan, H. *Adv. Synth. Catal.* **2008**, *350*, 453–464.
- (30) Nohair, B.; Especel, C.; Lafaye, G.; Marécot, P.; Hoang, L. C.; Barbier, J. J. *Mol. Catal. A Chem.* **2005**, *229*, 117–126.
- (31) Vajda, S.; Pellin, M. J.; Greeley, J. P.; Marshall, C. L.; Curtiss, L. A.; Ballentine, G. A.; Elam, J. W.; Catillon-Mucherie, S.; Redfern, P. C.; Mehmood, F.; Zapol, P. *Nat. Mater.* **2009**, *8*, 213–6.
- (32) Bukhtiyarov, V. I.; Moroz, B. L.; Bekk, N. E.; Prosvirin, I. P. *Catal. Ind.* **2009**, *1*, 17–28.

- (33) Park, J.; Joo, J.; Kwon, S. G.; Jang, Y.; Hyeon, T. *Angew. Chem. Int. Ed. Engl.* **2007**, *46*, 4630–60.
- (34) Cheong, S.; Watt, J. D.; Tilley, R. D. *Nanoscale* **2010**, *2*, 2045–53.
- (35) Xie, J.; Yang, X.; Han, B.; Shao-Horn, Y.; Wang, D. *ACS Nano* **2013**, *7*, 6337–6345.
- (36) Yacamán, M. J.; Ascencio, J. a.; Liu, H. B.; Gardea-Torresdey, J. J. *Vac. Sci. Technol. B Microelectron. Nanom. Struct.* **2001**, *19*, 1091.
- (37) Guisbiers, G.; Abudukelimu, G.; Hourlier, D. *Nanoscale Res. Lett.* **2011**, *6*, 396.
- (38) Wang, D.; Li, Y. *Adv. Mater.* **2011**, *23*, 1044–60.
- (39) Maroun, F.; Ozanam, F.; Magnussen, O. M.; Behm, R. J. *Science* **2001**, *293*, 1811–4.
- (40) Lin, W. F.; Zei, M. S.; Eiswirth, M.; Ertl, G.; Iwasita, T.; Vielstich, W. *J. Phys. Chem. B* **1999**, *103*, 6968–6977.
- (41) Mavrikakis, M.; Hammer, B.; Nørskov, J. *Phys. Rev. Lett.* **1998**, *81*, 2819–2822.
- (42) Oca, M. G. M. De; Plana, D.; Lazaro, M. J.; Fermin, D. J. *J. Phys. Chem. C* **2012**, *116*, 692–699.
- (43) Teng, X.; Black, D.; Watkins, N. J.; Gao, Y.; Yang, H. *Nano Lett.* **2003**, *3*, 261–264.
- (44) Zhong, C. J.; Maye, M. M. *Adv. Mater.* **2001**, *13*, 1507–1511.
- (45) Sasaki, K.; Wang, J. X.; Naohara, H.; Marinkovic, N.; More, K.; Inada, H.; Adzic, R. R. *Electrochim. Acta* **2010**, *55*, 2645–2652.
- (46) Strasser, P.; Koh, S.; Anniyev, T.; Greeley, J.; More, K.; Yu, C.; Liu, Z.; Kaya, S.; Nordlund, D.; Ogasawara, H.; Toney, M. F.; Nilsson, A. *Nat. Chem.* **2010**, *2*, 454–60.
- (47) Yang, H. *Angew. Chem. Int. Ed. Engl.* **2011**, *50*, 2674–6.
- (48) Tedsree, K.; Li, T.; Jones, S.; Chan, C. W. A.; Yu, K. M. K.; Bagot, P. A. J.; Marquis, E. A.; Smith, G. D. W.; Tsang, S. C. E. *Nat. Nanotechnol.* **2011**, *6*, 302–7.
- (49) Weber, M. J.; Mackus, A. J. M.; Verheijen, M. A.; van der Marel, C.; Kessels, W. M. *M. Chem. Mater.* **2012**, *24*, 2973–2977.

- (50) Lei, Y.; Liu, B.; Lu, J.; Lobo-Lapidus, R. J.; Wu, T.; Feng, H.; Xia, X.; Mane, A. U.; Libera, J. A.; Greeley, J. P.; Miller, J. T.; Elam, J. W. *Chem. Mater.* **2012**, *24*, 3525–3533.
- (51) Peterson, E. E.; Bell, A. T. *Catalyst deactivation*; Marcel Dekker Inc.: New York, USA, 1987.
- (52) Zhdanov, V. P. *Surf. Rev. Lett.* **2008**, *15*, 217–220.
- (53) Datye, A. K.; Xu, Q.; Kharas, K. C.; McCarty, J. M. *Catal. Today* **2006**, *111*, 59–67.
- (54) Stoldt, C. R.; Jenks, C. J.; Thiel, P. A.; Cadilhe, A. M.; Evans, J. W. *J. Chem. Phys.* **1999**, *111*, 5157.
- (55) Budiman, R.; Ruda, H. *Phys. Rev. B* **2002**, *65*, 045315.
- (56) Tao, F.; Grass, M. E.; Zhang, Y.; Butcher, D. R.; Renzas, J. R.; Liu, Z.; Chung, J. Y.; Mun, B. S.; Salmeron, M.; Somorjai, G. A. *Science (80-.)*. **2008**, *322*, 932–934.
- (57) Yu, Y.; Xin, H. L.; Hovden, R.; Wang, D.; Rus, E. D.; Mundy, J. A.; Muller, D. A.; Abruña, H. D. *Nano Lett.* **2012**, *12*, 4417–4423.
- (58) Yeung, C. M. Y.; Yu, K. M. K.; Fu, Q. J.; Thompsett, D.; Petch, M. I.; Tsang, S. C. *J. Am. Chem. Soc.* **2005**, *127*, 18010–1.
- (59) Lu, J.; Fu, B.; Kung, M. C.; Xiao, G.; Elam, J. W.; Kung, H. H.; Stair, P. C. *Science (80-.)*. **2012**, *335*, 1205–8.
- (60) Köhler, K.; Heidenreich, R. G.; Krauter, J. G. E.; Pietsch, J. *Chemistry* **2002**, *8*, 622–31.
- (61) Pryjomska-Ray, I.; Gniewek, A.; Trzeciak, A. M.; Ziółkowski, J. J.; Tylus, W. *Top. Catal.* **2006**, *40*, 173–184.
- (62) Phan, N. T. S.; Van Der Sluys, M.; Jones, C. W. *Adv. Synth. Catal.* **2006**, *348*, 609–679.
- (63) Wagner, M. *Top. Catal.* **2000**, *13*, 319–326.
- (64) Inaba, M.; Ito, H.; Tsuji, H.; Wada, T.; Banno, M.; Yamada, H.; Saito, M.; Tasaka, A. *ECS Trans.* **2010**, *33*, 231–238.

- (65) Oezaslan, M.; Heggen, M.; Strasser, P. *J. Am. Chem. Soc.* **2012**, *134*, 514–24.
- (66) Barcaro, G.; Fortunelli, A.; Polak, M.; Rubinovich, L. *Nano Lett.* **2011**, *11*, 1766–1769.
- (67) Petit, C.; Repain, V. In *Engineering Materials*; Alloyeau, D.; Mottet, C.; Ricolleau, C., Eds.; Engineering Materials; Springer London: London, 2012; pp. 1–23.
- (68) Zhou, B.; Balee, R. A. Y.; Groenendaal, R. *Nanotechnol. Law Bus.* **2005**, *2*, 222–229.
- (69) Schwarz, J. A.; Contescu, C.; Contescu, A. *Chem. Rev.* **1995**, *95*, 477–510.
- (70) Fendler, J. H.; Meldrum, F. C. *Adv. Mater.* **1995**, *7*, 607–632.
- (71) Wegener, S. L.; Marks, T. J.; Stair, P. C. *Acc. Chem. Res.* **2012**, *45*, 206–14.
- (72) Teranishi, T.; Miyake, M. *Chem. Mater.* **1998**, *10*, 594–600.
- (73) Herricks, T.; Chen, J.; Xia, Y. *Nano Lett.* **2004**, *4*, 2367–2371.
- (74) Bönemann, H.; Richards, R. M. *Eur. J. Inorg. Chem.* **2001**, *2001*, 2455–2480.
- (75) Zhang, Q.; Xie, J.; Yu, Y.; Lee, J. Y. *Nanoscale* **2010**, *2*, 1962–75.
- (76) Panigrahi, S.; Kundu, S.; Ghosh, S.; Nath, S.; Pal, T. *J. Nanoparticle Res.* **2004**, *6*, 411–414.
- (77) Van Hying, D. L.; Zukoski, C. F. *Langmuir* **1998**, *14*, 7034–7046.
- (78) Wang, H.; Qiao, X.; Chen, J.; Ding, S. *Colloids Surfaces A Physicochem. Eng. Asp.* **2005**, *256*, 111–115.
- (79) Kéki, S.; Török, J.; Deák, G.; Daróczy, L.; Zsuga, M. *J. Colloid Interface Sci.* **2000**, *229*, 550–553.
- (80) Semagina, N.; Joannet, E.; Parra, S.; Sulman, E.; Renken, A.; Kiwi-Minsker, L. *Appl. Catal. A Gen.* **2005**, *280*, 141–147.
- (81) Pachón, L. D.; Rothenberg, G. *Appl. Organomet. Chem.* **2008**, *22*, 288–299.
- (82) Pileni, M. P. *J. Phys. Chem.* **1993**, *97*, 6961–6973.

- (83) Magno, L. M.; Sigle, W.; van Aken, P. A.; Angelescu, D. G.; Stubenrauch, C. *Chem. Mater.* **2010**, *22*, 6263–6271.
- (84) Ingelstein, H. H.; Beziat, J.-C.; Bergkvist, K.; Palmqvist, A.; Skoglundh, M.; QiuHong, H.; Falk, L. K. L.; Holmberg, K. *Langmuir* **2002**, *18*, 1811–1818.
- (85) Yashima, M.; Falk, L. K.; Palmqvist, A. E.; Holmberg, K. *J Colloid Interface Sci.* **2003**, *15*, 348.
- (86) Varanda, L. C.; Jafelicci, M. *J. Am. Chem. Soc.* **2006**, *128*, 11062–6.
- (87) Brust, M.; Walker, M.; Bethell, D.; Schiffrin, D. J.; Whyman, R. *J. Chem. Soc., Chem. Comm.* **1994**, *1*, 801–802.
- (88) Wikander, K.; Petit, C.; Holmberg, K.; Pileni, M.-P. *Langmuir* **2006**, *22*, 4863–8.
- (89) Demortiere, A.; Launois, P.; Goubet, N.; Albouy, P.; Petit, C. *J. Phys. Chem. B* **2008**, *112*, 14583–14592.
- (90) Jiang, H.; Akita, T.; Ishida, T.; Haruta, M.; Xu, Q. *JACS* **2011**, *133*, 1304–1306.
- (91) Chen, T.-Y.; Lin, T.-L.; Luo, T.-J. M.; Choi, Y.; Lee, J.-F. *Chemphyschem* **2010**, *11*, 2383–92.
- (92) Peng, Z.; Yang, H. *Nano Today* **2009**, *4*, 143–164.
- (93) Habas, S. E.; Lee, H.; Radmilovic, V.; Somorjai, G. A.; Yang, P. *Nat. Mater.* **2007**, *6*, 692–7.
- (94) Meille, V. *Appl. Catal. A Gen.* **2006**, *315*, 1–17.
- (95) Wiedwald, U.; Han, L.; Biskupek, J.; Kaiser, U.; Ziemann, P. *Beilstein J. Nanotechnol.* **2010**, *1*, 24–47.
- (96) Marceau, E.; Carrier, X.; Che, M.; Clause, O.; Marcilly, C. *Ion exchange and Impregantion*; Wiley VCH Verlag GmbH: Weinheim, 2008.
- (97) Agrafiotis, C.; Tsetsekou, A.; Stournaras, C. J.; Julbe, A.; Dalmazio, L.; Guizard, C.; Boretto, G.; Debenedetti, M.; Parussa, F. *Appl. Catal. B Environ.* **2001**, *34*, 149–159.
- (98) Siegel, R. W. *Annu. Rev. Mater. Sci.* **1991**, *21*, 559–578.

- (99) Wegner, K.; Walker, B.; Tsantilis, S.; Pratsinis, S. E. *Chem. Eng. Sci.* **2002**, *57*, 1753–1762.
- (100) Penuelas, J.; Andrezza-Vignolle, C.; Andrezza, P.; Ouerghi, A.; Bouet, N. *Surf. Sci.* **2008**, *602*, 545–551.
- (101) Esaki, L. *Molecular Beam epitaxy and Heterostructures*; Series, N. A., Ed.; Eds: L.L. .; Martinus Nijhoff Publishers, The Netherlands, 1985.
- (102) Tournus, F.; Blanc, N.; Tamion, A.; Hillenkamp, M.; Dupuis, V. *Phys. Rev. B* **2010**, *81*, 1–4.
- (103) Weber, A. P.; Seipenbusch, M.; Kasper, G. *J. Phys. Chem. A* **2001**, *105*, 8958–8963.
- (104) Surangalikal, H.; Ouyang, X.; Besser, R. S. *Chem. Eng. J.* **2003**, *93*, 217–224.
- (105) Urban, F. K.; Hosseini-Tehrani, A.; Griffiths, P.; Khabari, A.; Kim, Y.-W.; Petrov, I. *J. Vac. Sci. Technol. B Microelectron. Nanom. Struct.* **2002**, *20*, 995.
- (106) Dolbec, R.; Irissou, E.; Chaker, M.; Guay, D.; Rosei, F.; El Khakani, M. *Phys. Rev. B* **2004**, *70*, 1–4.
- (107) Alloyeau, D.; Ricolleau, C.; Mottet, C.; Oikawa, T.; Langlois, C.; Le Bouar, Y.; Braidy, N.; Loiseau, a *Nat. Mater.* **2009**, *8*, 940–6.
- (108) Adachi, M.; Tsukui, S.; Okuyama, K. *J. Nanoparticle Res.* **2003**, *5*, 31–37.
- (109) Profijt, H. B.; Potts, S. E.; van de Sanden, M. C. M.; Kessels, W. M. M. *J. Vac. Sci. Technol. A Vacuum, Surfaces, Film.* **2011**, *29*, 050801.
- (110) Leskelä, M.; Ritala, M. *Angew. Chem. Int. Ed. Engl.* **2003**, *42*, 5548–54.
- (111) Solanki, R.; Pathangey, B. *Electrochem. Solid-State Lett.* **2000**, *3*, 479–480.
- (112) Klaus, J. W.; Ferro, S. J.; George, S. M. *Thin Solid Films* **2000**, *360*, 145–153.
- (113) George, S. M. *Chem. Rev.* **2010**, *110*, 111–31.
- (114) Elam, J. W.; Zinovev, A.; Han, C. Y.; Wang, H. H.; Welp, U.; Hryn, J. N.; Pellin, M. J. *Thin Solid Films* **2006**, *515*, 1664–1673.

- (115) Knoops, H. C. M.; Mackus, A. J. M.; Donders, M. E.; van de Sanden, M. C. M.; Notten, P. H. L.; Kessels, W. M. M. *Electrochem. Solid-State Lett.* **2009**, *12*, G34.
- (116) Leick, N.; Verkuijlen, R. O. F.; Lamagna, L.; Langereis, E.; Rushworth, S.; Roozeboom, F.; van de Sanden, M. C. M.; Kessels, W. M. M. *J. Vac. Sci. Technol. A Vacuum, Surfaces, Film.* **2011**, *29*, 021016.
- (117) Ding, S.-J.; Chen, H.-B.; Cui, X.-M.; Chen, S.; Sun, Q.-Q.; Zhou, P.; Lu, H.-L.; Zhang, D. W.; Shen, C. *Nanoscale Res. Lett.* **2013**, *8*, 80.
- (118) Aaltonen, B. T.; Alen, P.; Ritala, M.; Leskelä, M. *Chem. Vap. Depos.* **2003**, *9*, 45–49.
- (119) Zahmakiran, M.; Ayvali, T.; Philippot, K. *Langmuir* **2012**, *28*, 4908.
- (120) Heo, J.; Eom, D.; Lee, S. Y.; Won, S.-J.; Park, S.; Hwang, C. S.; Kim, H. J. *Chem. Mater.* **2009**, *21*, 4006–4011.
- (121) Zhang, M.; Chen, W.; Ding, S.-J.; Wang, X.-P.; Zhang, D. W.; Wang, L.-K. *J. Vac. Sci. Technol. A Vacuum, Surfaces, Film.* **2007**, *25*, 775.
- (122) Kim, S. K.; Lee, S. Y.; Lee, S. W.; Hwang, G. W.; Hwang, C. S.; Lee, J. W.; Jeong, J. J. *Electrochem. Soc.* **2007**, *154*, D95.
- (123) Yim, S.-S.; Lee, M.-S.; Kim, K.-S.; Kim, K.-B. *Appl. Phys. Lett.* **2006**, *89*, 093115.
- (124) Eom, T.-K.; Sari, W.; Choi, K.-J.; Shin, W.-C.; Kim, J. H.; Lee, D.-J.; Kim, K.-B.; Sohn, H.; Kim, S.-H. *Electrochem. Solid-State Lett.* **2009**, *12*, D85.
- (125) Biener, J.; Baumann, T. F.; Wang, Y.; Nelson, E. J.; Kucheyev, S. O.; Hamza, A. V.; Kemell, M.; Ritala, M.; Leskelä, M. *Nanotechnology* **2007**, *18*, 055303.
- (126) Lee, D.-J.; Yim, S.-S.; Kim, K.-S.; Kim, S.-H.; Kim, K.-B. *Electrochem. Solid-State Lett.* **2008**, *11*, K61.
- (127) Kwon, S.-H.; Kwon, O.-K.; Kim, J.-H.; Oh, H.-R.; Kim, K.-H.; Kang, S.-W. *J. Electrochem. Soc.* **2008**, *155*, H296.
- (128) Lee, D.-J.; Yim, S.-S.; Kim, K.-S.; Kim, S.-H.; Kim, K.-B. *Nanotechnology* **2011**, *22*, 095305.
- (129) Yim, S.-S.; Lee, D.-J.; Kim, K.-S.; Lee, M.-S.; Kim, S.-H.; Kim, K.-B. *Electrochem. Solid-State Lett.* **2008**, *11*, K89.

- (130) Zhang, M.; Chen, W.; Ding, S.-J.; Liu, Z.-Y.; Huang, Y.; Liao, Z.-W.; Zhang, D. W. *J. Phys. D. Appl. Phys.* **2008**, *41*, 032007.
- (131) Lee, D.-J.; Yim, S.-S.; Kim, K.-S.; Kim, S.-H.; Kim, K.-B. *J. Appl. Phys.* **2010**, *107*, 013707.
- (132) Farmer, D. B.; Gordon, R. G. *J. Appl. Phys.* **2007**, *101*, 124503.
- (133) Di, X.; Methaapanon, R.; Geyer, S. M.; Brennan, S.; Bent, S. F. *Chem. Mater.* **2013**, *25*, 3458–3463.
- (134) Serp, P.; Chateau, L.; Feurer, R.; Kiennemann, A.; Kalck, P. *J. Mol. Catal. A Chem.* **1998**, *136*, 269–278.
- (135) Shelef, M.; McCabe, R. *Catal. Today* **2000**, *62*, 35–50.
- (136) Park, K. J.; Parsons, G. N. *Appl. Phys. Lett.* **2006**, *89*, 043111.
- (137) Aaltonen, T.; Ritala, M.; Leskelä, M. *Electrochem. Solid-State Lett.* **2005**, *8*, C99.
- (138) Chiu, S.-Y.; Wang, Y.-L.; Chang, S.-C.; Feng, M.-S. *Thin Solid Films* **2005**, *478*, 293–298.
- (139) Cabot, A.; Arbiol, J.; Cornet, A.; Morante, J. R.; Chen, F.; Liu, M. *Thin Solid Films* **2003**, *436*, 64–69.
- (140) Kumar, P.; Malhotra, L. K. *Mater. Chem. Phys.* **2004**, *88*, 106–109.
- (141) Sun, Z., Shen, B. *Rare. Met. Mat. Eng.* **2004**, *33*, 889.
- (142) Paglieri, S. N.; Way, J. D. *Sep. Purif. Rev.* **2002**, *31*, 1–169.
- (143) Hegedus, L. L.; Gumbleton, J. J. In *Proceedings of the 9th Automotive Materials Conference: Ceramic Engineering and Science Proceedings*; John Wiley & Sons, Inc., 2008; pp. 403–428.
- (144) Arenz, M.; Mayrhofer, K. J. J.; Stamenkovic, V.; Blizanac, B. B.; Tomoyuki, T.; Ross, P. N.; Markovic, N. M. *J. Am. Chem. Soc.* **2005**, *127*, 6819–29.
- (145) Kim, Y.-S.; Shin, J.; Cho, J.-H.; Ten Eyck, G. A.; Liu, D.-L.; Pimanpang, S.; Lu, T.-M.; Senkevich, J. J.; Shin, H.-S. *Surf. Coatings Technol.* **2006**, *200*, 5760–5766.

- (146) Ten Eyck, G. A.; Senkevich, J. J.; Tang, F.; Liu, D.; Pimanpang, S.; Karaback, T.; Wang, G.-C.; Lu, T.-M.; Jezewski, C.; Lanford, W. A. *Chem. Vap. Depos.* **2005**, *11*, 60–66.
- (147) Feng, H.; Elam, J. W.; Libera, J. A.; Setthapun, W.; Stair, P. C. *Chem. Mater.* **2010**, *22*, 3133–3142.
- (148) Lu, J.; Stair, P. C. *Angew. Chem. Int. Ed. Engl.* **2010**, *49*, 2547–51.
- (149) Goldstein, D. N.; George, S. M. *Appl. Phys. Lett.* **2009**, *95*, 143106.
- (150) Goldstein, D. N.; George, S. M. *Thin Solid Films* **2011**, *519*, 5339–5347.
- (151) Lu, J.; Stair, P. C. *Langmuir* **2010**, *26*, 16486–95.
- (152) Feng, H.; Libera, J. A.; Stair, P. C.; Miller, J. T.; Elam, J. W. *ACS Catal.* **2011**, *1*, 665–673.
- (153) Liang, X.; Lyon, L. B.; Jiang, Y.-B.; Weimer, A. W. *J. Nanoparticle Res.* **2012**, *14*.
- (154) Lu, J.; Liu, B.; Greeley, J. P.; Feng, Z.; Libera, J. A.; Lei, Y.; Bedzyk, M. J.; Stair, P. C.; Elam, J. W. *Chem. Mater.* **2012**, *24*, 2047–2055.
- (155) Feng, H.; Lu, J.; Stair, P. C.; Elam, J. W. *Catal. Letters* **2011**, *141*, 512–517.
- (156) Rikkinen, E.; Santasalo-Aarnio, A.; Airaksinen, S.; Borghei, M.; Viitanen, V.; Sainio, J.; Kauppinen, E. I.; Kallio, T.; Krause, A.; Outi, I. *J. Phys. Chem. C* **2011**, *115*, 23067–23073.
- (157) Elam, J. W.; Zinovev, A. V.; Pellin, M. J.; Comstock, D. J.; Hersam, M. C. *ECS Trans.* **2007**, *3*, 271–278.
- (158) Lei, Y.; Lu, J.; Luo, X.; Wu, T.; Du, P.; Zhang, X.; Ren, Y.; Wen, J.; Miller, D. J.; Miller, J. T.; Sun, Y.-K.; Elam, J. W.; Amine, K. *Nano Lett.* **2013**, *13*, 4182–9.
- (159) Lei, Y.; Lu, J.; Zhao, H.; Liu, B.; Low, K.-B.; Wu, T.; Libera, J. A.; Greeley, J. P.; Chupas, P. J.; Miller, J. T.; Elam, J. W. *J. Phys. Chem. C* **2013**, *117*, 11141–11148.
- (160) Lu, J.; Elam, J. W.; Stair, P. C. *Acc. Chem. Res.* **2013**, *article AS*.

- (161) Dai, Y.; Lim, B.; Yang, Y.; Cobley, C. M.; Li, W.; Cho, E. C.; Grayson, B.; Fanson, P. T.; Campbell, C. T.; Sun, Y.; Xia, Y. *Angew. Chemie* **2010**, *122*, 8341–8344.
- (162) Prokes, S. M.; Glembocki, O. J.; Cleveland, E.; Caldwell, J. D.; Foos, E.; Niinisto, J.; Ritala, M. *Appl. Phys. Lett.* **2012**, *100*, 053106.
- (163) Kariniemi, M.; Niinisto, J.; Hatanp, T.; Kemell, M.; Sajavaara, T.; Ritala, M. *Chem. Mater.* **2011**, *23*, 2901–2907.
- (164) Chalker, P. R.; Romani, S.; Marshall, P. A.; Rosseinsky, M. J.; Rushworth, S.; Williams, P. A. *Nanotechnology* **2010**, *21*, 405602.
- (165) Niskanen, a.; Hatanpää, T.; Arstila, K.; Leskelä, M.; Ritala, M. *Chem. Vap. Depos.* **2007**, *13*, 408–413.
- (166) In *Gmelin Handbook of Inorganic Chemistry*; Springer-Verlag: New York, 1986; p. 43.
- (167) Hamalainen, J.; Sajavaara, T.; Puukilainen, E.; Ritala, M.; Leskela, M. *Chem. Mater.* **2012**, *24*, 55–60.
- (168) Lim, Y. H.; Yoo, H.; Choi, B. H.; Lee, J. H.; Lee, H.-N.; Lee, H. K. *Phys. Status Solidi* **2011**, *8*, 891–894.
- (169) Silvennoinen, R. J.; Jylhä, O. J. T.; Lindblad, M.; Österholm, H.; Krause, A. O. I. *Catal. Letters* **2007**, *114*, 135–144.
- (170) Yinghuai, Z.; Chenyan, K.; Peng, A. T.; Emi, A.; Monalisa, W.; Kui-Jin Louis, L.; Hosmane, N. S.; Maguire, J. A. *Inorg. Chem.* **2008**, *47*, 5756–61.
- (171) Hämäläinen, J.; Puukilainen, E.; Kemell, M.; Costelle, L.; Ritala, M.; Leskelä, M. *Chem. Mater.* **2009**, *21*, 4868–4872.
- (172) Kemell, M.; Pore, V.; Ritala, M.; Leskelä, M. *Chem. Vap. Depos.* **2006**, *12*, 419–422.
- (173) Vuori, H.; Silvennoinen, R. J.; Lindblad, M.; Österholm, H.; Krause, A. O. I. *Catal. Letters* **2009**, *131*, 7–15.
- (174) Hämäläinen, J.; Hatanpää, T.; Puukilainen, E.; Costelle, L.; Pilvi, T.; Ritala, M.; Leskelä, M. *J. Mater. Chem.* **2010**, *20*, 7669.
- (175) Vuori, H.; Pasanen, A.; Lindblad, M.; Valden, M.; Niemelä, M. V.; Krause, A. O. I. *Appl. Surf. Sci.* **2011**, *257*, 4204–4210.

- (176) Setthapun, W.; Williams, W. D.; Kim, S. M.; Feng, H.; Elam, J. W.; Rabuffetti, F. A.; Poepfelmeier, K. R.; Stair, P. C.; Stach, E. A.; Ribeiro, F. H.; Miller, J. T.; Marshall, C. L. *J. Phys. Chem. C* **2010**, *114*, 9758–9771.
- (177) Kemell, M.; Härkönen, E.; Pore, V.; Ritala, M.; Leskelä, M. *Nanotechnology* **2010**, *21*, 035301.
- (178) King, J. S.; Wittstock, A.; Biener, J.; Kucheyev, S. O.; Wang, Y. M.; Baumann, T. F.; Giri, S. K.; Hamza, A. V.; Baeumer, M.; Bent, S. F. *Nano Lett.* **2008**, *8*, 2405–9.
- (179) Liu, C.; Wang, C.-C.; Kei, C.-C.; Hsueh, Y.-C.; Perng, T.-P. *Small* **2009**, *5*, 1535–8.
- (180) Christensen, S. T.; Elam, J. W.; Rabuffetti, F. A.; Ma, Q.; Weigand, S. J.; Lee, B.; Seifert, S.; Stair, P. C.; Poepfelmeier, K. R.; Hersam, M. C.; Bedzyk, M. J. *Small* **2009**, *5*, 750–7.
- (181) Christensen, S. T.; Elam, J. W.; Lee, B.; Feng, Z.; Bedzyk, M. J.; Hersam, M. C. **2009**, *3*, 516–521.
- (182) Li, J.; Liang, X.; King, D. M.; Jiang, Y.-B.; Weimer, A. W. *Appl. Catal. B Environ.* **2010**, *97*, 220–226.
- (183) Shim, J. H.; Jiang, X.; Bent, S. F.; Prinz, F. B. *J. Electrochem. Soc.* **2010**, *157*, B793.
- (184) Novak, S.; Lee, B.; Yang, X.; Misra, V. *J. Electrochem. Soc.* **2010**, *157*, H589.
- (185) Zhou, Y.; King, D. M.; Liang, X.; Li, J.; Weimer, A. W. *Appl. Catal. B Environ.* **2010**, *101*, 54–60.
- (186) Lin, Y.-H.; Hsueh, Y.-C.; Lee, P.-S.; Wang, C.-C.; Chen, J.-R.; Wu, J.-M.; Perng, T.-P.; Shih, H. C. *J. Electrochem. Soc.* **2010**, *157*, K206.
- (187) Lashdaf, M.; Lahtinen, J.; Lindblad, M.; Venäläinen, T.; Krause, A. O. I. *Appl. Catal. A Gen.* **2004**, *276*, 129–137.
- (188) Shresta, P.; Gu, D.; Tran, N. H.; Tapily, K.; Baumgart, H.; Namkoong, G. *ECS Trans.* **2010**, *33*, 127.
- (189) Baker, L.; Cavanagh, A. S.; Seghete, D.; George, S. M.; Mackus, A. J. M.; Kessels, W. M. M.; Liu, Z. Y.; Wagner, F. T. *J. Appl. Phys.* **2011**, *109*, 084333.

- (190) Christensen, S. T.; Elam, J. W.; Lee, B.; Feng, Z.; Bedzyk, M. J.; Hersam, M. C. *Chem. Mater.* **2009**, *21*, 516–521.
- (191) Gu, D.; Baumgart, H.; Tapily, K.; Shrestha, P.; Namkoong, G.; Ao, X.; Müller, F. *Nano Res.* **2010**, *4*, 164–170.
- (192) Lee, H.; Mullings, M. N.; Jiang, X.; Clemens, B. M.; Bent, S. F. *Chem. Mater.* **2012**, *24*, 4051–4059.
- (193) Zhou, Y.; Muhich, C. L.; Neltner, B. T.; Weimer, A. W.; Musgrave, C. B. *J. Phys. Chem. C* **2012**, *116*, 12114–12123.
- (194) Enterkin, J. A.; Setthapun, W.; Elam, J. W.; Christensen, S. T.; Rabuffetti, F. A.; Marks, L. D.; Stair, P. C.; Poepfelmeier, K. R.; Marshall, C. L. *ACS Catal.* **2011**, *1*, 629–635.
- (195) Hales, J. H.; Kallesøe, C.; Lund-Olesen, T.; Johansson, A.-C.; Fanøe, H. C.; Yu, Y.; Lund, P. B.; Vig, A. L.; Tynelius, O.; Christensen, L. H. *Fuel Cells Bull.* **2012**, *2012*, 12–16.
- (196) Goulas, A.; Ruud van Ommen, J. *J. Mater. Chem. A* **2013**, *1*, 4647.
- (197) Mackus, A. J. M.; Verheijen, M. A.; Leick, N.; Bol, A. A.; Kessels, W. M. M. *Chem. Mater.* **2013**, *25*, 1905–1911.
- (198) Dai, P.; Xie, J.; Mayer, M. T.; Yang, X.; Zhan, J.; Wang, D. *Angew. Chemie* **2013**, *125*, 1–6.
- (199) Dasgupta, N. P.; Liu, C.; Andrews, S.; Prinz, F. B.; Yang, P. *JACS* **2013**.
- (200) Liang, X.; Jiang, C. *J. Nanoparticle Res.* **2013**, *15*, 1890.
- (201) Sun, S.; Zhang, G.; Gauquelin, N.; Chen, N.; Zhou, J.; Yang, S.; Chen, W.; Meng, X.; Geng, D.; Banis, M. N.; Li, R.; Ye, S.; Knights, S.; Botton, G. A.; Sham, T.-K.; Sun, X. *Sci. Rep.* **2013**, *3*, 1775.
- (202) Su, C.; Hsueh, Y.; Kei, C.; Lin, C.; Perng, T. *J. Phys. Chem. C* **2013**, *117*, 11610.
- (203) Xu, R.; Selvaraj, S. K.; Jursich, G.; Feinerman, A.; Takoudis, C. *ECS J. Solid State Sci. Technol.* **2013**, *2*, P452–P456.

- (204) Erkens, I. J. M.; Blauw, M. A.; Verheijen, M. A.; Roozeboom, F.; Kessels, W. M. M. *ECS Trans.* **2013**, *58*, 203–214.
- (205) Haruta, M. *Chem. Rec.* **2003**, *3*, 75–87.
- (206) Barry, S. T.; Coyle, J. P.; Kariniemi, M.; Niinisto, J.; Ritala, M.; Leskela, M. In *12th International Conference on Atomic Layer Deposition (ALD 2012), Dresden, Germany*; 2012.
- (207) Molenbroek, A. M.; Haukka, S.; Clausen, B. S. *J. Phys. Chem. B* **1998**, *102*, 10680–10689.
- (208) Christensen, S. T.; Feng, H.; Libera, J. L.; Guo, N.; Miller, J. T.; Stair, P. C.; Elam, J. W. *Nano Lett.* **2010**, *10*, 3047–51.
- (209) Sairanen, E.; Figueiredo, M. C.; Karinen, R.; Santasalo-Aarnio, A.; Jiang, H.; Sainio, J.; Kallio, T.; Lehtonen, J. *Appl. Catal. B Environ.* **2014**, *148-149*, 11–21.
- (210) Johansson, A.-C.; Larsen, J. V.; Verheijen, M. A.; Haugshøj, K. B.; F. Clausen, H.; Kessels, W. M. M.; H. Christensen, L.; Thomsen, E. V. *J. Catal.* **2014**, *311*, 481–486.
- (211) Johansson, A.-C.; Yang, R. B.; Haugshøj, K. B.; Larsen, J. V.; H. Christensen, L.; Thomsen, E. V. *Int. J. Hydrogen Energy* **2013**, *38*, 11406.
- (212) Sivakov, V. A.; Höflich, K.; Becker, M.; Berger, A.; Stelzner, T.; Elers, K.-E.; Pore, V.; Ritala, M.; Christiansen, S. H. *Chemphyschem* **2010**, *11*, 1995–2000.
- (213) Hsu, I. J.; Kimmel, Y. C.; Jiang, X.; Willis, B. G.; Chen, J. G. *Chem. Commun. (Camb)*. **2012**, *48*, 1063–5.
- (214) Lu, J.; Low, K.-B.; Lei, Y.; Libera, J. a.; Nicholls, A.; Stair, P. C.; Elam, J. W. *Nat. Commun.* **2014**, *5*, 1–9.
- (215) Mackus, A. J. M.; Mulders, J. J. L.; van de Sanden, M. C. M.; Kessels, W. M. M. *J. Appl. Phys.* **2010**, *107*, 116102.
- (216) Mackus, A. J. M.; Dielissen, S. A. F.; Mulders, J. J. L.; Kessels, W. M. M. *Nanoscale* **2012**, *4*, 4477–4480.
- (217) Canlas, C. P.; Lu, J.; Ray, N. A.; Grosso-Giordano, N. A.; Lee, S.; Elam, J. W.; Winans, R. E.; Van Duyne, R. P.; Stair, P. C.; Notestein, J. M. *Nat. Chem.* **2012**, *4*, 1030–6.

- (218) Dasgupta, N. P.; Jung, H. J.; Trejo, O.; McDowell, M. T.; Hryciw, A.; Brongersma, M.; Sinclair, R.; Prinz, F. B. *Nano Lett.* **2011**, *11*, 934–40.
- (219) Hicks, J.; Bergstrom, D.; Hattendorf, M.; Jopling, J.; Maiz, J.; Pae, S.; Prasad, C.; Wiedemer, J. *Intel Technol. J.* **2008**, *12*, 131.
- (220) Bohr, M.; Mistry, K. Presentation “Intels Revolutionary 22 nm Transistor Technology.”
- (221) McCormick, J. A.; Cloutier, B. L.; Weimer, A. W.; George, S. M. *J. Vac. Sci. Technol. A Vacuum, Surfaces, Film.* **2007**, *25*, 67.
- (222) Wank, J. R.; George, S. M.; Weimer, A. W. *J. Am. Ceram. Soc.* **2004**, *87*, 762–765.
- (223) King, D. M.; Liang, X.; Weimer, A. W. *Powder Technol.* **2012**, *221*, 13–25.
- (224) Scheffe, J. R.; Francés, A.; King, D. M.; Liang, X.; Branch, B. a.; Cavanagh, A. S.; George, S. M.; Weimer, A. W. *Thin Solid Films* **2009**, *517*, 1874–1879.
- (225) Hsueh, Y.-C.; Wang, C.-C.; Kei, C.-C.; Lin, Y.-H.; Liu, C.; Perng, T.-P. *J. Catal.* **2012**, *294*, 63–68.
- (226) Karinen, R.; Airaksinen, S.; Kiviranta, P.; Keskinen, K.; Linnekoski, J.; Uusi-Kyyny, P.; Krause, A. O. I. *Top. Catal.* **2011**, *54*, 1206–1212.
- (227) Lowe, H.; Ehrfeld, W. *Electrochem. Acta* **1999**, *44*, 3679–3689.
- (228) Kolb, G.; Schürer, J.; Tiemann, D.; Wichert, M.; Zapf, R.; Hessel, V.; Löwe, H. *J. Power Sources* **2007**, *171*, 198–204.
- (229) Sekol, R. C.; Kumar, G.; Carmo, M.; Gittleson, F.; Hardesty-Dyck, N.; Mukherjee, S.; Schroers, J.; Taylor, A. D. *Small* **2013**, *9*, 2081–5, 2026.
- (230) Kolb, G., Zapf, R., Hessel, V., Lowe, H. *Appl. Catal. A* **2004**, *277*, 155.
- (231) Mies, M. J. M.; van den Bosch, J. L. P.; Rebrov, E. V.; Jansen, J. C.; de Croon, M. H. J. M.; Schouten, J. C. *Catal. Today* **2005**, *110*, 38–46.
- (232) Cominos, V.; Hessel, V.; Hofmann, C.; Kolb, G.; Zapf, R.; Ziogas, A.; Delsman, E. R.; Schouten, J. C. *Catal. Today* **2005**, *110*, 140–153.

- (233) Zapf, R.; Berresheim, K.; Bolz, H.; Gnaser, H. *Trans IChemE* **2003**, *81*, 721–729.

Chapter 3

Preparation of noble metal nanoparticles by atomic layer deposition: preparation details, analysis and underlying physical mechanisms

3.1 Introduction

Heterogeneous catalysis is the focus of a tremendous amount of research, because it benefits many important applications, such as industrial chemistry, oil refinery, or the automobile industry through catalytic converters.¹⁻⁴ Noble metal nanoparticles (NPs) supported on large area oxides are one of the most important classes of heterogeneous catalysts,^{1,3,5,6} and they are used in various chemical processes. For example, Pt and Pd nanoparticles (NPs) supported on Al_2O_3 are used in many technologies such as oil refining,^{1,2,7} hydrogen storage,⁸ sensing,⁹ automotive emissions catalytic conversion¹⁰ and fuel cells.^{11,12}

Atomic Layer Deposition (ALD) is a deposition technique that has the ability to control film growth at the atomic level, using self-limiting chemistry through alternating pulses of precursors and co-reactants.¹³ Recently, ALD has been used as an alternative and robust route to produce noble metal NPs. ALD is an interesting alternative to other techniques because it allows the deposition of the nanomaterials to occur on substrates with demanding 3D surface topologies including materials with high surface-to-volume ratios.¹³ ALD has been explored by various research groups as a way to deposit noble metal NPs on challenging substrates (e.g. carbon nanotubes), for example for fuel cell catalyst applications.¹⁴⁻¹⁸ Furthermore, the synthesized NPs can be used for catalysis applications without the need for post treatment steps (e.g. chemical processes for removal of contaminants, annealing, etc.). This new route is very versatile, since ALD can be employed to design metallic NPs with different compositions in alloyed¹⁹ or core/shell^{20,21} structures. Various materials can be grown by ALD, and among them noble metals such as Pt or Pd are the most used for catalysis applications. Several studies in the past decade were devoted to obtaining a deeper understanding of the reaction mechanisms of noble metal ALD processes.²²⁻²⁴ Despite some recent investigations about the precise mechanisms of ALD nucleation,²⁵⁻²⁷ there are still several open questions related to what takes place at the atomic scale and what influences the resulting NPs properties. Therefore, more understanding is required to improve ALD processes and develop novel applications of the NPs.

Both the catalytic activity and selectivity of noble metal NPs can be highly dependent on their size and composition,²⁸ but also on their shape and the atomic arrangement on their surfaces.^{7,29-33} In this work, the morphological properties that we will discuss are the crystallinity, the crystal orientation, the shape, the island density, and the size distribution of the NPs. The control of these NP morphological properties is crucial if one wants to optimize each catalytic system,^{32,34,35} where the exact relationship between the NPs morphology and their catalytic performance is usually depending on the reaction that needs to be cata-

lyzed.³³ As seen in Chapter 2, independently of the chemical reactions to be catalyzed, the “ideal” system containing (monometallic) nanocatalysts is usually characterized by a high NP density, an appropriate (eventually 3D structured) oxide substrate on which the NPs are deposited, a specific diameter comprised between 1 and 10 nm with a narrow size distribution, and crystal surfaces with an open structure.

The characterization of supported NPs is challenging because of their small size, but various techniques can be used. In particular, transmission electron microscopes (TEM) are very powerful instruments to observe NPs. A precise investigation of the evolution of density, size and shape of the NPs prepared by ALD can lead to an improved control of their properties, and it is therefore an important research goal.

Due to their prominent role in catalysis, noble metal NPs are also grown using physical vapor deposition (PVD) based techniques (such as vapor flow condensation, see chapter 2 for more details). There are strong similarities between noble metal NPs grown by these techniques and those grown by ALD. In particular, surface diffusion processes play a major role in thin film nucleation and growth. Insight into the nucleation reaction mechanisms of ALD can therefore be obtained by acknowledging these similarities and by studying relevant surface science literature. Because surface reactions that take place during ALD nucleation can be similar to surface reactions in catalysis, relevant information on the surface reactions during nucleation can be found in catalysis literature as well.

This chapter is meant to provide some background information on the experimental aspects of the preparation of NPs by ALD, their analysis by TEM, and the underlying physical mechanisms that play a role during the formation of the NPs. The chapter is divided in three parts. The experimental section is given first, and mainly describes the ALD process parameters and the principle of TEM, the main analysis technique of the NPs used in this work. The second part aims to use the TEM data to extract information on the morphological properties such as the surface density and the size distribution of Pd and Pt NPs supported on alumina prepared using our ALD processes. Finally, the third part presents an overview of the main underlying physical mechanisms that can take place during the different stages of NP growth. The focus is on the materials Pt and Pd, but many of the described mechanisms are expected to occur during the ALD of other noble metals as well.

3.2 Experimental part

3.2.1 ALD reactor

All depositions have been carried out in an open-load home-built ALD reactor, as described extensively by Langereis et al.³⁶ A schematic representation and a photo of the set-up used in this work are given in Figure 3.1.

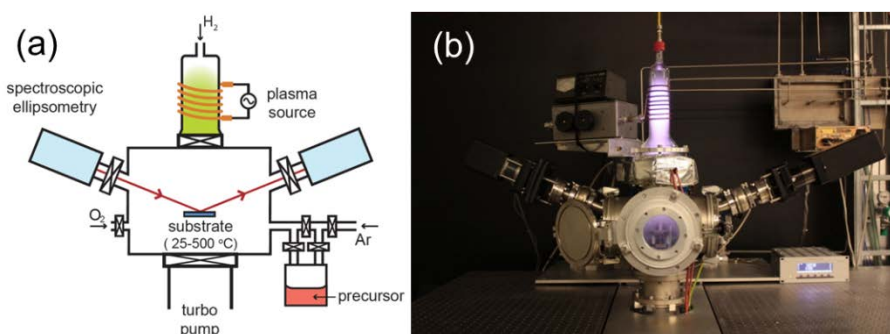


Figure 3.1. (a) Schematic overview and (b) photo of the remote plasma ALD reactor used in this work.

The reactor consists of a deposition chamber which is connected to a remote inductively coupled plasma source, a pump unit, and precursor and co-reactant dosing systems. The pump unit and plasma source were connected to the chamber through gate valves. A combination of a turbo-molecular pump and a rotary pump were used to pump down the chamber. The ALD reactor is an open-load reactor equipped with a 100 mm diameter (4 inch) substrate holder. The total volume of the reactor is approximately $9 \times 10^6 \text{ mm}^3$, and the inner active total surface of the reactor is $146 \times 10^3 \text{ mm}^2$. Additionally, there is the substrate stage surface of approximately $57 \times 10^3 \text{ mm}^2$.

Before the NPs deposition, the (inner) walls were coated with a film of 10-20 nm of the material (Pd or Pt) to be deposited (wall conditioning). This wall conditioning appears to be important for the reproducibility of the experiments. Furthermore, the reactor walls were permanently heated to approximately 90°C to avoid any precursor condensation.

3.2.2 Pd and Pt ALD process parameters

The Pd and Pt ALD processes used in this chapter have been employed to prepare NPs on Al₂O₃ substrates. The precursors, methylcyclopentadienyl(trimethyl)platinum (MeCpPtMe₃, 98%) and palladium hexafluoroacetate (Pd(hfac)₂, 99%), were obtained from Sigma-Aldrich and were used as received. The precursor Pd(hfac)₂ was obtained as a powder and directly transferred in the bubbler. The precursor MeCpPtMe₃ (also purchased from Sigma-Aldrich) was received in a “sticky” phase and was heated at 50°C in order to transfer it as a liquid to the bubbler. Because the precursor molecules are air-sensitive, the transfers to the bubblers have been carried out in a glove box under N₂ atmosphere. The detailed ALD baseline process parameters are given in the Table 3.1.

Table 3.1. Detailed baseline process parameters of the ALD processes

	Pt ALD process	Pd ALD process
Precursor	MeCpPtMe ₃	Pd(hfac) ₂
Precursor exposure time (s) *	3	3
Ar purge time (s)	3	5
Pump time (s)	4	5
Co-reactant	O ₂ gas at 1 mbar	H ₂ plasma at 0.01 mbar
Co-reactant exposure time (s)	5	5
Pump time (s)	8	
Bubbler temperature (°C)	30	50
Substrate temperature (°C)	300	100
Reactor wall temperature (°C)	90	
Reactor base pressure (mbar)	≤10 ⁻⁶	

* Ar was used as a carrier gas.

3.2.3 Substrates

For process development and thin film studies, the depositions were carried out on Si wafers covered with 250 nm Al_2O_3 prepared by ALD. For NPs studies, the substrates employed were Si_3N_4 TEM windows,³⁷ as schematically shown in Figure 3.2. Silicon nitride membranes are chemically, thermally and mechanically robust even for a membrane thickness of 17 nm. These Si_3N_4 TEM windows allow for a good transmission of the electron beam, are easy to handle and can be coated with different materials, which make them optimal substrates for our studies. In this work, the Si_3N_4 TEM window substrates were coated with 3 nm of Al_2O_3 using ALD (see Figure 3.2) in order to study the NP nucleation on this oxide surface. In case of a thermal ALD process, the NP deposition could potentially take place at the back side of the TEM window as well, which is not wanted in our study case. This implies that the substrate stage and the TEM windows used for the deposition of NPs by ALD must be very flat and smooth to ensure good contact and thus prevent deposition on the backside. A deposition of NPs on both the front and the back side of TEM windows would be revealed by a partial overlapping of NPs in the TEM images, which was not the case in our studies. While the deposition took place on the TEM window(s), the deposition growth rate was monitored in parallel on a “seed layer”. The “seed layer” is a Si wafer covered by ~15 nm Pt or Pd, which is used in order to verify the stable conditions of the process during the depositions of NPs. For this purpose, the typical, linear ALD film growth was verified by *in-situ* spectroscopic ellipsometry on this “seed layer”.

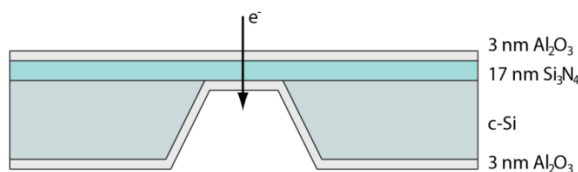


Figure 3.2. Schematic cross-section of TEM windows typically used in this work.

3.2.4 Transmission Electron Microscopy (TEM)

Supported metallic NPs can be characterized using various analysis techniques, such as scanning probe microscopy techniques (scanning tunnelling microscopy and atomic force microscopy) or X-ray based techniques (e.g. using synchrotron radiation). In this work, we are using a transmission electron microscope (TEM),

a powerful instrument which makes use of highly energetic electrons (in the range of 60-300 keV) in order to image objects at extremely high resolution. TEM analysis can reveal information on topography, morphology, composition and crystallinity of objects at the sub-nanometer level. The size distribution and the surface density of NPs can directly be extracted from TEM studies.³⁸ Therefore, this technique is of great use for the analysis of the NPs prepared by ALD.

The basic TEM geometry is shown in Figure 3.3. After being emitted by the source (electron gun), the diameter and intensity of electron beam is controlled using a series of electromagnetic lenses and apertures. Deflectors are aimed to control the direction of the beam with respect to the optical axis. The electron beam reaches the sample and interacts with it before being transmitted (the incident electrons all have the same energy when hitting the sample). Because electrons are easily stopped or deflected by matter, the samples must be very thin ($< 0.5 \mu\text{m}$) to have electron transmission. After passing through the sample, transmitted electrons are focused by the objective lens. The following aperture situated below the sample determines which of the scattered electrons will form the image of the TEM. The last step of the electron beam is to go through the magnifying system part, which is composed of intermediate and projector lenses. The imaging is achieved using a CCD detector and a viewing screen.^{38,39} It has to be noted that the electromagnetic lenses used in TEMs are not perfect but have aberrations. These aberrations degrade the resulting image quality. The most important aberration is astigmatism, and the stigmators placed in the TEM column are aimed to correct this distortion. Optical aberrations can degrade the image quality as well, but the latest TEM systems can be equipped with aberration correctors to correct spherical aberrations, and with an (in-column) energy filter to correct chromatic aberrations.

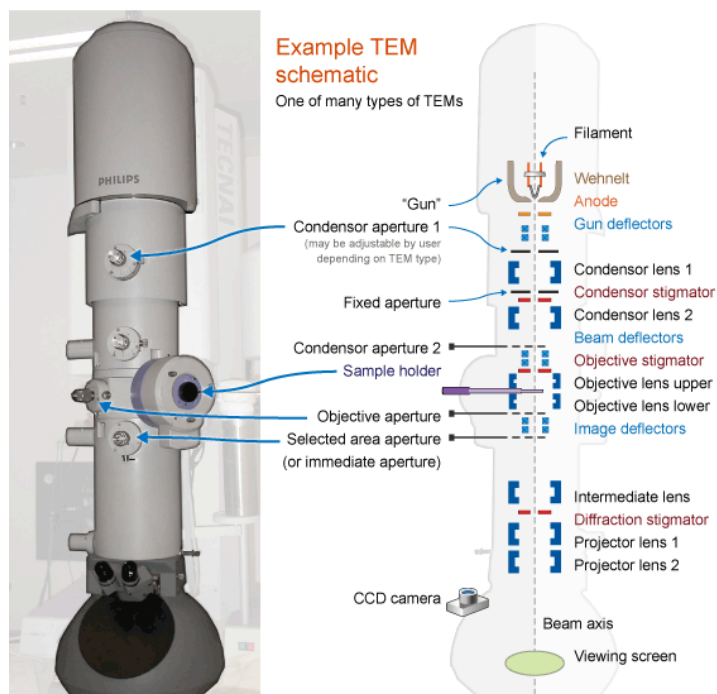


Figure 3.3. A cut-away diagram of the internal structure of a TEM (taken from <http://www.ammrf.org.au/myscope/tem/introduction>).

When studying crystalline samples, the TEM image contrast is dominated by diffraction contrast. The electron diffraction mode is obtained by tuning the microscope lenses such that the back focal plane of the lens is focused on the CCD camera. In this mode, sharp diffraction spots or diffraction disks can be formed.

In the imaging mode, different types of imaging can be carried out. The (retractable) objective aperture situated in the objective lens below the sample (i.e. in the back focal plane of the upper objective lens) can be selective to either the direct (central) electron beam for bright field (BF) imaging, or to one or some of the diffracted electron beams for dark field (DF) imaging.³⁹ BF and DF TEM imaging are the most used imaging modes for crystalline materials.

Scanning TEM (STEM) is a specific mode of TEM, in which a convergent electron beam is focused into a narrow spot which is scanned over the sample. The transmitted electrons are collected at each probe position.⁴⁰ The main advantage of STEM (when compared to TEM) is that elemental composition and atomic bonding state can be directly correlated to the position within an atomic resolution image. Similarly to conventional TEM, BF and DF are the two main imaging modes. BF imaging in STEM makes use of a circular detector centered

on the optical axis, whereas annular DF imaging requires an annular detector centered around the optical axis. The images of BF and annular DF can be recorded simultaneously. Figure 3.4 illustrates the STEM imaging system.

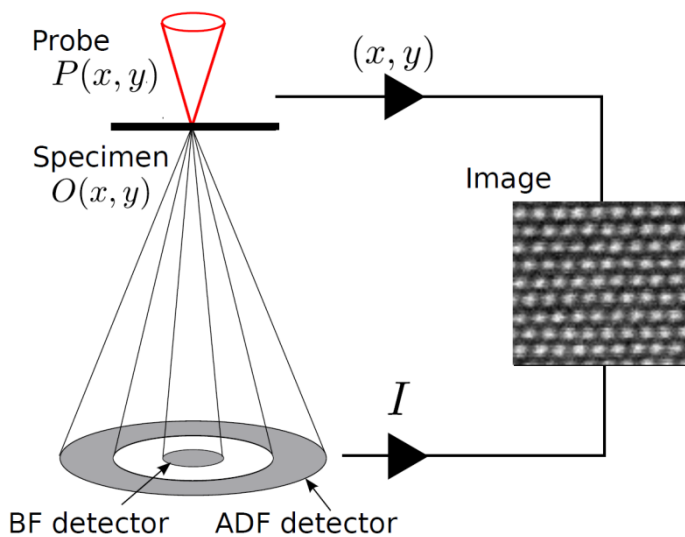


Figure 3.4. Representative illustration of the STEM imaging system. BF holds for bright field and ADF for annular dark field (taken from reference⁴¹).

The high angle annular dark field (HAADF) imaging employs an annular detector with a large radius (high angle) to allow the detection of electrons scattered to high angles. Images with their intensity dependent on the atomic number Z are obtained using this imaging mode. Because of the difference in atomic numbers, the HAADF mode is therefore particularly suitable for the imaging of metallic NPs on oxide substrates.

The electron beam used during TEM/STEM irradiates the surface of the sample with sufficient energy to produce the emission of characteristic X-rays from the sample, allowing for an elemental composition study (with energy-dispersive X-ray spectroscopy (EDX-EDS)) as well. The serial imaging used in STEM requires the use of long scanning times (10-40 s) compared to conventional TEM (less than 1 s), but STEM allows the collection of different types of signals. Analysis techniques such as EDX-EDS, electron energy loss spectroscopy (EELS) and HAADF imaging can be performed simultaneously.^{42,43}

The TEMs used during this doctoral project were an FEI Tecnai F30ST operated at 300 kV and a Cs probe-corrected JEOL ARM 200F operated at 200 kV. The obtained images were analyzed using the imageJ and iTEM software

packages to determine the NPs surface density and size distribution. Manual counting of the particle size and distribution was necessary in certain cases to include the smallest particles (<1 nm) which were not counted by automated software routines.

It has to be noted that in case of high currents, the electron beam can be responsible for a change in the NP morphology during imaging. As observed in our studies, prolonged irradiation results in a 'smearing-out' of the NPs by enhanced surface diffusion of atoms over the oxide surface. It should also be mentioned that the electron beam can accelerate the surface migration of metal atoms, as we observed during STEM studies of areas containing single Pt atoms on an Al₂O₃ substrate. During our TEM studies, special care was taken to leave the original NPs shape intact. For example, the series of images were monitored continuously to make sure that the original shape remained unaltered during acquisition, while also small probe sizes with reduced beam currents were used.

Note about *in-situ* TEM:

Because NPs can undergo structural and chemical variations in response to different environments (oxidising, reducing) and catalytic reactions, there is an increasing interest to study supported NPs under "real" conditions. In the last few years, *in-situ* TEM became an important field of research, because it enables the study of the catalysts at conditions close to operation conditions in e.g. catalysis.⁴⁴

Dedicated *in-situ* TEMs have been developed by various instrument manufacturers, ranging from unique instruments based on customer-oriented modifications of existing equipment (FEI, Jeol, Hitachi) to commercial products (such as the FEI Titan ETEM G2 - environmental TEM). These instruments include gas supplies in a limited volume in the close vicinity of the sample and differential pumping apertures to maintain good vacuum conditions in the rest of the microscope column. The gas pressure in the sample area is a few mbar. This option has several characteristics, being advantageous or disadvantageous depending on the topic of research: Most of the gas molecules never reach the thin slice of the TEM sample, and the pressures reached are orders of magnitude lower than the normal operation conditions of a catalytic process. Whether these TEM studies are representative of "real" conditions is still under debate. The alternative approach is to use a "standard" TEM system and include a reactor cell in the sample holder. In the last few years, several commercial suppliers of various types of *in-situ* TEM holders have emerged (Poseidon 200 Liquid Flow Cell, Aduro TEM holder, etc.).

Various *in-situ* TEM studies of nanocatalysts have already been published in the literature, and therefore contribute to the advancement of this field of science. For example, Pt/Al₂O₃ catalyst reduction through calcination was studied under H₂ environment. The influence of the reaction temperature was studied in detail by stepwise heating the sample up to 250°C and monitoring the changes in the NPs morphology for each step.⁴⁵ (De)hydrogenation and oxidation of crystalline Pd nanocatalysts (sputtered on SiN membrane) using a nanoreactor operated at hydrogen and oxygen gas pressures in the range of 1 bar and temperatures up to 700 °C has also been studied.^{46,47} The possibilities offered by these *in-situ* TEM studies can thus lead to valuable knowledge for the catalysis community.

3.3 Characterization of ALD Pd and Pt nanoparticles morphological properties

In this section, the morphological properties of Pd and Pt NPs prepared by ALD will be discussed. These properties have been extracted from bright field TEM studies. Figures 3.5 and 3.6 present BF TEM images showing the nucleation and growth of Pd and Pt, respectively, on Al₂O₃ substrates as a function of the number of ALD cycles. The ALD recipes described in the experimental section 3.2.2 were used.

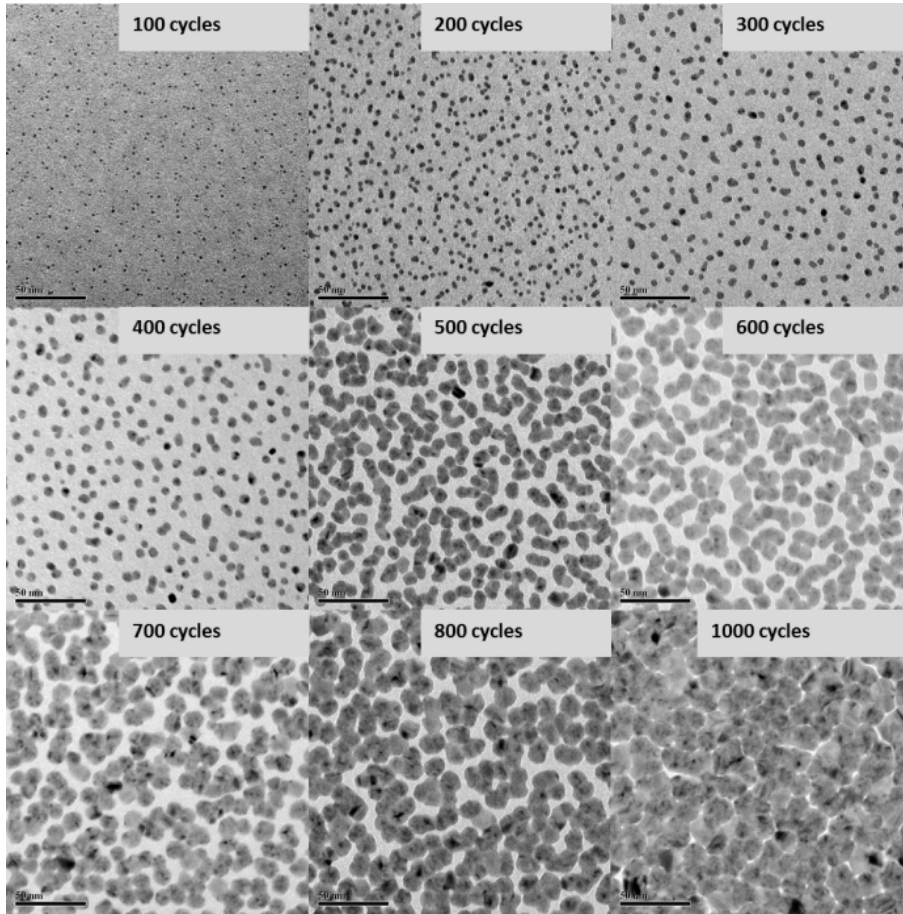


Figure 3.5. BF TEM images of the nucleation and growth of Pd presented as a function of the number of ALD cycles (indicated in the upper right corner of each image). The substrates used were Al_2O_3 covered Si_3N_4 membranes. The scale bar is 50 nm in every image.

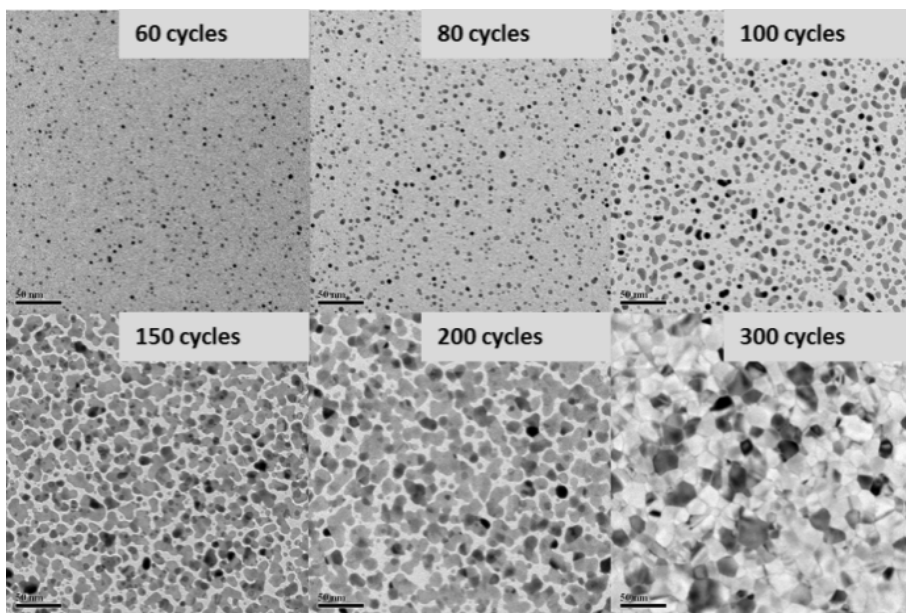


Figure 3.6. BF TEM images of the nucleation and growth of Pt presented as a function of the number of ALD cycles (indicated in the upper right corner of each image). The substrates used were Al_2O_3 covered Si_3N_4 membranes. The scale bar is 50 nm in every image.

3.3.1 Crystallinity and shape

Both Pd and Pt ALD start with the formation of discrete nanoparticles (NPs). The differences in grey scales between the different Pd and Pt NPs in the TEM images presented in Figure 3.5 and Figure 3.6 are due to diffraction contrast, demonstrating the fact that the NPs obtained are crystalline. The differences in intensity are due to the differences in crystal orientation with respect to the electron beam. At the magnifications used in these BFTEM studies, these NPs seem to have a circular shape. However, considering their limited size, atomic resolution TEM studies would be needed to reveal their actual projected shape. Grazing-incidence X-Ray diffraction studies carried out on Pd thin films of 15 nm revealed that the Pd films deposited using our process had the face-centered cubic (fcc) crystal structure. No evidence for texture was present in such a thin film implying that the initial stage of ALD starts with randomly oriented particles. Thus, even if the particles have a faceted morphology exhibiting the most common facets, i.e. $\{111\}$ and $\{100\}$, these facets may still not be recognizable in the projection into a BFTEM image because of their random orientation. In addi-

tion, the projected circular shape in the TEM images may indicate a half-spherical shape of the NPs, but it is presumptuous to precise a 3D shape without any other data than these (top view) images. It would require either high resolution STEM tomography or imaging of NPs deposited on 3-D substrates to obtain more information on the actual 3-D shape. For example, Figure 3.7 shows a HAADF-STEM image of Pt NPs supported on the tip of an Al_2O_3 coated GaP nanowire. The large particle at the extremity of the nanowire is a gold particle, which is used during the growth process of the nanowire.

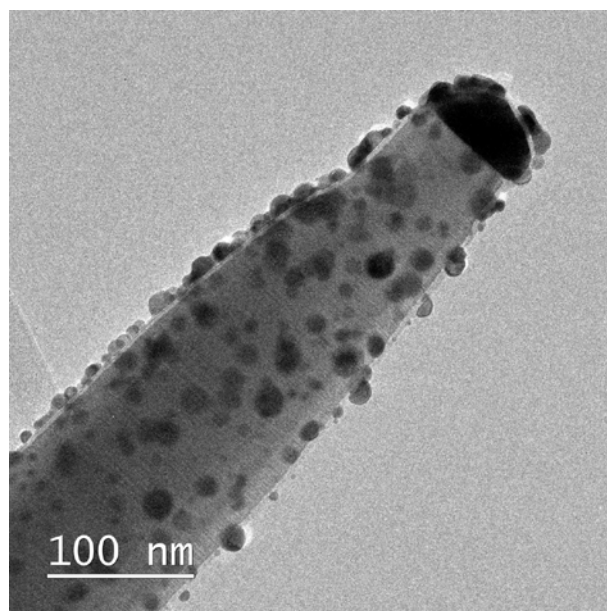


Figure 3.7. BF-TEM image of Pt NPs supported on the tip of an Al_2O_3 coated GaP nanowire.

The NPs seem to present a semi-spherical geometry, but the precise 3D shape (e.g. semi-spherical) and faceting of the ALD prepared NPs strongly depend on the substrate surface and other parameters (e.g. gas environment, impurities) and might considerably change with the NPs growth.⁴⁸ The determination of these properties after a precise number of ALD cycles was not a primary focus of our study. Some insights can also be obtained from the ALD literature. For example, ALD of Pt has been carried out in order to deposit Pt NPs on SrTiO_3 (STO) nanocuboids, and it has been shown that the NPs are crystalline and grow epitaxially.^{49,50} The orientation of the facets has been found to be consistent with the surface free energies of the materials and corresponds to the lowest energy of the system. Sairanen *et al.* found that Pt NPs supported on carbon present a hexagonal shape for consistency with the projection of thermodynamically ideal cub-

octahedron.⁵¹ Therefore, these NP shapes are expected to be stable even under catalysis and different environments conditions. Changing the surface energies of the substrate would change the faceting (e.g. ratio of exposed Pt(111) to Pt(100) facets) which could change the overall catalytic performance.⁵⁰

Xie *et al.* grew Pt NPs onto TiSi₂ substrates by ALD and observed multiple twinned NPs, exposing a large number of (111) surface atoms (see Figure 3.8).⁵² This indicates that the shape of NPs can strongly depend on the underlying substrate.

Lei *et al.* prepared Pd NPs on TiO₂ and on porous carbon substrates. The NPs were found to be crystalline and faceted, and showed lattice fringes consistent with the d-spacing for the Pd (111) plane.^{25,53}

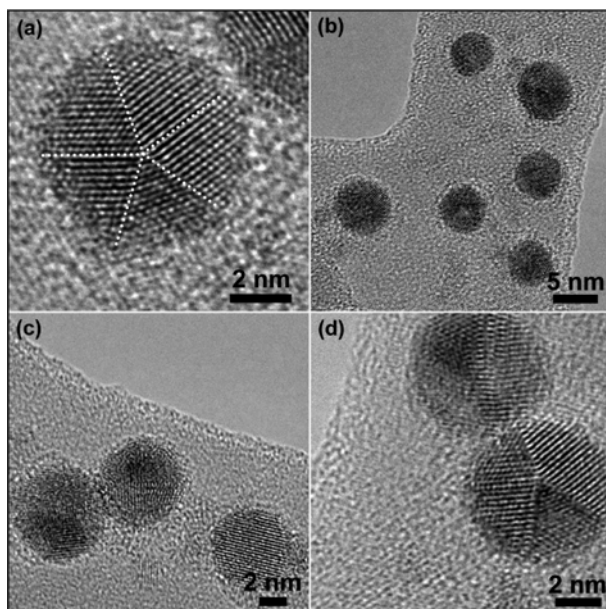


Figure 3.8. HRTEM image of multiple-twinned Pt nanoparticles deposited on TiSi₂ by ALD. (a) A 5-fold twinning effect is observed in the high-resolution TEM image with zone axis (110). (b-d) High yield of multiple twinned Pt nanoparticles (taken from Reference⁵²).

3.3.2 Size evolution

The NPs grow with the increase of the number of cycles. The NP size can therefore easily be tuned by changing the number of ALD cycles. After a few hundreds of cycles, the NPs merge and finally coalesce to form a closed film. A change in contrast between different NPs can be observed for both Pd and Pt NPs. This is primarily due to differences in crystal orientations with respect to the electron beam.

Many interesting properties of NPs can be extracted from the TEM images presented in Figures 3.5 and 3.6. Figure 3.9 presents the surface density evolution of Pd and Pt NPs as a function of the number of ALD cycles. The typical density shows a sharp initial increase to reach a maximum value of around 10^{12} NPs/cm² for both Pd and Pt NPs. This density subsequently decreases with the coalescence of the single NPs. It is known from the literature that metal NPs prepared by PVD techniques generally present a maximal density between 10^{10} and 10^{12} NPs/cm².⁵⁴⁻⁵⁷ This maximal density of NPs is very typical for PVD and is basically linked to the deposition rate and the hopping rate of the adatoms.^{55,57-59} This value is in good agreement with the maximal density values observed during ALD which are in the range of 10^{12} NPs/cm². Note however that this density value concerns the particles which are visible in our TEM images and can thus depend on the resolution of the instrument. Sub-nanometer sized particles (such as individual atoms or clusters of a few atoms) may not be discernable or accurately measurable using an uncorrected STEM such as the FEI Tecnai F30ST used for this study. Thus, only the NPs with a diameter larger than 0.5 nm have been considered.

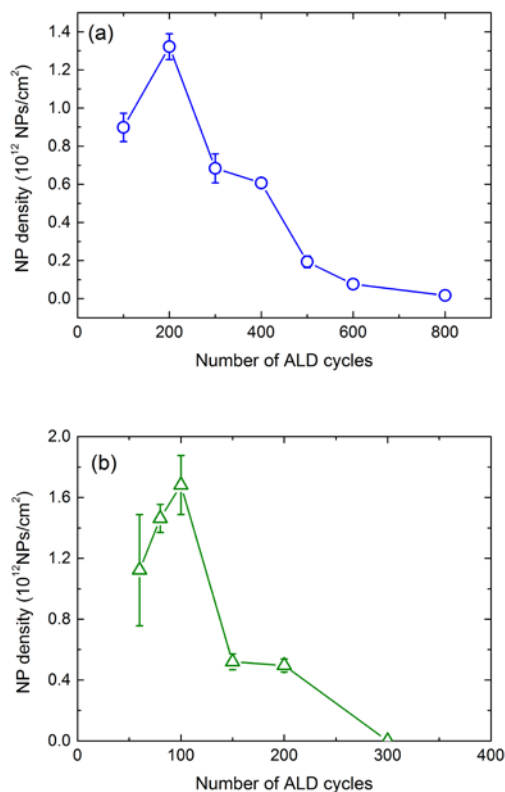


Figure 3.9. NP surface density evolution as a function of the number of cycles for (a) Pd and (b) Pt ALD as determined from the TEM images presented in Figure 3.5 and 3.6. The error bars correspond to the standard deviations and are given when different images of the same sample have been analyzed.

The size of NPs (the diameter for the case of circularly shaped NPs) is an important parameter for their final application in catalysis. To get more insight into the differences observed in Pd and Pt NPs prepared by our ALD processes, their size distributions as a function of the number of ALD cycles have been studied and are presented in Figure 3.10. The data have been obtained by measuring the diameter of each NP present in the image and by subsequently categorizing the NPs in different diameter sections with an 0.5 nm interval. The area studied depends on the resolution of the TEM image. For example, for the studies based on Figures 3.5 and 3.6, the area studied was approximately $0.4 \mu\text{m}^2$ per

BFTEM image. In general, the data have been obtained from and averaged over three images.

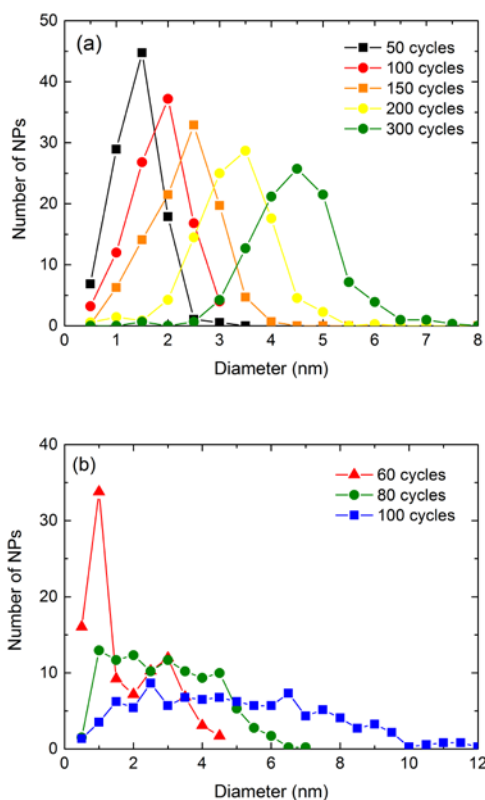


Figure 3.10. Size distribution of (a) Pd NPs and (b) Pt NPs determined from the TEM images presented in Figure 3.5 and 3.6.

The nucleation of both Pd and Pt ALD results in nano-sized particles, which are often desired for heterogeneous catalysis applications. Pd ALD results in a unimodal and very narrow size distribution of NPs. The narrow size distribution of the Pd NPs obtained is particularly relevant for catalysis, since a precise NP diameter is often desired in order to obtain a high activity or selectivity. It is very plausible that the growth rate for NPs and thin films is different as they are likely ruled by different mechanisms. Furthermore, the process was optimized for thin film growth meaning that the growth for the NPs was even not fully saturated. The Pd NP diameter can be easily and precisely tuned from 1 to 5 nm by simply increasing the number of ALD cycles. In fact, the average diameter of the Pd NPs increases at a rate of ~ 0.014 nm/cycle. This corresponds to a radial growth rate of ~ 0.007 nm/cycle. This NP radial growth rate can be compared to

the film growth rate. The film growth rate normally obtained with this Pd process has a value of ~ 0.017 nm/cycle (see Chapter 4 for details), which is substantially higher than the NPs radial growth rate observed. The Pt ALD process, on the other hand, results in NPs with a much broader size distribution (compared to the Pd NPs). The average diameter of the Pt NPs increases at a rate of ~ 0.08 nm/cycle, corresponding to a radial growth rate of ~ 0.040 nm/cycle. This is only slightly lower than the film growth rate of ~ 0.045 nm/cycle normally obtained with this process.^{22,60} Summarizing, the Pd and Pt NP growth behavior and size distributions present considerable differences. Those differences can possibly be related to the process conditions (e.g. precursor exposure, temperature, co-reactant), but also to the substrate surface properties (e.g. presence of polluting ligands). In fact, the NP growth strongly depends on the surface chemistry of the process, which affects the diffusion of adatoms and the NP growth. The physical mechanisms and processes taking place at the surface during nucleation will now be described.

3.4 Physical mechanisms and processes taking place during nucleation

The nucleation of metals during ALD on oxide surfaces begins with the formation of isolated NPs. The growth mechanism includes the adsorption of precursor molecules at the substrate surface (see section 3.4.2) followed by the diffusion of metal adatoms to form clusters or to join growing NPs (see the sections 3.4.3 and 3.4.4). The formation of these islands is mainly due to the difference in surface energies between the substrate and the material deposited, as described below.

3.4.1 The island growth mode

Thermodynamically, the surface energy (or surface tension) is defined as the reversible work required to create a certain surface area (by cleavage).⁶¹ If the interatomic bonds of a material are strong, the surface energy is high because the bulk cohesion is high. Typically, strongly bonded metals have high surface energies. Depending on the material, this surface energy can be anisotropic and thus is different depending on the surface orientation.^{62,63}

Under thermodynamic equilibrium conditions, the growth mode of a film depends on the surface energies of the substrate (γ_s) and of the deposited material (γ_m), as well as on the interfacial energy (γ_i). The growth mode is related to the

magnitude of $\Delta\gamma$, where $\Delta\gamma = \gamma_m + \gamma_i - \gamma_s$. Thermodynamically, the initial stage of film deposition can occur by the following three different modes (as depicted in Figure 3.11):^{58,64}

a. Frank-van der Merwe (“layer growth”): the adsorbate material forms a complete monolayer before a second layer starts. This growth mode takes place when $\Delta\gamma < 0$.

b. Volmer-Weber (“island growth”): the adsorbate forms 3D islands on the surface. This growth mode takes place when $\Delta\gamma > 0$.

c. Stranski-Krastanov (“layer plus island growth”): the adsorbate forms first monolayers and then 3-dimensional islands with the increasing thickness. This growth mode takes place when $\Delta\gamma \sim 0$.

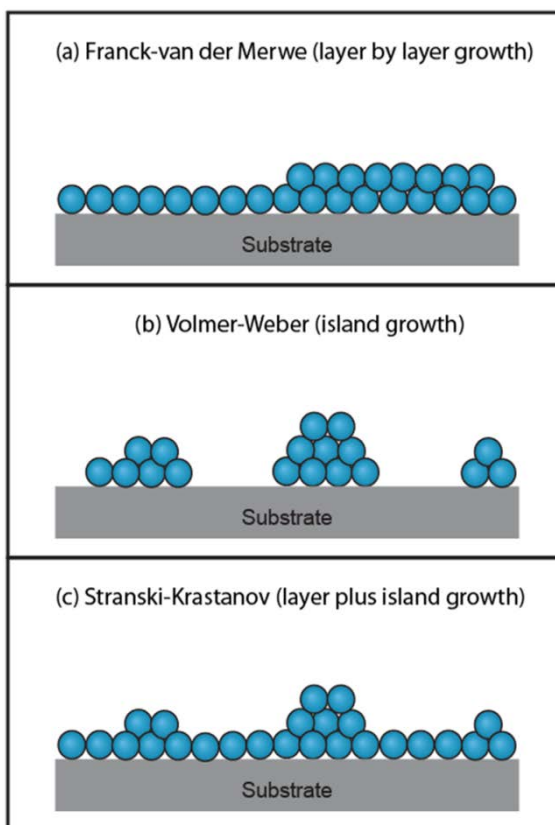


Figure 3.11: Schematic representation of the three growth modes: (a) Frank-van der Merwe (layer by layer growth); (b) Volmer-Weber (island growth) and (c) Stranski-Krastanov (layer plus island growth).

Typically, the Frank-van der Merwe and the Stranski-Krastanov modes take place when a lower surface energy film is deposited on a larger surface energy substrate ($\gamma_m < \gamma_s$). The adatoms arriving at the surface migrate to form 2D islands usually shaped as fractals, which expand by capturing other migrating adatoms until forming a monolayer or a layer and islands. The Volmer-Weber mode, resulting in the growth of 3D islands, basically occurs when the deposited material surface energy is larger than the substrate one ($\gamma_m > \gamma_s$).^{57,58,64} The surface free energy of metals is usually larger than that of oxides,⁶⁵ therefore the Volmer-Weber growth mode takes generally place during the deposition of metals on oxide substrates.^{58,65}

For example, the surface energy of Al_2O_3 is typically comprised between 650 and 925 mJ/cm^2 ,^{65,66} whereas the surface energies of metals Pd and Pt are respectively ~ 1200 - 1500 mJ/cm^2 and ~ 1400 - 1700 mJ/cm^2 depending on the crystal orientations.⁶⁶⁻⁶⁸ The surface energies can also be seen as the binding energies between atoms. This so-called cohesive energy protects the NP from dissociation. Pd has a cohesive energy value of 376 kJ/mol (corresponding to 3.89 eV/atom), whereas Pt has even a higher value of 564 kJ/mol (corresponding to 5.84 eV/atom).⁶⁹ Thus, thermodynamically, NPs in which atoms are closely packed together are in general likely to be formed in order to reduce the total free energy of the system. NPs preferably form a compact shape, as the atoms at the edge find thermodynamically stable positions and form closely packed structures through faceting (e.g. octahedron).⁷⁰ However, the principle of energy minimization is usually not sufficient to predict the exact growth of a material, especially when considering that the deposition does not take place under thermodynamic equilibrium conditions. Therefore, kinetics related to the deposition process parameters must also be considered. The early stage of NPs growth involves the arrival and accommodation of adatoms at the substrate surface and their diffusion. Using conventional physical vapor deposition (PVD) techniques (e.g. vapor condensation), the metal atoms are typically deposited uniformly over the whole oxide surface, and by surface diffusion they first form 2D islands, and then 3D islands with a certain contact angle and shape. During ALD, the deposited metal atoms are likely to initially form islands as well, as has been observed for Pd and Pt ALD on Al_2O_3 substrates (see the TEM images presented in Figure 3.5 and Figure 3.6). The compact NP shape seen for Pd and Pt NPs is probably the sign that the atomic diffusion along the NPs edges plays also an important role.

The ALD reaction mechanisms are different at these catalytically active island surfaces when compared to oxide surfaces. Because the catalytic activity of the noble metal surfaces enables the decomposition of the incoming precursor

molecules, the deposition of metal atoms is enhanced at the noble metal island surfaces with respect to the oxide surfaces. This leads to an enhanced 3D island growth.

The island growth observed during metal ALD on oxide is therefore a combination of a Volmer-Weber growth mode related to the surface energies, and of an enhanced 3D island growth related to reaction mechanisms such as the catalytic enhancement of certain ALD reactions. This island growth throughout the ALD process will be further discussed in 3.4.3 where the diffusion processes are described.

3.4.2 Initial reactions between the precursor molecules and the oxide surface

The first aspect to take into consideration is the interaction between the precursor molecules and the oxide substrate surface. The precursor molecules, when physisorbed at the surface, can diffuse and then potentially react with surface groups in order to get chemisorbed.

For example, let us consider the cases of Pd and Pt ALD on a starting oxide surface. For Pd ALD, it is commonly accepted that the Pd(hfac)₂ precursor reacts with hydroxyl groups, to create one Pd(hfac) molecule at the surface and releases one Hhfac molecule to the gas phase.^{71,72} For Pt ALD, the methyl ligands of the MeCpPtMe₃ precursor are expected to initially react with the surface hydroxyls groups as well, leading to the formation of CH₄.^{23,73} These chemical reactions, which are taking place between the precursor molecules and the surface groups, form the first step of film growth by ALD on the oxide surface. The fact that precursor molecules react chemically with the substrate surface groups implies that their diffusion is limited afterwards. Then, the pump/purge step applied at the end of the first half-cycle removes the excessive amount of precursor molecules, leaving only the molecules which reacted with the surface groups. This ensures the self-limiting nature of the first half-reaction.

After the initial precursor adsorption and purge/pump steps, the coreactant is introduced in order to remove the ligands and to reduce the metals to their metallic state. Considering the specific case of Pd ALD from Pd(hfac)₂, the H₂ plasma (or the commonly used formalin) co-reactant effectively removes the precursor hfac ligands and reduces the Pd(II) to Pd(0) state, leaving single Pd atoms at the substrate surface.^{71,74,75} Because Pd has a very strong affinity to hydrogen, it is plausible that H atoms remain chemisorbed at the Pd single atoms and clusters surfaces.^{8,76} However, it is also known that hfac ligands strongly react with the alumina substrate and remain present even after the co-reactant and

pump step, and these remaining ligands can pollute the alumina surface.^{77,78} For Pt ALD, it is known that the use of oxygen as co-reactant combusts the ligands effectively, releasing CH₄, CO₂ and water.²⁴ The ALD cycle finally results in the deposition of Pt single atoms with chemisorbed O atoms, and the species formed are a mixture of PtO and PtO₂ molecules. The majority of PtO and PtO₂ are then reduced during the precursor adsorption due to the precursor ligands in the next cycle.^{27,73,79} Ligands pollution can also happen for Pt ALD, but probably to a less extent than for Pd ALD.⁷⁹

Subsequently, the diffusion of the adatoms over the substrate surface enables the formation of NPs to take place and influences their resulting morphology. Thus, in order to elucidate the processes behind the formation of NPs, the focus is now on understanding the surface diffusion processes taking place during the nucleation stage of ALD.

3.4.3 Surface diffusion of metal atoms and formation of NPs

The first ALD cycles likely lead to atoms at the substrate surface. The basic kinetic approach to describe the surface diffusion processes of individual adatoms uses the Arrhenius form. These atomic surface processes are regulated by the surface diffusion coefficient D which can be expressed by

$$D = \frac{\nu a^2}{4} \exp(-\Delta E_a/k_B T)$$

Where ν is the vibrational frequency or hopping attempt frequency, a is effective hopping distance between sites (0.2-0.5 nm),⁵⁷ ΔE_a the potential energy barrier from site to site, k_B the Boltzmann constant and T the substrate temperature.^{57,80} For an adatom on a surface, the hopping attempt frequency ν (also called vibrational frequency) is in the order of 10^{13} s^{-1} .⁷⁰

At low surface coverage, the adatoms move mainly by hopping from one site to another by surmounting an energy barrier ΔE_a . It is known from literature that isolated atoms of metals such as Pd or Pt on oxide and metal surfaces are highly mobile at room (and ALD) temperature, due to the low hopping activation energies ΔE_a which are in the range of 0.3-0.5 eV (for Pt and Pd atoms on γ -Al₂O₃ surfaces).⁸¹⁻⁸³ Thus, these single adatoms can diffuse over the surface and undergo several processes. Figure 3.12 illustrates these atomic processes taking place during nucleation and growth on the surface. These atomistic processes include capture at special sites such as kinks, steps or vacancies,⁸⁴ but also binding of atoms which can imply the nucleation of clusters. Another important pro-

cess is the capture by existing clusters or NPs. The hopping mechanism from one site to another can take place on the oxide substrate surface or at the surface of the islands of metal atoms. The atoms can also diffuse along the island edges or “jump” on the island top. Furthermore, interdiffusion mechanisms (such as atomic or vacancy exchange) can also take place during the island restructuring and growth. Other possibilities are the atomic dissolution into the substrate and re-evaporation, but those processes are unlikely under ALD conditions.⁵⁸

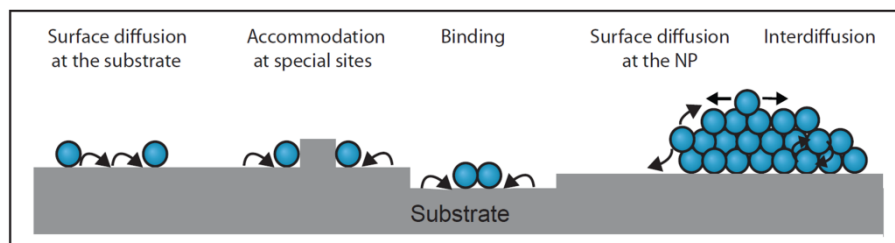


Figure 3.12. Schematic diagram of atomic processes taking place during nucleation and growth on surfaces. Adatoms are likely to accommodate at special sites at the substrate surface such as kinks or steps. Surface diffusion of the adatoms can take place at the substrate surface, and at the NPs edges or surfaces. Interdiffusion within the NP is also possible.

When the deposited atoms meet each other, they form dimers or trimers, and become larger 2D islands when more atoms join. It is known from the literature that isolated adatoms of metals as Pt or Pd on oxides can diffuse rapidly from site to site across the oxide until finding a metal cluster.⁸¹ If the metal adatoms deposition rate is constant, the surface diffusion dictates the average distance that an adatom moves at the surface before meeting another adatom to create a new island or joining an existing island.⁸⁰ These 2D particles can grow laterally, but also vertically to form 3D islands. The small islands shape is the result of the close-packing of atoms around the central atom, and the very small clusters rearrange themselves into a new structure when an atom is added. For example, trimer forms an equilateral triangle and with the increasing number of atoms, multiple and more complex structures can be found. The formation of closely packed structure such as cuboctahedron is likely to happen because of the reduced surface energy of the system. Interestingly, the formation of exceptionally stable clusters can take place for a specific number of atoms, when electronic and geometric “shells” are optimal (“magic clusters”).^{85–87}

As mentioned earlier, Pd and Pt clusters grow in a 3D structure due to strong metal-metal binding energies that overcome metal-surface interactions.⁸³ The growth in height of the NPs can be the effect of several mechanisms. Firstly, it can occur if atoms from the substrate surface diffuse upwards along the parti-

cle side facets. The diffusion of atoms over the surface of the NP or within the NP allows for a process of minimization to reduce the total surface free energy. Secondly, when the precursor molecules are exposed to the substrate surface, they do not only react at the surfaces of the oxide, but also on the facets of the NPs, and thus enable the deposition of metal atoms directly at the NPs top. As mentioned earlier, an increased vertical growth takes place because of the higher deposition rate at the NPs surfaces than at the oxide surfaces due to the catalytic nature of the NPs.

Surface diffusion processes can be affected by specific aspects of the ALD process. Logically, each ALD process has specific conditions such as, for example, the temperature, the pressure, or the use of plasmas. Those process parameters can considerably change the diffusion possibilities. We believe that the diffusion of newly deposited metal atoms can be hindered if ligands or carbon contaminants pollute the surface, and this may affect the adatoms diffusion length and the probability to form new islands. Furthermore, the species deposited or formed may undergo changes during the ALD cycle and this affects the diffusion rates. For example, Pd and Pt materials are known to be able to adsorb H and O atoms,^{8,24,76} which can modify the properties of the NPs such as their diffusion rates. In Pt ALD, the PtO and PtO₂ species (formed after the first cycle) have a different diffusion rate than the Pt atoms (formed after the introduction of the precursor).^{79,88}

Also, different substrate surfaces will influence the diffusion processes. Substrates are not ideal and perfect, they can have roughness or can be 3D structured, and they can have multiple defects and steps which are difficult to predict. The spatial distribution of clusters on perfect surfaces is typically not random, because their formation tends to be less likely in the immediate vicinity of existing clusters. However, especially when considering amorphous substrates which present numerous defects/steps randomly distributed that can act as nucleation sites, NPs can be located at these more random specific defects/steps at the surface. It is important to note that ALD allows for the tuning of the NPs density using some process modifications, for example by applying surface treatments⁸⁹ or by increasing the co-reactant pressure or composition.^{79,90-93}

3.4.4 NPs growth and ripening

After the initial NPs have formed, the NPs can proceed growth by different mechanisms. First, the NPs logically grow with the addition of newly deposited

atoms on their surface or in their vicinity (through adatoms diffusion towards the NPs). This “growth from adatoms” is depicted in the Figure 3.13a. Then, upon further growth, the NPs can meet each other and merge, leading to bigger NPs as well. This merging process is shown in Figure 3.13b.

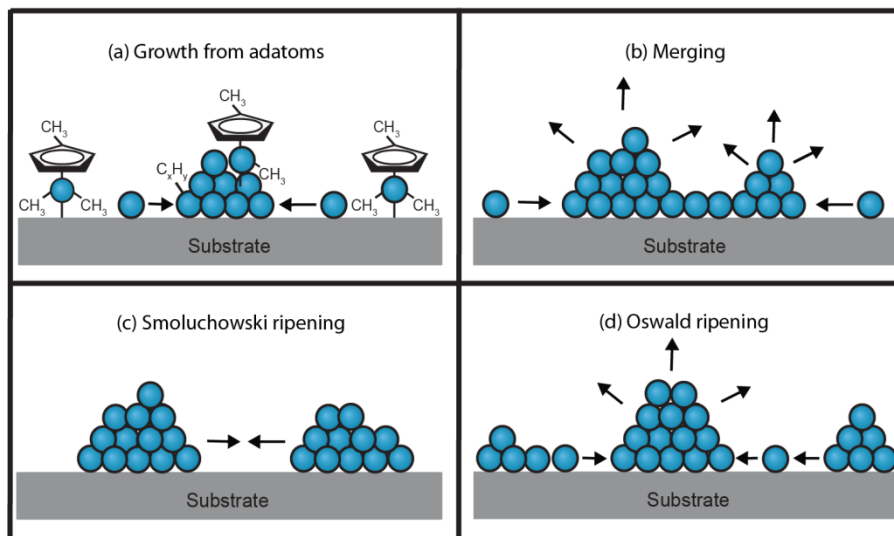


Figure 3.13. Nanoparticle growth from (a) adatoms, (b) Merging, (c) Smoluchowski ripening and (d) Ostwald ripening.

In addition, the NPs can diffuse as well over the surface. The ripening of NPs can occur through the displacement of individual atoms, sections of the cluster, or the entire cluster moving at once.⁹³ Thus, the NPs deposited on a surface can also grow by ripening processes which do not involve the arrival of new adatoms: the Smoluchowski ripening (depicted in Figure 3.13c) and the Ostwald ripening (depicted in Figure 3.13d).^{80,94–97}

The Smoluchowski ripening is the migration or diffusion of the whole NP at the surface, which eventually results in the merging of NPs. The particle diffusion process is characterized by the displacement of the center of mass of a particle. In general, smaller particles (clusters) diffuse faster than bigger particles.⁵⁹ The coalescence of two islands typically results in the formation of one island which restructures its shape in order to reduce its surface energy. The Ostwald ripening can be seen as the net diffusion of atoms from small NPs to larger NPs, resulting in the redistribution of mass between NPs. As a result larger NPs will grow at the expense of smaller NPs. This thermodynamical process also leads to a reduction of the surface energy of the NPs.^{80,94} Thus, the ripening processes are in favor of the formation of large NPs,⁸⁸ and the stability of NPs increases consid-

erably with their increasing size. Such ripening processes may also take place during ALD nucleation. If these surface diffusion processes are important, a large part of the oxide surface can be re-exposed to incoming precursor molecules and new nucleation events can occur.

The narrow size distribution of Pd NPs observed in Figure 3.5 can be an indication that Ostwald ripening, based on the diffusion of atoms at the surface, is probably not an important phenomenon in this ALD process. This hypothesis is in agreement with the possibility that the surface is covered with polluting ligands during Pd ALD, which can hinder surface diffusion processes. Pt ALD is based on combustion chemistry at 300°C and the removal of the precursor ligands is likely to be more efficient in this process. The preparation of Pt NPs, presenting a broader size distribution (see Figure 3.6), is therefore likely to be more affected by the surface diffusion of Pt atoms during ALD and thus by potential Ostwald ripening processes.

As mentioned previously, certain surface reactions can be catalysed at the surfaces of NPs of noble metal, which tend to cause an increased 3D growth. The catalytic activity of noble metals can break the bonds of ALD precursor molecules and can therefore lead to a higher deposition rate of metal atoms at the metal NPs than at the oxide surface. In addition, the catalytic reactions can be strongly dependent on the particle size, which implies that the type and rate of these reactions at the noble metal NP surface and in their vicinity change during the nucleation stage because the NPs grow in size with the number of ALD cycles. Spillover effects can also take place. For example, during Pt ALD nucleation, dissociative chemisorption of O₂ occurs on the NPs during the O₂ pulse, but not on the oxide.⁷⁹ The O atoms that are formed during that reaction can subsequently spillover to the surface and participate in the combustion of precursor ligands adsorbed at this substrate surface in the vicinity of the NPs. Similarly, Pd NPs can act as “storage matrix” for H atoms, which can spillover to the surface and participate in the ALD reactions at the vicinity of the NPs.^{8,76} It is therefore important to differentiate between the reactions that take place on a NP, within its periphery, and on the oxide surface.

3.4.5 Additional remarks

Even if the number of ALD cycles it takes to form NPs from deposited atoms depends mainly on the density of metal adatoms and their surface diffusion, the determination of this number of cycles is not trivial.

Substantial differences have been observed in the literature. It is likely that the ALD process and the reactor type used have a considerable influence on the number of cycles needed to form NPs. For example, it has been reported that Pd and Pt clusters/NPs of 1 nm were deposited using only 4 and 5 ALD cycles, respectively.^{98,99} This number of cycles is one order of magnitude smaller than for our results (where 1 nm sized NPs were observed after 50-100 cycles). However it has to be noted that the precursor time sequences applied were long (more than 10 minutes just for a half-cycle) compared to the ones we applied in our studies (1-3 s), and the pressure and temperature applied have been different than the ones used in this work. In addition, the ALD reactors used had a different design. These differences can influence the amount of metal atoms deposited at the surface, their diffusion and therefore the formation of NPs. We believe that the number of cycles needed for the preparation of NPs is strongly dependent on the process parameters such as the precursor exposure (in terms of time and pressure), and that the saturation conditions during the initial stage of ALD and during steady-state growth of the film are very different. The processes used in the present work have been optimized for (steady-state) film growth. It is possible that they are not in self-limiting saturated conditions for the nucleation stage, but in “under saturation” conditions. The ratio between the noble metal and the oxide surface during ALD nucleation is constantly changing. The evolution of the ratio noble metal / oxide makes it difficult to define the saturation conditions during this initial stage of ALD. The “under saturation” conditions used may also be an explanation for the low growth rate of NPs (compared to film growth) that we observed. We believe that initial long exposures (in terms of time and pressure) of the precursor molecules during the first ALD cycles would enable the deposition of (much) more metal atoms at the substrate surface. The determination of the precise saturation conditions at this initial stage requires future research. This research would enable a more efficient deposition of NPs and could help to determine which precise parameters influence the formation of NPs.

3.5 Conclusions

This chapter provides background information on the ALD processes used in this work for the preparation of NPs as well as the basics of NP analysis by TEM. We illustrated the nucleation of metal films by ALD with the specific cases of Pd and Pt on Al₂O₃ surfaces. A physical description of the NPs obtained has been extracted from the TEM data. Based on literature reports in the field of ALD, catalysis and surface science, several physical and chemical processes influencing noble metal nucleation and growth have been presented. The initial reactions between the precursor molecules and the substrate surface, the atomic-scale sur-

face diffusion processes, the formation and growth of discrete NPs from adatoms, as well as the ripening processes that these NPs can undergo have been addressed. The relevance of these processes for our ALD processes has been discussed.

For both Pd and Pt ALD on Al_2O_3 surfaces, crystalline NPs have been obtained which grow in size with the number of ALD cycles. The surface density obtained using our ALD processes presents a maximum value of $\sim 10^{12}$ NPs/cm², which is in line with maximum density values obtained with PVD techniques. The island growth mode obtained for ALD of metals on oxide surfaces is the result of a Volmer-Weber type growth which is related to the difference in surface energies between the noble metals and the oxide substrate. However it is also affected by an enhanced 3D island growth related to the specific surface chemistry of the metal ALD processes such as the catalytic decomposition of the incoming precursor molecules at the surface of the noble metals. It has been found that Pd and Pt ALD result in different NPs growth behaviors and size distributions. Pd NPs grow slower and present a more uni-modal and very narrow size distribution than Pt NPs. One hypothesis to explain these differences is that surface diffusion processes such as Ostwald ripening are more likely to happen for Pt ALD than for Pd ALD. The lower surface diffusion rate during Pd ALD can possibly be explained by pollution of the oxide surface by remaining ligands, leading to a slower but preferential ALD growth on the initially formed noble metal NPs and thus to a narrow size distribution.

The results and studies presented in this chapter indicate that surface diffusion processes play a major role in the formation of NPs and their final morphological properties. We have elucidated what we believe are the most important processes taking place during the initial stage of Pd and Pt ALD, namely the interaction between the precursor molecules and the oxide substrate surface, the surface diffusion of metal atoms and the formation of NPs, as well as the growth of the NPs themselves. The processes described are likely to happen for other noble metal ALD systems as well. We believe that a deep understanding of the surface chemistry and kinetics is required in order to further optimize the NPs morphology and to develop new ALD processes. In addition, the fact that Pd ALD yields NPs with uni-modal and narrow size distribution will be exploited in Chapter 5 and 6 where Pd NPs are used as core material for the synthesis of core/shell structured NPs.

References

- (1) Thomas, J. M.; Thomas, W. J. *Principles and practice of heterogeneous catalysis*; VCH: Weinheim, 1997; p. 669.
- (2) Bowker, M. *The Basis and Applications of Heterogeneous Catalysis*; Oxford University Press Inc.: New York, U.S.A., 1998; p. 96.
- (3) Prasad, R.; Kennedy, L. A.; Ruckenstein, E. *Catal. Rev. - Sci. Eng.* **1984**, *26*.
- (4) Richardson, J. T. *Principles of Catalyst Development*; Plenum: New York, U.S.A., 1989; p. 288.
- (5) Bell, A. T. *Science* **2003**, *299*, 1688–91.
- (6) Twigg, M. V. *Catalyst Handbook*; 2nd ed.; Manson: London, 1996; p. 608.
- (7) Piccolo, L.; Valcarcel, A.; Bausach, M.; Thomazeau, C.; Uzio, D.; Berhault, G. *Phys. Chem. Chem. Phys.* **2008**, *10*, 5504–6.
- (8) Yamauchi, M.; Ikeda, R.; Kitagawa, H.; Takata, M. *J. Phys. Chem. C* **2008**, *112*, 3294–3299.
- (9) Lal, S.; Link, S.; Halas, N. J. *Nat. Photonics* **2007**, *1*, 641–648.
- (10) Kašpar, J.; Fornasiero, P.; Hickey, N. *Catal. Today* **2003**, *77*, 419–449.
- (11) Jiang, X.; Huang, H.; Prinz, F. B.; Bent, S. F. *Chem. Mater.* **2008**, *20*, 3897–3905.
- (12) Osaka, T.; Iida, H.; Tominaka, S.; Hachisu, T. *Isr. J. Chem.* **2008**, *48*, 333–347.
- (13) Leskelä, M.; Ritala, M. *Angew. Chem. Int. Ed. Engl.* **2003**, *42*, 5548–54.
- (14) Hsueh, Y.-C.; Wang, C.-C.; Kei, C.-C.; Lin, Y.-H.; Liu, C.; Perng, T.-P. *J. Catal.* **2012**, *294*, 63–68.
- (15) Hales, J. H.; Kallesøe, C.; Lund-Olesen, T.; Johansson, A.-C.; Fanøe, H. C.; Yu, Y.; Lund, P. B.; Vig, a. L.; Tynelius, O.; Christensen, L. H. *Fuel Cells Bull.* **2012**, *2012*, 12–16.
- (16) Liu, C.; Wang, C.-C.; Kei, C.-C.; Hsueh, Y.-C.; Perng, T.-P. *Small* **2009**, *5*, 1535–8.
- (17) Shim, J. H.; Jiang, X.; Bent, S. F.; Prinz, F. B. *J. Electrochem. Soc.* **2010**, *157*, B793.

- (18) King, J. S.; Wittstock, A.; Biener, J.; Kucheyev, S. O.; Wang, Y. M.; Baumann, T. F.; Giri, S. K.; Hamza, A. V.; Baeumer, M.; Bent, S. F. *Nano Lett.* **2008**, *8*, 2405–9.
- (19) Christensen, S. T.; Feng, H.; Libera, J. L.; Guo, N.; Miller, J. T.; Stair, P. C.; Elam, J. W. *Nano Lett.* **2010**, *10*, 3047–51.
- (20) Weber, M. J.; Mackus, A. J. M.; Verheijen, M. A.; van der Marel, C.; Kessels, W. M. M. *Chem. Mater.* **2012**, *24*, 2973–2977.
- (21) Lu, J.; Low, K.-B.; Lei, Y.; Libera, J. A.; Nicholls, A.; Stair, P. C.; Elam, J. W. *Nat. Commun.* **2014**, *5*, 1–9.
- (22) Aaltonen, T.; Ritala, M.; Sajavaara, T.; Keinonen, J. *Chem. Mater.* **2003**, *15*, 1924–1928.
- (23) Elliott, S. D. *Langmuir* **2010**, *26*, 9179–82.
- (24) Mackus, A. J. M.; Leick, N.; Baker, L.; Kessels, W. M. M. *Chem. Mater.* **2012**, *24*, 1752–1761.
- (25) Lei, Y.; Lu, J.; Zhao, H.; Liu, B.; Low, K.-B.; Wu, T.; Libera, J. A.; Greeley, J. P.; Chupas, P. J.; Miller, J. T.; Elam, J. W. *J. Phys. Chem. C* **2013**, *117*, 11141–11148.
- (26) Mack, J. F.; Van Stockum, P. B.; Yemane, Y. T.; Logar, M.; Iwadate, H.; Prinz, F. B. *Chem. Mater.* **2012**, *24*, 4357–4362.
- (27) Setthapun, W.; Williams, W. D.; Kim, S. M.; Feng, H.; Elam, J. W.; Rabuffetti, F. A.; Poeppelmeier, K. R.; Stair, P. C.; Stach, E. A.; Ribeiro, F. H.; Miller, J. T.; Marshall, C. L. *J. Phys. Chem. C* **2010**, *114*, 9758–9771.
- (28) Shao, M.; Peles, A.; Shoemaker, K. *Nano Lett.* **2011**, *11*, 3714–3719.
- (29) Li, Y.; Somorjai, G. A. *Nano Lett.* **2010**, *10*, 2289–95.
- (30) Rioux, R. M.; Song, H.; Grass, M.; Habas, S.; Niesz, K.; Hoefelmeyer, J. D.; Yang, P.; Somorjai, G. A. *Top. Catal.* **2006**, *39*, 167–174.
- (31) Grass, M. E.; Joo, S. H.; Zhang, Y.; Somorjai, G. A. *J. Phys. Chem. C* **2009**, *113*, 8616–8623.
- (32) Stakheev, A. Y.; Mashkovskii, I. S.; Baeva, G. N.; Telegina, N. S. *Russ. J. Gen. Chem.* **2010**, *80*, 618–629.

- (33) Heiz, U.; Bullock, E. L. *J. Mater. Chem.* **2004**, *14*, 564.
- (34) Rainer, D. .; Goodman, D. . *J. Mol. Catal. A Chem.* **1998**, *131*, 259–283.
- (35) Datye, A. K.; Xu, Q.; Kharas, K. C.; McCarty, J. M. *Catal. Today* **2006**, *111*, 59–67.
- (36) Langereis, E.; Knoops, H. C. M.; Mackus, A. J. M.; Roozeboom, F.; van de Sanden, M. C. M.; Kessels, W. M. M. *J. Appl. Phys.* **2007**, *102*, 083517.
- (37) Jacobs, J. W. M.; Verhoeven, J. F. C. M. *J. Microsc.* **1986**, *143*, 103–116.
- (38) Williams, D. B.; Carter, C. B. *Transmission Electron Microscope. A Textbook for Materials Science*; Springer, Ed.; Springer-Verlag, 1996.
- (39) Reimer, L.; Kohl, H. *Transmission Electron Microscopy: Physics of Image Formation*; Springer-Verlag, 2008.
- (40) Pennycook, S. J.; Nellist, P. D. *Scanning Transmission Electron Microscopy, Imaging and Analysis*; Springer-Verlag, 2011; p. 762.
- (41) Kauko, H. Quantitative scanning transmission electron microscopy studies on heterostructured GaAs nanowires, Norwegian University of Science and Technology, 2013, p. 128.
- (42) Von Heimendahl, M.; Bell, W.; Thomas, G. *J. Appl. Phys.* **1964**, *35*, 3614.
- (43) Egerton, R. F. *Electron Energy-Loss Spectroscopy in the Electron Microscope*; 3rd ed.; Springer-Verlag, 1996; p. 491.
- (44) Hansen, T. W.; Wagner, J. B.; Hansen, P. L.; Dahl, S.; Topsøe, H.; Jacobsen, C. J. *Science (80-.)*. **2001**, *294*, 1508–1510.
- (45) Puspitasari, I.; Vendelbo, S.; Morana, B.; Mele, L.; Santagata, F.; Creemer, J.; Saputra, P.; Kooyman, P. J. In *EMC2012 Proceedings*; 2012.
- (46) Yokosawa, T.; Alan, T.; Pandraud, G.; Dam, B.; Zandbergen, H. *Ultramicroscopy* **2012**, *112*, 47–52.
- (47) Yokosawa, T.; Wu, M. Y.; Pandraud, G.; Dam, B.; Zandbergen, H. W. In *EMC2012 Proceedings*; 2012.
- (48) Schauermaun, S.; Nilius, N.; Shaikhutdinov, S.; Freund, H.-J. *Acc. Chem. Res.* **2013**, *46*, 1673–1681.

- (49) Enterkin, J. A.; Setthapun, W.; Elam, J. W.; Christensen, S. T.; Rabuffetti, F. A.; Marks, L. D.; Stair, P. C.; Poeppelmeier, K. R.; Marshall, C. L. *ACS Catal.* **2011**, *1*, 629–635.
- (50) Enterkin, J. A.; Poeppelmeier, K. R.; Marks, L. D. *Nano Lett.* **2011**, *11*, 993–997.
- (51) Sairanen, E.; Figueiredo, M. C.; Karinen, R.; Santasalo-Aarnio, A.; Jiang, H.; Sainio, J.; Kallio, T.; Lehtonen, J. *Appl. Catal. B Environ.* **2014**, *148-149*, 11–21.
- (52) Xie, J.; Yang, X.; Han, B.; Shao-Horn, Y.; Wang, D. *ACS Nano* **2013**, *7*, 6337–6345.
- (53) Lei, Y.; Lu, J.; Luo, X.; Wu, T.; Du, P.; Zhang, X.; Ren, Y.; Wen, J.; Miller, D. J.; Miller, J. T.; Sun, Y.-K.; Elam, J. W.; Amine, K. *Nano Lett.* **2013**, *13*, 4182–9.
- (54) Pashley, D. W. *Advan. Phys.* **1965**, *14*, 327.
- (55) Lewis, B. J. *Vac. Sci. Technol.* **1967**, *4*, 209.
- (56) Blackman, J. A.; Wilding, A. *Europhys. Lett.* **1991**, *16*, 115–120.
- (57) Venables, J. A. *Surf. Sci.* **1994**, *299-300*, 798–817.
- (58) Venables, J. A.; Spiller, G. D. T.; Hanbucken, M. *Rep. Prog. Phys.* **1984**, *47*, 399–459.
- (59) Venables, J. A. *Introduction to Surface and Thin Film Processes*; Cambridge University Press, 2000; p. 372.
- (60) Knoops, H. C. M.; Mackus, A. J. M.; Donders, M. E.; van de Sanden, M. C. M.; Notten, P. H. L.; Kessels, W. M. M. *Electrochem. Solid-State Lett.* **2009**, *12*, G34.
- (61) Galanikis, I.; Papanikolaou, N.; Dederichs, P. H. *Surf. Sci.* **2002**, *511*, 1–12.
- (62) Liu, F.; Hohage, M.; Lagally, M. G. *Surface and Interfaces of Solids. Encycl. Appl. Phys.*
- (63) Luth, H. *Surfaces and Interfaces of Solid materials*; Springer-Verlag, 1995; p. 495.
- (64) Bauer, E. *Zeitschrift fur Krist.* **1958**, *110*, 372–394.
- (65) Campbell, C. T. *Surf. Sci. Rep.* **1997**, *27*, 1–111.

- (66) Chatain, D.; Rivollet, I.; Eustathopoulos, N. *J. Chim. Phys.* **1983**, *86*, 561.
- (67) Todd, B. D.; Lynden-Bell, R. M. *Surf. Sci.* **1993**, *281*, 191.
- (68) Foiles, S. M.; Baskes, M. I.; Daw, M. S. *Phys. Rev. B* **1986**, *33*, 7983.
- (69) Kittel, C. *Introduction to Solid State Physics*; 8th Editio.; John Wiley & Sons, Inc.: Hoboken, NJ, USA, 2005.
- (70) Chen, P.; Wang, T. Y.; Luo, M. F. *J. Chem. Phys.* **2007**, *127*, 144714.
- (71) Elam, J. W.; Zinovev, A.; Han, C. Y.; Wang, H. H.; Welp, U.; Hryn, J. N.; Pellin, M. J. *Thin Solid Films* **2006**, *515*, 1664–1673.
- (72) Feng, H.; Libera, J. A.; Stair, P. C.; Miller, J. T.; Elam, J. W. *ACS Catal.* **2011**, *1*, 665–673.
- (73) Kessels, W. M. M.; Knoops, H. C. M.; Dielissen, S. A. F.; Mackus, A. J. M.; van de Sanden, M. C. M. *Appl. Phys. Lett.* **2009**, *95*, 013114.
- (74) Ten Eyck, G. A.; Senkevich, J. J.; Tang, F.; Liu, D.; Pimanpang, S.; Karaback, T.; Wang, G.-C.; Lu, T.-M.; Jezewski, C.; Lanford, W. A. *Chem. Vap. Depos.* **2005**, *11*, 60–66.
- (75) Ten Eyck, G. A.; Pimanpang, S.; Bakhru, H.; Lu, T.-M.; Wang, G.-C. *Chem. Vap. Depos.* **2006**, *12*, 290–294.
- (76) Yamauchi, M.; Kobayashi, H.; Kitagawa, H. *Chemphyschem* **2009**, *10*, 2566–76.
- (77) Goldstein, D. N.; George, S. M. *Appl. Phys. Lett.* **2009**, *95*, 143106.
- (78) Goldstein, D. N.; George, S. M. *Thin Solid Films* **2011**, *519*, 5339–5347.
- (79) Mackus, A. J. M.; Verheijen, M. A.; Leick, N.; Bol, A. A.; Kessels, W. M. M. *Chem. Mater.* **2013**, *25*, 1905–1911.
- (80) Zhang, Z. *Science (80-)*. **1997**, *276*, 377–383.
- (81) Campbell, C. T. *Acc. Chem. Res.* **2013**, *46*, 1712–1719.
- (82) Aaron Deskins, N.; Mei, D.; Dupuis, M. *Surf. Sci.* **2009**, *603*, 2793–2807.
- (83) Valero, M.; Raybaud, P.; Sautet, P. *Phys. Rev. B* **2007**, *75*, 1–12.

- (84) Kajikawa, Y. *Mater. Chem. Phys.* **2008**, *112*, 311–318.
- (85) Liu, X.; Bauer, M.; Bertagnolli, H.; Roduner, E.; van Slageren, J.; Phillipp, F. *Phys. Rev. Lett.* **2006**, *97*, 253401.
- (86) Watari, N.; Ohnishi, S. *Phys. Rev. B* **1998**, *58*, 1665.
- (87) Schmid, G.; Klein, N.; Morun, B.; Lehnert, A. *Pure Appl. Chem.* **1990**, *62*, 1175–1177.
- (88) Simonsen, S. B.; Chorkendorff, I.; Dahl, S.; Skoglundh, M.; Sehested, J.; Helveg, S. *J. Am. Chem. Soc.* **2010**, *132*, 7968–75.
- (89) Lee, H.; Mullings, M. N.; Jiang, X.; Clemens, B. M.; Bent, S. F. *Chem. Mater.* **2012**, *24*, 4051–4059.
- (90) Lee, D.-J.; Yim, S.-S.; Kim, K.-S.; Kim, S.-H.; Kim, K.-B. *Nanotechnology* **2011**, *22*, 095305.
- (91) Lu, J.; Stair, P. C. *Angew. Chem. Int. Ed. Engl.* **2010**, *49*, 2547–51.
- (92) Lee, D.-J.; Yim, S.-S.; Kim, K.-S.; Kim, S.-H.; Kim, K.-B. *Electrochem. Solid-State Lett.* **2008**, *11*, K61.
- (93) Oura, K.; Lifshitz, V. G.; Saranin, A. A.; Zotov, A. V.; Katayama, M. *Surface Science: An Introduction*; Springer-Verlag, 2003; p. 465.
- (94) Simonsen, S. B.; Chorkendorff, I.; Dahl, S.; Skoglundh, M.; Sehested, J.; Helveg, S. *J. Catal.* **2011**, *281*, 147–155.
- (95) Wynblatt, P.; Gjosteis, N. A. *Acta Met.* **1976**, *24*, 1165–1174.
- (96) Stoldt, C. R.; Jenks, C. J.; Thiel, P. A.; Cadilhe, A. M.; Evans, J. W. *J. Chem. Phys.* **1999**, *111*, 5157.
- (97) Budiman, R.; Ruda, H. *Phys. Rev. B* **2002**, *65*, 045315.
- (98) Lu, J.; Stair, P. C. *Langmuir* **2010**, *26*, 16486–95.
- (99) Goulas, A.; Ruud van Ommen, J. J. *Mater. Chem. A* **2013**, *1*, 4647.

Chapter 4

*Atomic Layer Deposition of High-Purity Palladium Films from Pd(hfac)₂ and H₂ and O₂ Plasmas**

Abstract: A plasma-assisted atomic layer deposition (ALD) process has been developed that allows for low temperature (100°C) synthesis of virtually 100% pure palladium thin films with low resistivity of $24 \pm 3 \mu\Omega \cdot \text{cm}$ on oxide substrates. This process is based on Pd(hfac)₂ (hfac= hexafluoroacetylacetonate) precursor dosing followed by sequential H₂ plasma and O₂ plasma steps in a so-called ABC-type ALD process. Gas-phase infrared spectroscopy studies revealed that the O₂ plasma pulse is required to remove carbon contaminants from the Pd surface that remain after the H₂ plasma reduction step. Omitting the O₂ plasma step, i.e. Pd ALD from Pd(hfac)₂ and H₂ plasma in a typical AB-like ALD process, leads to a carbon contamination of >10% and significantly higher resistivity values. From transmission electron microscopy it has also been observed that the ABC-type process leads to a faster nucleation of the Pd nanoparticles formed during the initial stage of film growth. As this novel process allows for the deposition of high purity Pd at low temperatures, it opens up prospects for various applications of Pd thin films and nanoparticles.

* This work has been published as: M. J. Weber, A. J. M. Mackus, M. A. Verheijen, V. Longo, A. A. Bol, and W. M. M. Kessels, *The Journal of Physical Chemistry C*, 118 (16), 8702–8711 (2014).

4.1 Introduction

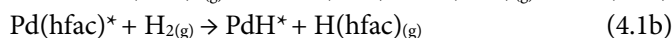
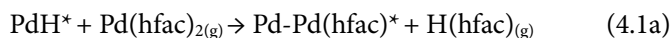
Atomic layer deposition (ALD) enables film growth with control at the atomic level due to its self-limiting surface chemistry during alternating precursor and co-reactant pulses. Therefore, ALD is nowadays considered as the method of choice to deposit conformal ultrathin films of a wide variety of materials for a growing number of applications.^{1,2} ALD is particularly suited to deposit binary compounds due to its binary reaction sequence while ternary and other multiple compound materials can be prepared by combining cycles of individual materials in a super-cycle fashion. ALD of single-element materials is typically much more challenging. Viable processes are often lacking, although ALD of several metals, in particular Pt-group metals, has been reported.³⁻⁵ Another challenge in metal ALD is the nucleation of the film on certain classes of materials.² In case of metal ALD on oxides, the nucleation takes typically place through the formation of islands (Volmer-Weber growth) as can be understood from surface energy considerations. The islands grow cycle after cycle and eventually coalesce to form a continuous film.⁶⁻⁸ This nucleation stage, and hence the formation of a closed film, can take many cycles and therefore limits the viability of ALD for ultrathin film growth significantly.

Among the metals which are currently receiving interest in the ALD community is palladium. Palladium thin films have a wide variety of nanoscale applications. For example, they can be applied as metal contacts⁹ in nanoelectronics or as materials for energy storage.¹⁰ Nanoscale Pd is also of interest due to its catalytic properties, for example in gas sensing applications.^{11,12} Many of these applications, can benefit from conformal deposition by ALD while low temperature processes are often preferred, especially when temperature-sensitive materials are involved.¹³

ALD of Pd is not trivial and ALD processes with different precursors have been attempted in recent years. Pd(keim)₂ (keim₂ = CF₃C(O)CHC(NBuⁿ)CF₃) with O₂ as co-reactant led to metallic Pd films, but with poor adhesion on alumina substrates and, more importantly, without reaching self-limiting growth when increasing the precursor pulse time.¹⁴ ALD was therefore not achieved for this process. ALD based on Pd(thd)₂ (thd = 2,2,6,6-tetramethyl-3,5-heptanedionato) and O₃ also led to unsatisfactory results, since the films were non-uniform¹⁵ and partly oxidized while they also revealed significant incorporation of precursor ligand fragments.¹⁶ To date, the best results have been achieved with Pd hexafluoroacetylacetonate Pd(hfac)₂ (Pd(C₅HF₆O₂)₂), which is currently the most adopted precursor for Pd ALD.^{7,17,18}

Unlike many other ALD processes for Pt-group metals, attempts to develop an ALD process for Pd using Pd(hfac)₂ as precursor and O₂ as co-reactant

were unsuccessful. As reviewed by Hämäläinen *et al.*, neither ALD of Pd or of its oxide, PdO, was achieved by this precursor when combined with O₂ dosing or exposure to any other oxidizing agent.¹⁹ The presence of fluorine in the precursor has been suggested as a possible reason.¹⁹ Instead, it has been reported that ALD processes based on Pd(hfac)₂ require a true reducing agent. In the pioneering work of Senkevich *et al.*, it was shown that Pd can be deposited by an ALD process using H₂ as co-reactant.²⁰ H₂ is known to dissociate on a Pd surface²¹ and the dissociated H₂ can reduce the Pd²⁺ metal ions to Pd⁰. Moreover, the H atoms react with the hfac ligands to create Hhfac reaction products in an ALD chemistry such as:



where the asterisks (*) denote the surface species. This process was demonstrated for ALD of Pd on an electron-beam deposited Ir surface and on a Pd “seed” layer prepared by Pd(hfac)₂ and glyoxylic acid.²⁰ Actually, the issue of this process is that it needs a starting surface that can dissociate H₂, such as an Ir or Pd surface, in order to initialize ALD growth.

Elam and co-workers demonstrated that the nucleation and growth of Pd films can be achieved also on oxide surfaces using stronger reducing agents than H₂ gas. Using formalin as co-reactant, they successfully deposited Pd films on Al₂O₃, which were found to be pure and to have good material properties.¹⁸ This Pd ALD process based on Pd(hfac)₂ and formalin dosing was however only effective at 200°C and did not result in growth at 100°C. It also showed nucleation difficulties on oxide surfaces. In case of Pd ALD from Pd(hfac)₂ and formalin on Al₂O₃, the reaction is likely to start with the precursor Pd(hfac)₂ adsorbing at hydroxyl groups.^{7,18,22} Recent studies^{23,24} have shown that this Pd(hfac)₂ adsorption results in both Pd(hfac)* and Al(hfac)* surface species. The Al(hfac)* species act as site blockers for precursor adsorption during the following ALD cycles. This surface poisoning by hfac ligands has been found to be partly responsible for the long nucleation delay usually observed in Pd ALD.²⁴

An alternative to formalin is to make use of H atoms, for example generated by a H₂ plasma. Plasmas, consisting of electrons, ions, radical species and other excited neutrals, provide additional reactivity to the surface reducing energy barriers for surface reactions and allowing for processes at lower temperature than for strictly thermal ALD processes.²⁵ When using a H₂ plasma as co-reactant during Pd ALD, it directly provides the H atoms necessary for the Pd to nucleate and the ALD reactions to occur even on oxide surfaces. Ten Eyck *et al.*

successfully demonstrated that the use of plasmas (H_2 plasmas and $\text{H}_2\text{-N}_2$ plasmas) allows the Pd nucleation from $\text{Pd}(\text{hfac})_2$ to occur on various surfaces at low temperatures (80°C).^{26,27} However, the material resulting from Pd plasma-assisted ALD process was not characterized in detail in their work.

In this article, the deposition of Pd films on Al_2O_3 by plasma-assisted ALD is further explored. The plasma-assisted ALD process based on $\text{Pd}(\text{hfac})_2$ and H_2 plasma dosing, a so-called AB-type ALD process, is first investigated in more detail than done by Ten Eyck *et al.* More extensive analysis of the material properties revealed that the films prepared by this “AB process” contain a relatively high fraction of carbon. Therefore, a second process was developed which consisted of three reaction steps per cycle. This is a so-called three-step cycle or ABC cycle, as opposed to a typical, binary AB cycle. The co-reactant step in this “ABC process” consisted of H_2 plasma exposure followed by O_2 plasma exposure. Similar three-step ALD cycles have already been successfully applied for the deposition of Rh,¹⁵ Pt^{5,15,28}, Pd¹⁵ and Ir^{15,29} thin films. However in these cases the O_2 -based step was followed by a H_2 -based step (either H_2 gas or H_2 plasma) while in this work it is the other way around: ALD of Pd is achieved when the H_2 plasma is followed by the O_2 plasma. When reversing the order of co-reactants, i.e., first the O_2 plasma and afterwards the H_2 plasma, no film growth could be achieved (see Appendix 4.5.1). In addition to a study of the material properties, revealing significantly improved Pd thin films for the ABC process over the AB process, gas-phase infrared spectroscopy studies were carried out yielding insight into the reaction mechanism for this newly developed ABC process. Moreover, the nucleation of Pd prepared by both the AB and the ABC processes was studied by transmission electron microscopy (TEM) revealing faster nucleation of Pd on Al_2O_3 when using the ABC process. It was therefore established that Pd with improved material and process properties can be obtained with the ABC process, even well below substrate temperatures of 200°C .

4.2 Experimental section

All depositions have been carried out in an home-built open-load ALD reactor, described elsewhere.³⁰ Briefly, the reactor chamber is connected to a remote inductively coupled plasma source and a turbomolecular pump through gate valves. The base pressure was approximately 1×10^{-6} Torr. The precursor $\text{Pd}(\text{hfac})_2$ was obtained from Sigma-Aldrich and used as received. It was dosed with Ar as a carrier gas from a stainless steel bubbler connected to the reactor which was heated to 50°C in order to get an adequate vapor pressure. If not specified other-

wise, the substrate holder was heated to 100°C and the reactor walls were permanently heated to approximately 80-90°C to avoid condensation.

The ALD precursor step, similar for both ALD processes presented here, consisted of 3 s of Pd(hfac)₂ dosing, which was sufficient to achieve saturation. An Ar purge step and a pump step of 5 s each were applied directly after the precursor pulse. For the AB process, hydrogen gas at a pressure of 8 mTorr was subsequently dosed for 2.5 s, followed by a H₂ plasma at 100 W which was applied for 5 s. The ALD cycle was completed with a 6 s pump down time. The ABC process, had the same H₂ gas and H₂ plasma step, but subsequently O₂ gas at 8 mTorr was introduced for 1 s before a O₂ plasma at 100 W was applied for 1 s. The O₂ step was separated from the H₂ step by a pumping time of 6 s. The reactor chamber was then pumped down for 8 s to complete the ALD cycle.

The depositions were carried out on Si wafers covered with 250 nm Al₂O₃ prepared by ALD. Before each deposition, the substrates were first exposed to an O₂ plasma at 100 W for 3 minutes in order to remove the surface C contamination.

The composition of the films was analyzed by X-ray photoelectron spectroscopy (XPS) on a ThermoFisher Scientific K Alpha XPS equipped with an Al K α source (X-ray spot 400 μm^2). Depth profiling was carried out through Ar ion sputtering. The elemental composition of the Pd film has been also determined by Rutherford backscattering spectrometry (RBS) at AccTec B.V. A monoenergetic beam of 2 MeV ⁴He⁺ ions was used at normal incidence. The microstructure of the films was studied using grazing incidence X-ray diffraction (GI-XRD) with a PANalytical X'pert PRO MRD equipped with a Cu K α source (1.54 Å radiation). Moreover, the thickness and mass density have been measured by X-ray reflectometry (XRR) on the same diffractometer. The root-mean square (RMS) surface roughness was determined over a 2x2 μm^2 area by atomic force microscopy (AFM) using a NT-MDT Solver P47 SPM. Electrical resistivity was measured at room temperature with a Signatone four-point probe (FPP) in combination with a Keithley 2400 sourcemeter acting both as a voltage meter and a current source.

To monitor the Pd film thickness *in-situ* during the ALD process, spectroscopic ellipsometry (SE) measurements were carried out every 10 ALD cycles using a J.A. Woollam, Inc M2000U visible and near-infrared ellipsometer (0.7 – 5.0 eV) at an angle of incidence of 68°. The SE data were analyzed by modeling the dielectric functions of the films with a Kramers-Kronig-consistent B-spline parametrization.³¹⁻³⁴

Gas phase infrared spectroscopy measurements were carried out with a Bruker Optics Vector 22 FT-IR, which has a mid-infrared radiation source that

produces a broad spectrum of infrared light ($\sim 4000\text{-}350\text{ cm}^{-1}$). The infrared beam was passed through the ALD reactor through KBr windows which could be protected by gate valves. At the other side of the reactor, the infrared light was focused on a liquid N_2 cooled Mercury Cadmium Telluride (MCT) detector (Bruker D 313, Range: $10000\text{-}750\text{ cm}^{-1}$) using a gold parabolic mirror. See Ref. ³⁵ for more details. During the infrared spectroscopy measurements, the reactions products were trapped in the reaction chamber by closing the gate valve to the turbomolecular pump. Measurements were carried out with a resolution of 4 cm^{-1} and with 64 scans per measurement. To improve the signal-to-noise ratio data was averaged over multiple measurements. Every measurement took place after three full ALD cycles in order to (re)condition the reactor every time. The spectra shown in this work are differential spectra showing the changes after carrying out one single process step.

The nucleation of the Pd films was studied using scanning transmission electron microscopy (STEM) using a FEI Tecnai 300 kV system in high angle annular dark field (HAADF) mode. The substrates used were Si_3N_4 TEM windows covered by 3 nm Al_2O_3 prepared by ALD. Measurements took place on samples on which Pd was deposited with a varying number of cycles.

4.3 Results and discussion

4.3.1. Material properties for the AB process

The material properties of the ALD process based on $\text{Pd}(\text{hfac})_2$ and H_2 plasma dosing, the so-called “AB process”, were investigated first for a substrate temperature of 100°C . The results are summarized in Table 4.1.

Table 4.1. Properties of Pd films prepared by plasma-assisted ALD using Pd(hfac)₂ as precursor and a H₂ plasma (“AB process”) or a H₂ plasma followed by a O₂ plasma (“ABC process”) as co-reactants. The substrates were Si(100) wafers with 250 nm thick Al₂O₃ films and the substrate temperature was 100°C. *In situ* spectroscopic ellipsometry (SE), X-Ray reflectometry (XRR), atomic force microscopy (AFM), Rutherford backscattering spectroscopy (RBS), X-Ray photoelectron spectroscopy (XPS) and four-point probe (FPP) measurements were used for analysis of the films. The films were ~20 nm thick, except for the XPS analysis which took place on films of ~30 nm in thickness.

Properties	Analysis technique	AB process	ABC process
Growth-per-cycle (Å/cycle)	SE	0.17±0.05	0.13±0.05
Growth-per-cycle (atoms.cm ⁻² .cycle ⁻¹)	RBS	(0.9±0.1)×10 ¹⁴	(0.7±0.1)×10 ¹⁴
Mass density (g/cm ³)	XRR	11.0±0.5	11.7±0.5
Resistivity (μΩ.cm)	FPP	48±5	24±3
C content (at. %)	XPS	14±3	< 2 ^a
	RBS	11±5	< 5 ^a
RMS roughness (nm)	AFM	1.0±0.3	1.3±0.3
	XRR	1.3±0.3	1.4±0.3

^a Detection limit of the technique

One of the most striking results is that the films contain a relatively high C content. RBS, which is generally not very sensitive to light elements such as C when using 2 MeV ⁴He⁺ ions, yielded a C content of 11±5 at.%, whereas XPS revealed 14±3 at.%. The XPS depth profiling results, carried out on a film with a thickness of 41 nm, are shown in Figure 4.1a.

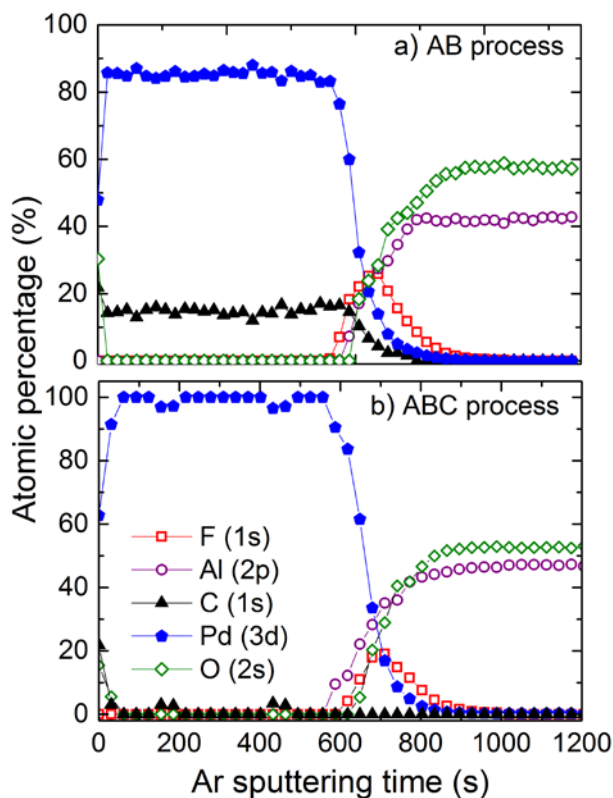


Figure 4.1. XPS depth profile of the Pd films prepared by ALD with (a) the AB process, and (b) the ABC process (A: Pd(hfac)₂ precursor step; B: H₂ plasma step; C: O₂ plasma step). The films were ~30 nm thick and the substrates were Si(100) wafers covered with 250 nm thick Al₂O₃ films prepared by ALD. The electron configurations of the electrons related to the spectral peaks used for composition analysis have been indicated.

The C content is constant over the full thickness of the film showing that C atoms from the precursor ligands were incorporated in the film during growth. Extending the H₂ plasma exposure in the ALD cycle from 5 s to 20 s did not affect the level of C contamination. XPS revealed also traces of F at the interface between Pd and the Al₂O₃ substrate. This points to incomplete ligand removal during the first ALD cycles, possibly related to the presence of Al(hfac)* surface groups.^{23,24}

The resistivity of the Pd films was determined by four-point probe (FPP) measurements. These revealed a resistivity of $48 \pm 5 \mu\Omega \cdot \text{cm}$ even for films thicknesses up to ~40 nm (Pd bulk resistivity is $9.8 \mu\Omega \cdot \text{cm}$ ³⁶). For the formalin-based

process, Elam *et al.* obtained a resistivity of 14 $\mu\Omega\cdot\text{cm}$ for a 42 nm film prepared at 200°C.¹⁸ The presence of carbon within the film is likely responsible for the higher resistivity for the films prepared by the AB process.

GI-XRD measurements were carried out in order to study the microstructure of the films. The spectrum, shown in Figure 4.2a, revealed that the films had the face-centered cubic (fcc) crystal structure.

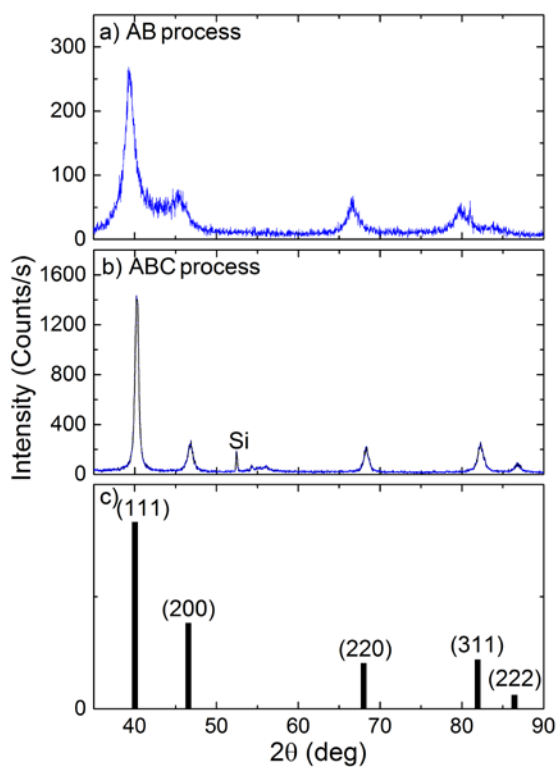


Figure 4.2. Grazing incidence XRD spectrum of (a) a 16 nm Pd film deposited by the AB process; (b) a 15 nm Pd film deposited by the ABC process; and (c) the corresponding Pd powder spectrum. The substrates for (a) and (b) were Si(100) wafers covered with 50 nm thick Al₂O₃ films prepared by ALD. All peaks could be assigned to the face-centered-cubic (fcc) Pd crystal structure. The acquisition time used to generate the spectrum in (a) was 8 hours while that for the spectrum in (b) was 55 hours leading to a different signal-to-noise ratio.

From the (111) peak full width at half maximum (FWHM), an average grain size of 4 ± 1 nm was extracted. Furthermore, when compared to the powder spectrum in Figure 4.2c, it is clear that the peaks are shifted to slightly lower 2θ

angles. The deviation is constant for all peaks implying an isotropic expansion of the lattice. The calculated unit cell dimension of 0.398 nm is larger than for pure Pd (0.391 nm) and the incorporation of C atoms in the Pd film can be responsible for this lattice expansion.^{37,38} Using formalin as co-reactant, Elam *et al.* obtained pure Pd films with a fcc crystal structure without a peak shift in the XRD spectrum.¹⁸ Ten Eyck *et al.*, on the other hand, obtained amorphous Pd films for their H₂ plasma-based process, most likely due to a large C content.²⁶ The mass density of the films prepared by the AB process was 11.0±0.5 g/cm³ (see Table 1), which is somewhat lower than the mass density of bulk Pd (12.0 g/cm³).³⁶

AFM measurements revealed a RMS roughness of 1.0 nm for a 17 nm thick film, whereas the RMS roughness was 1.3 nm for a 41 nm. These values can be compared to a RMS roughness of 4.2 nm for a 42 nm film synthesized by thermal ALD.¹⁸ This demonstrates that plasma-assisted ALD is a technique that can be used to synthesize smooth Pd films.

From these results it can be concluded that the Pd films prepared by the AB process contain a relatively high C content. One possible origin of this high C content is the decomposition of the hfac precursor ligands on the Pd surface,^{39,40} which is catalytically active towards breaking of C-C, C-O and C-H bonds.^{41,42} Previous studies on chemical vapor deposition of Cu(hfac)₂ have shown that the chemical reactions between hfac and transition metal surfaces are complex and Cu(hfac)₂ and Hhfac decomposition products (CF₃, CO, HF and fluorine containing fragments) were evident above 300 K on Pt⁴³ and Cu⁴⁰ surfaces. Lin *et al.* also observed the decomposition of surface-bound hfac ligands at 300 K on Cu, leaving small amounts of graphitic carbon at the surface.⁴⁴ Most of these decomposition products should desorb from the surface around 300 K,⁴³ but there are potentially some C containing reaction products that remain. Apparently the H₂ plasma is not effective in fully removing these C species from the surface. Another possible reason for the C contamination in the films is that the volatile reaction products are dissociated in the H₂ plasma and redeposited on the surface during the plasma step.⁴⁵ However, it was verified that the (thermal) process based on Pd(hfac)₂ and H₂ gas, carried out on a Pt seed layer, also contained a high C content (and overall similar material properties) as the AB process with H₂ plasma (see Appendix 4.5.2). This indicates that decomposition of the hfac ligands at the Pd surface is mainly responsible for the C contamination observed.

4.3.2. Material properties for the ABC process

As O₂ plasmas are known to be very effective for the removal of organic contaminants on various surfaces, it is plausible that an O₂ plasma would be more effi-

cient in removing the C atoms from the surface. O₂ plasmas have already been used as co-reactant in other ALD processes of Pt-group metals such as Pt and Ru.^{3,5,46} Due to the high reduction potentials of the Pt-group metals, O₂ plasma-based processes can still yield metal films and not their oxide counterparts.⁴⁷ Moreover, a potential oxidized surface (region) can be reduced by precursor ligands during the next precursor dosing step. Therefore, a new ALD process was developed in which the H₂ plasma was followed by an O₂ plasma. This so-called “ABC process” is identical to the H₂ process with the exception that there is an additional O₂ plasma step after the H₂ plasma step. The idea behind this process is that the majority of the hfac ligands are removed by the H₂ plasma, after which the remaining C atoms are eliminated from the surface by the O₂ plasma. Potentially oxidized top atomic layers can be reduced during the next cycle. The material properties resulting from this ABC process were again investigated for a substrate temperature of 100°C and are summarized in Table 1.

With RBS no C could be detected in the films above the detection limit (~5 at.%) of the technique while the XPS depth profiling results shown in Figure 1b revealed only a small C signal on top of the film, most likely adventitious carbon resulting from the air exposure of the samples. No C could be detected in the bulk of the film above the XPS detection limit of ~2 at%. Similar to the AB process, again traces of F were found at the interface between Pd and the Al₂O₃, most likely due to Al(hfac)* surface groups that poison the Al₂O₃ surface. It is also noted that no O could be detected in the films showing that the films are virtually 100% pure Pd. These results indicate therefore that the additional O₂ plasma is very effective in removing C from the surface and that the ABC process is able to deposit high-purity Pd films.

A higher purity of the films also showed an effect in the FPP measurements which revealed a resistivity of 24±3 μΩ.cm. This resistivity is two times lower than the one obtained with the AB process (48±5 μΩ.cm). The improved resistivity can also (partially) be attributed to a difference in microstructure of the Pd films. The GI-XRD spectrum, shown in Figure 4.2b, revealed a fcc crystal structure. This spectrum clearly differs from the powder spectrum in Figure 2c. Firstly, the (111) peak in Figure 4.2b has a much higher relative intensity than it would have in the case of absence of texture (Figure 4.2c). This peak is present at ~40°. In the GI-XRD measurement geometry used, we detect the (111) planes that are oriented ~20° away from the substrate surface orientation. The high intensity combined with the ~20° angle with respect to the surface normal implies a broad distribution of (111) orientations around the surface normal, i.e. an imperfect (111) texture. Secondly, the (111) peak is much sharper than the other peaks, implying that the (111) oriented grains have a larger average grain size (of

16±4 nm) than the crystals with other orientations. This grain size is significantly larger than the grain size obtained for the H₂ process. Summarizing these observations, we can conclude that in this thin layer a clear onset to (111) texture is present. Still, all peaks present in the powder spectrum are also present in Figure 4.2b, implying that part of the ensemble of crystals has random orientations. Possibly, this contribution is coming from the nucleation layer. The value of the unit cell dimension of 0.390 nm, extracted from the peak positions, is also a proof of an improved crystallinity of the films. The RMS roughness value obtained from AFM measurements was 1.3±0.3 nm for a film thickness ~20 nm. From these results, it can be concluded that the ABC process leads to improved material properties compared to those obtained by the AB process.

4.3.3. Gas-phase infrared spectroscopy

In our previous work, gas-phase infrared spectroscopy was found to be a powerful method to obtain understanding of the surface chemistry during Pt ALD.^{28,48} Therefore, the method was employed here to obtain information on the reaction products created in the various steps of the ALD cycle of the ABC process and hence to gain insight into the reaction mechanisms taking place. As outlined earlier, it is expected that the H₂ plasma removes the majority of the hfac ligands present on the surface after Pd(hfac)₂ dosing but that the O₂ plasma is necessary to eliminate all C atoms remaining on the surface after the H₂ plasma step. The gas-phase spectra recorded for the ABC process are depicted in Figure 4.3.

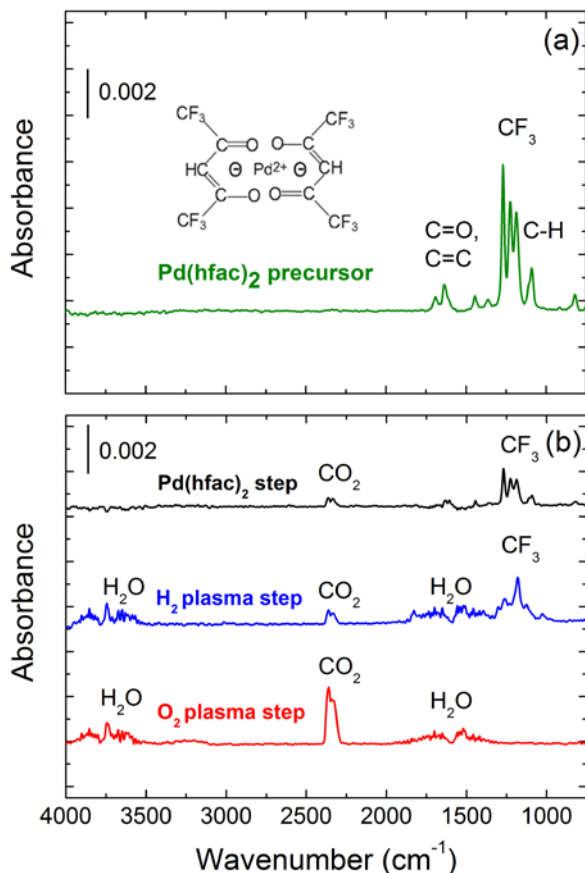


Figure 4.3. Differential spectra obtained by gas-phase infrared spectroscopy for (a) the Pd(hfac)₂ precursor and (b) the various steps in the cycle of the ABC process: the Pd(hfac)₂ step; the H₂ plasma step; and the O₂ plasma step. The resolution was 4 cm⁻¹ and every spectrum was averaged over 3 ALD cycles with 64 scans per measurement. The main absorbance peaks have been assigned in the graph. The inset in (a) shows the Pd(hfac)₂ precursor.

These are differential spectra showing the change in gas phase species after one single step of the ALD process. The substrate and the reactor walls were all heated to 100°C. Figure 3a shows the spectrum corresponding to the precursor molecules. This “precursor only” spectrum was obtained after dosing the precursor into the reactor chamber after making sure that the surface was completely saturated with precursor species. The spectra in Figure 4.3b show the gas phase species as present in the reactor chamber after carrying out the three steps of the ALD cycle for the ABC process, i.e., the precursor/reactant molecules as well as the reaction products released from the surface during the Pd(hfac)₂ dos-

ing step, the H₂ plasma step and the O₂ plasma step. Prior to the measurements, at least three cycles of the ABC process were carried out in order to condition the reactor while the data in the spectra were averaged over three cycles to improve the signal-to-noise ratio. Extended pulses and measurement times were also required, not only for a good signal-to-noise ratio, but also to ensure that the film growth on the reactor walls was saturated (and not only on the substrate holder). The precursor-only spectrum in Figure 4.3a shows several absorption peaks in the region 1100-1350 cm⁻¹, which can be attributed to CF₃ symmetric and asymmetric stretching vibrations.^{49,50} The peak present at 1108 cm⁻¹ can be assigned to the bending vibration of C-H.^{50,51} The other peaks visible in the region between 1450 and 1700 cm⁻¹ are due to the stretching vibrations of C=C^{23,49-51} and C=O.^{50,51} All these absorption peaks result from the Pd(hfac)₂ precursor.

The spectrum recorded after the precursor pulse in Figure 4.3b, which was taken as part of a sequence of full ALD cycles, shows CF₃ symmetric and asymmetric stretching vibrations, very similar to those as observed for precursor-only. These are a signature of the precursor and they imply that Pd(hfac)₂ dosing reached saturation because not all precursor molecules were consumed. The spectrum also shows a peak due to CO₂ at 2360 cm⁻¹ wavenumbers. The O atoms in the CO₂ can stem from the precursor itself but also from oxidized top atomic layers after the O₂ plasma step from the previous ALD cycle. The ligands of the incoming precursor will oxidize when they react at the PdO* surface, while reducing the oxidized top atomic layers at the same time. This is similar to observations by gas-phase infrared spectroscopy for the Pt ALD process from MeCpPtMe₃ and O₂ gas.⁴⁸

The spectrum after the H₂ plasma step also shows a strong signal in the region of 1100-1350 cm⁻¹ mainly related to CF₃ stretching vibrations. The signature of the peaks is slightly different from those observed for precursor-only and for the precursor dosing step. Likely these absorption peaks can be related to Hhfac reaction products created during the H₂ step but they can also potentially be due to fragments of the ligand that contain C-C, C-H, C-O or C-F bonds.⁵⁰ Such fragments can originate from ligands that get dissociated in the plasma or decomposed at the catalytic Pd surface.^{43,44} Furthermore broad absorption bands are present in the regions around 1570 cm⁻¹ and 3780 cm⁻¹ which can be attributed to the formation of H₂O during the H₂ plasma step. These, as well as the CO₂ absorbance peaks around 2360 cm⁻¹ indicate the presence of O atoms at the surface after the precursor step. The O atoms could originate from the precursor ligands themselves or they can be a remnant of the O₂ plasma step in the previous ALD cycle. For example, the reduction of the oxidized top atomic layers might not yet be complete after the precursor dosing step.

The absorbance spectrum recorded after the O₂ plasma pulse clearly shows the release of H₂O and CO₂ reaction products from the surface. This spectrum confirms the necessity of using an O₂ plasma step after the H₂ plasma step. The relatively large absorption peak of CO₂ shows that a significant fraction of the hydrocarbon fragments remaining from the precursor ligands were not eliminated during the H₂ plasma step. If the O₂ plasma step would have been omitted (i.e., the AB process), these C species would have remained on the surface and would have been incorporated into the Pd film after one cycle. This implies that the precursor fragments that are left after the H₂ plasma step pollute the surface, and thereby increase the C contamination within the film deposited with the H₂ plasma-assisted process. The observations therefore confirm that the use of an O₂ plasma step after the H₂ step is essential for decreasing the C content and hence for depositing high purity Pd films by plasma-assisted ALD.

4.3.4. Nucleation and steady-state film growth

As mentioned in the Introduction, the nucleation of metal films by ALD can be manifesting itself by island growth and a long delay before film closure is achieved. Therefore, the nucleation phase and steady-state film growth were considered separately.

Scanning transmission electron microscopy (STEM) has been used to study nucleation and film closure for both the AB and ABC process. High angle annular dark field – STEM (HAADF-STEM) images are shown in Figure 4.4a (AB process) and Figure 4.4b (ABC process) after applying 100, 200, 400, 600 and 800 ALD cycles.

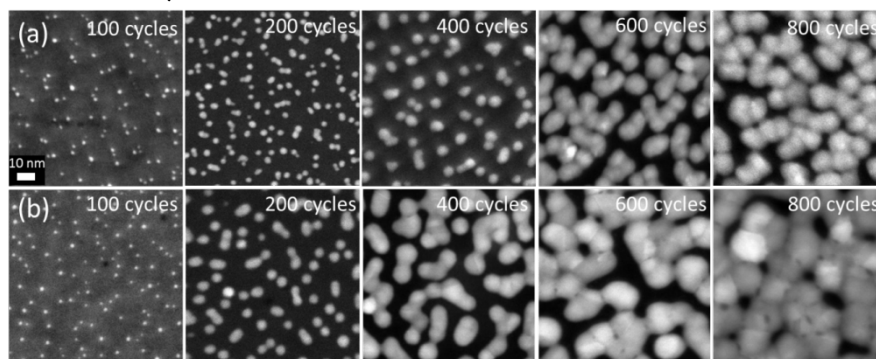


Figure 4.4. HAADF-STEM images of Pd nanoparticles obtained by applying 100, 200, 400, 600 and 800 ALD cycles of (a) the AB process and (b) the ABC process. The substrates were Si₃N₄ TEM windows covered with a 3 nm thick Al₂O₃ film prepared by ALD.

After 100 cycles, these figures clearly reveal island growth and a high density of nanoparticles (NPs). For both processes, their density is $(1.0 \pm 0.5) \times 10^{12} \text{ cm}^{-2}$ whereas their average size is $3 \pm 1 \text{ nm}$. After 200 cycles, the Pd NPs already begin to coalesce, and this phenomenon is slightly faster for the ABC process, leading to a larger surface coverage fraction, as shown in Figure 4.5.

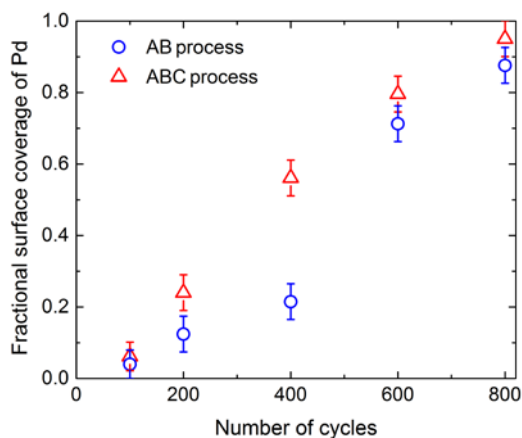


Figure 4.5. Fractional surface coverage of Pd as a function of the number of cycles for the AB and ABC processes. The data have been extracted from the STEM images in Figure 3.4.

This figure, which is based on the data in Figure 4.4, reveals that surface coverage for the ABC process is slightly enhanced over the surface coverage for the AB process when comparing data obtained at the same number of cycles. This appears to be especially the case after 400 cycles, where an absolute difference of 25% was observed. After 800 cycles, both films were almost reaching closure as can be concluded from the TEM images and the corresponding surface coverage fractions of 0.88 and 0.95 for the AB and the ABC processes, respectively.

The modest, but significant difference in particle growth rate between two processes might be a result of various effects taking place during the O_2 plasma step which is the only difference between the two processes. For example, it has been reported in the literature that adsorption of the $\text{Pd}(\text{hfac})_2$ precursor on Al_2O_3 leads to $\text{Al}(\text{hfac})^*$ surface species that inhibit the Pd particles to grow.²⁴ The O_2 plasma facilitates the removal of these poisoning precursor fragments, possibly allowing for more precursor molecules to adsorb at the surface. By surface diffusion, this increased availability of precursor molecules could increase the growth of the Pd NPs. Another possible effect caused by the O_2 plasma is

enhanced diffusion of the Pd surface species. For example, for ALD of Pt from (MeCp)PtMe₃ precursor and O₂ gas it was found that the surface diffusion of Pt species was enhanced in the presence of oxygen. This was most likely due to the formation of PtO_x species, leading to faster aggregation of Pt atoms into metal clusters that catalyze the surface reactions of ALD growth.⁵² A similar effect could occur for Pd when using the ABC process. A possible third effect is that the O atoms chemisorbed at the surface of the Pd NPs can eliminate hydrocarbon fragments more efficiently during the precursor step due to combustion-like reactions. This can potentially increase the density of active sites for precursor adsorption and enhance the growth rate of the NPs.⁵³

RBS yields the areal density of the Pd atoms in the film in terms of Pd atoms per cm². When divided by the number of cycles carried out to prepare the films, a first approximation of the growth-per-cycle (GPC) during steady state film growth can be obtained. This is only a first approximation as reduced Pd growth during the nucleation phase is not taken into account in this calculation. As shown in Table 4.1, the corresponding values of the growth-per-cycle are $(0.9 \pm 0.1) \times 10^{14}$ and $(0.7 \pm 0.1) \times 10^{14}$ Pd atoms per cycle and per cm² for the AB and ABC process, respectively. This indicates an enhanced Pd growth for the AB process compared to the ABC process, certainly when taking the slightly slower film closure for the AB process into account (see Figures 4.4 and 4.5).

Information on the growth-per-cycle during steady-state film growth has also been obtained by *in situ* spectroscopic ellipsometry (SE). Analysis of the SE data relies on optical modeling and due to the simplicity of the model, not taking into account the island growth during the nucleation phase, the thickness values during the nucleation phase are not very reliable. However the increase in thickness during steady-state growth is reliable and from this data the GPC during steady-state film growth can be extracted (see Appendix 4.5.3). After the nucleation phase the growth-per-cycle was constant for both the AB process and the ABC process with values of 0.17 ± 0.01 Å/cycle and 0.13 ± 0.01 Å/cycle, respectively. These values can be compared to the GPC of 0.22 Å/cycle reported by Ten Eyck *et al.* for plasma-assisted ALD on SiO₂²⁶ and 0.2 Å/cycle reported by Elam *et al.* for the formalin-based process at 200°C.¹⁸

Both RBS and *in situ* SE indicate that the growth-per-cycle is lower for the ABC process than for the AB process. In terms of thickness, the difference between the two processes cannot be attributed to the incorporation of a significant C content in the Pd films obtained by the AB process because with RBS the actual GPC-value in terms of Pd atoms is obtained. Instead, the difference between the two processes is likely due to the nature of the film surface after carrying out a full ALD cycle. For the AB process, it is likely that the Pd is covered by H atoms

after the H₂ step^{54,55} whereas for the ABC process the film surface consists most likely of PdO_x after the O₂ step.⁵⁶⁻⁵⁸ Apparently, Pd(hfac)₂ adsorption on the PdH* surface is more effective than on a PdO* surface. On the PdH* surface it can be expected that ligand elimination through reaction (4.1a) is prominent whereas combustion-like reactions will most likely take place for the precursor ligands for the PdO* surface.

4.3.5. Temperature dependence

The investigation of the material properties provided by the ALD processes was extended over a larger substrate temperature range with insight into the film growth and surface chemistry obtained. Therefore the growth-per-cycle, resistivity and C content of the films prepared by both the AB process and ABC process were studied for substrate temperatures between 50 and 200°C. The resulting data, obtained for Pd films of 20-25 nm in thickness, are presented in Figure 4.6.

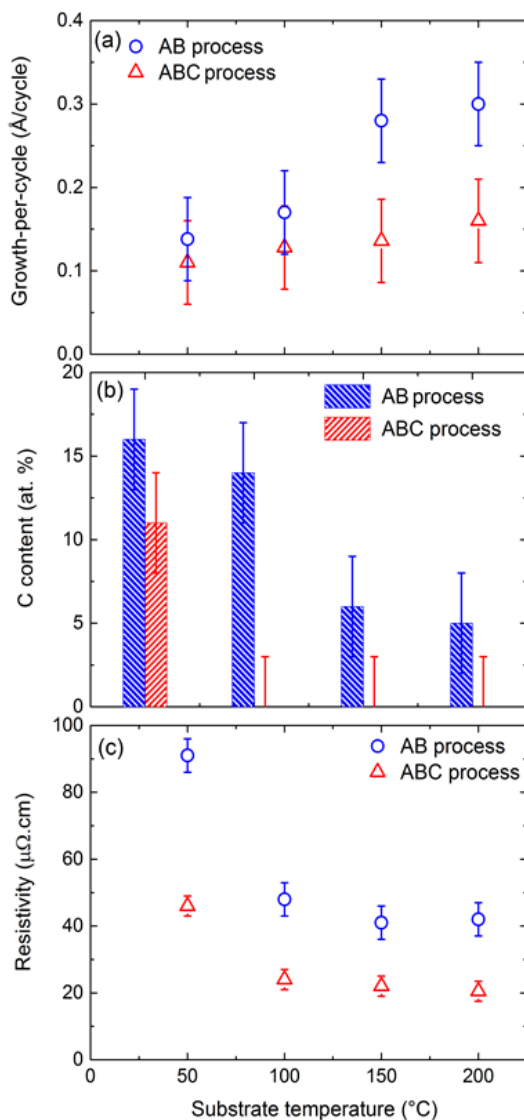


Figure 4.6. (a) Growth-per-cycle (GPC), (b) C content and (c) resistivity as a function of substrate temperature for the AB and the ABC processes. The films thicknesses were between 20 and 25 nm. The substrates were Si(100) wafers covered with 250 nm Al₂O₃ films prepared by ALD. The GPC values were determined from the change in film thickness with number of ALD cycles during steady-state growth as monitored by *in situ* spectroscopic ellipsometry (SE). The resistivity values were determined by four point probe measurements. The C content was determined by X-ray photoelectron spectroscopy (XPS). The C content of the films prepared by the ABC process between 100 and 200°C was below the detection limit of 2 at.% of XPS.

The GPC, extracted from *in situ* SE, was determined for steady-state film growth. As is shown in Figure 4.6a, the growth-per-cycle for the ABC process is lower than the one of the AB process over the whole temperature range and not only for the case of 100°C as discussed in the previous section. This is consistent with the hypothesis that Pd(hfac)₂ adsorption on the PdH* surface is more effective than on a PdO* surface. Moreover for both processes, an increase of the growth-per-cycle with the temperature is observed, especially for the AB process that presents a GPC of 0.30±0.05 Å/cycle at 200°C. This indicates that one step involved in the adsorption of the Pd(hfac)₂ precursor is thermally activated, e.g. ligand elimination from the incoming precursor or the creation of reactive sites during the reactant steps. Such an increase has been observed before,¹⁴ however, the exact nature of the increased GPC values at higher temperatures is not yet understood.

The fact that elimination of ligand fractions from the surface is thermally activated can be concluded from the C content of the films given in Figure 4.6b. For both processes, higher substrate temperatures result in higher purity films. For the AB process the C content decreases monotonously with increasing substrate temperature from 16±3 at.% at 50 °C to 5±3 at.% at 200 °C. For the ABC process the C content was substantially lower, especially above 50°C. XPS revealed a C content of 10±3 at.% at 50°C but for higher temperatures the C content was below the detection limit of XPS (~2 at.%). This again confirms that high purity Pd films can be prepared by Pd(hfac)₂ dosing when combined with a H₂ plasma and an O₂ plasma as reactant step.

The improved purity of the films prepared at higher substrate temperatures and prepared by the ABC process is also manifested in the resistivity values shown in Figure 4.6c. For both processes the resistivity decreases with increasing substrate temperature and the resistivity of the films prepared by the ABC process is consistently lower than the resistivity of the films prepared by the AB process. The lowest resistivity is 21±3 μΩ.cm and was obtained for the ABC process at 200°C. Apart from a lower C content of the films, also an improved microstructure (e.g., larger grain size) can contribute to the lower resistivity values at higher temperatures.

4.4 Conclusion

It has been demonstrated that thin films of palladium of high purity and low resistivity can be deposited at substrate temperatures as low as 100°C using a new-

ly-developed ALD process. In this process Pd(hfac)₂ is used as precursor and the reactant step consists of a H₂ plasma step followed by an O₂ plasma step. This “ABC process” yields a significantly lower C content of the films than the ALD process in which only a H₂ plasma step is used as reactant (“AB process”). From gas phase infrared spectroscopy it was concluded that the O₂ plasma step is important to remove hydrocarbon fragments from the surface that remain after the H₂ plasma step.

The best material properties were obtained for the ABC process for temperatures between 100°C and 200°C, with only a very slight improvement in the properties when going to the higher side of this temperature window. For these conditions, the C content is below the XPS detection limit of ~2 at.%, the resistivity of the films is slightly higher than 20 μΩ.cm, and the mass density approaches the value of bulk Pd. The GPC increases slightly with increasing substrate temperature and the higher value at 200°C (0.26±0.05 Å/cycle) might be a reason to use this higher substrate temperature when preparing films with the substrate material permitting. However, if no substrate temperatures higher than 100°C can be tolerated the material properties are not significantly compromised.

The study of initial film growth on Al₂O₃ surfaces showed that nucleation takes place in the island growth mode for both processes. In both cases more than 800 cycles were required to achieve film closure. On the other hand, the nanoparticles obtained in the initial cycles can have interesting applications as well. Many applications in the field of heterogeneous catalysis can benefit from the high surface-to-volume ratio of nanoparticles of Pt-group metals.

In summary, it can be concluded that the newly-developed ALD process developed is a promising alternative to the Pd ALD process in which formalin is used as reactant. The plasma based process allows for deposition of high-purity Pd films and nanoparticles at lower temperatures and therefore unlocks potential applications in nanoelectronics, energy storage, catalysis, and possibly many other technologies.

Acknowledgments

We would like to thank M.J.F. van de Sande, J.J.A. Zeebregts and J.J.L.M. Meulendijks for their technical assistance. W. Keuning and S. Kalčík for the XRD/XRR and infrared spectroscopy measurements, respectively. The research leading to these results has received funding from the European Community's Seventh Framework Programme (FP7/2007-2013) under grant agreement num-

ber ENHANCE-238409, and by the Technology Foundation STW through the VICI program on “Nanomanufacturing”.

4.5 Appendix

4.5.1. Details on the ALD process using Pd(hfac)₂ as precursor and an O₂ plasma followed by H₂ plasma as co-reactant step

For Ir²⁹ and Pt²⁸, ALD processes have been reported that employ dosing of a metalorganic precursor in combination with a co-reactant step that consists of exposure to an oxidizing agent followed by exposure to a reducing agent. The rationale behind this approach is that the adsorbed precursor ligands are first combusted by the oxidizing agent after which the oxidized metal atoms in the surface layer can be reduced to the metallic state by the reducing agent. Oxidizing agents such as O₂ plasma or ozone can be used in this approach in combination with H₂ gas or H₂ plasma as reducing agent. For ALD of Pd, this approach has however been rather unsuccessful¹⁹ and so far ALD of Pd is typically only achieved by using a reductive chemistry such as with H₂ or formalin. Nevertheless, in this work several attempts were made to apply this approach for ALD of Pd using Pd(hfac)₂ as precursor and O₂ plasma and H₂ plasma in the co-reactant step. However, for all conditions investigated very poor results showing no or almost no growth were obtained.

One example of a result is shown in Figure 4.7. This figure shows an XPS survey scan of a film after 1000 cycles. The process parameters were similar to those reported in the manuscript with the exception of the reverse order of the co-reactants in this experiment. The substrates were Al₂O₃ films on Si and the substrate temperature was 100°C. The XPS result in Figure 4.7 was obtained after removing the surface contamination by a mild sputtering step. The XPS peaks reveal that the elements Pd, C, F, but also Al and O are present. The presence of Al peaks, originating from the Al₂O₃ substrate, is a sign that the film is very thin (< 5 nm). The presence of C and F peaks, clearly visible, indicates that the film is strongly contaminated by carbon and fluorine containing species. The film was too thin to enable a decent quantitative compositional analysis and furthermore presented a very high resistivity value of 10⁷ μΩ.cm, as measured by FPP.

One hypothesis to explain the fact that this approach is not viable for ALD of Pd from Pd(hfac)₂ is the presence of F in the precursor ligands. During the O₂ plasma step the adsorbed precursor ligands will undergo reactions with the plasma species leaving various fragments behind at the surface. It is known from

the literature that ALD based on the reaction between fluorinated metal precursors and a strong oxygen source can result in metal fluorides.⁵⁹ For example, CaF₂ thin films were prepared by an ALD process based on Ca(hfac)₂ and ozone at 300°C.⁵⁹ This shows that the hfac ligands are reactive with strong oxidizing agents, and hence it is possible that hfac ligands and O₂ plasma species lead to surface metal fluoride species and other by-products. Moreover, during the H₂ plasma step, H atoms can potentially react with adsorbed F atoms leading to HF species. These could induce etching which is also detrimental for ALD film growth.

For other ALD processes for which the O₂ plasma approach is viable, i.e. for ALD of Pt,²⁸ Ir²⁹ or Ru³, the precursors contain typically no F atoms but only C, H, and O. In these cases exclusively volatile by-products are created in the reaction with O₂ plasma species.⁶⁰

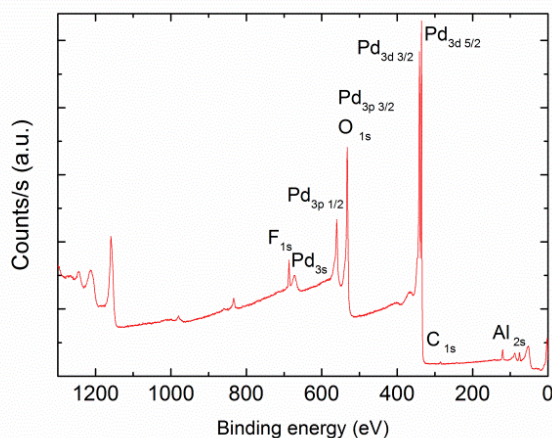


Figure 4.7. XPS survey scan of a film after carrying out 1000 cycles of the ALD process consisting of Pd(hfac)₂ dosing, O₂ plasma exposure and subsequently H₂ plasma exposure. The substrate was a Si wafer covered with a 250 nm ALD Al₂O₃ film. The deposition temperature was 100°C.

4.5.2. Properties of Pd films deposited by the (thermal) ALD process using Pd(hfac)₂ and H₂ gas dosing

Table 4.2. Properties of Pd films deposited by ALD using Pd(hfac)₂ as precursor and H₂ gas as co-reactant. Data obtained with H₂ plasma as co-reactant (i.e., the AB process in the manuscript) are given for easy comparison. The substrates were Si wafers with 250 nm thick Al₂O₃ films and the substrate temperature was 100°C. The process with H₂ gas as co-reactant took place on a 15 nm thick Pt seed layer. In situ spectroscopic ellipsometry (SE), atomic force microscopy (AFM), Rutherford backscattering spectroscopy (RBS) and four-point probe (FPP) measurements were used for analysis of the films. The films were ~30 nm thick.

Properties	Analysis technique	Pd(hfac) ₂ with H ₂ gas	Pd(hfac) ₂ with H ₂ plasma (AB process)
Growth-per-cycle (Å/cycle)	SE	0.16±0.05	0.17±0.05
Growth-per-cycle (atoms.cm ⁻² .cycle ⁻¹)	RBS	(0.9±0.1)×10 ¹⁴	(0.9±0.1)×10 ¹⁴
Mass density (g/cm ³)	XRR	10.5±0.5	11.0±0.5
Resistivity (μΩ.cm)	FPP	65±5	48±5
C content (at. %)	XPS	-	14±3
	RBS	12±5	11±5
RMS roughness (nm)	AFM	2.3±0.3	1.0±0.3
	XRR	-	1.3±0.3

4.5.3. Growth-per-cycle during steady-state film growth for the AB and ABC processes at 100°C

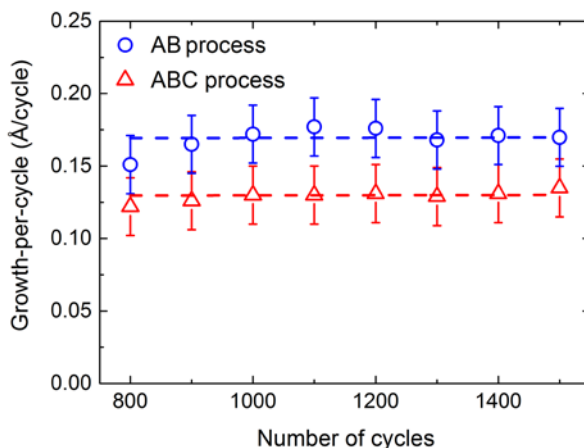


Figure 4.8. Growth-per-cycle (GPC) of Pd during steady-state ALD growth for the AB and ABC processes as determined by in situ spectroscopic ellipsometry. Data during the nucleation phase are omitted as the GPC as it is difficult to extract reliable data from spectroscopic ellipsometry when there is island growth. The GPC observed with the AB and the ABC processes are 0.13 ± 0.02 and 0.17 ± 0.02 Å/cycle, respectively. The substrates were Si wafers covered with a 250 nm ALD Al₂O₃ film. The deposition temperature was 100°C.

References

- (1) Leskelä, M.; Ritala, M. *Angew. Chem. Int. Ed. Engl.* **2003**, *42*, 5548–54.
- (2) George, S. M. *Chem. Rev.* **2010**, *110*, 111–31.
- (3) Leick, N.; Verkuijlen, R. O. F.; Lamagna, L.; Langereis, E.; Rushworth, S.; Roozeboom, F.; van de Sanden, M. C. M.; Kessels, W. M. M. *J. Vac. Sci. Technol. A Vacuum, Surfaces, Film.* **2011**, *29*, 021016.
- (4) Aaltonen, T.; Ritala, M.; Sammelselg, V.; Leskelä, M. *J. Electrochem. Soc.* **2004**, *151*, G489.

- (5) Knoop, H. C. M.; Mackus, A. J. M.; Donders, M. E.; van de Sanden, M. C. M.; Notten, P. H. L.; Kessels, W. M. M. *Electrochem. Solid-State Lett.* **2009**, *12*, G34.
- (6) Christensen, S. T.; Elam, J. W.; Rabuffetti, F. A.; Ma, Q.; Weigand, S. J.; Lee, B.; Seifert, S.; Stair, P. C.; Poeppelmeier, K. R.; Hersam, M. C.; Bedzyk, M. J. *Small* **2009**, *5*, 750–7.
- (7) Feng, H.; Libera, J. A.; Stair, P. C.; Miller, J. T.; Elam, J. W. *ACS Catal.* **2011**, *1*, 665–673.
- (8) Weber, M. J.; Mackus, A. J. M.; Verheijen, M. A.; van der Marel, C.; Kessels, W. M. M. *Chem. Mater.* **2012**, *24*, 2973–2977.
- (9) Chen, Z.; Appenzeller, J.; Knoch, J.; Lin, Y.; Avouris, P. *Nano Lett.* **2005**, *5*, 1497–502.
- (10) Paglieri, S. N.; Way, J. D. *Sep. Purif. Rev.* **2002**, *31*, 1–169.
- (11) Jakubik, W. P.; Urbańczyk, M. W.; Kochowski, S.; Bodzenta, J. *Sensors Actuators B Chem.* **2003**, *96*, 321–328.
- (12) Kumar, P.; Malhotra, L. K. *Mater. Chem. Phys.* **2004**, *88*, 106–109.
- (13) Mercedes, P. V.; Silipas, D.; Mecea, V. *Gas Sep. Purif.* **1990**, *4*, 137–140.
- (14) Aaltonen, T.; Ritala, M.; Tung, Y.-L.; Chi, Y.; Arstila, K.; Meinander, K.; Leskelä, M. J. *Mater. Res.* **2004**, *19*, 3353–3358.
- (15) Hämäläinen, J.; Puukilainen, E.; Sajavaara, T.; Ritala, M.; Leskelä, M. *Thin Solid Films* **2013**, *531*, 243–250.
- (16) Lashdaf, M.; Hatanpää, T.; Krause, A. O. I.; Lahtinen, J.; Lindblad, M.; Tiitta, M. *Appl. Catal. A Gen.* **2003**, *241*, 51–63.
- (17) Liang, X.; Lyon, L. B.; Jiang, Y.-B.; Weimer, A. W. *J. Nanoparticle Res.* **2012**, *14*.
- (18) Elam, J. W.; Zinovev, A.; Han, C. Y.; Wang, H. H.; Welp, U.; Hryn, J. N.; Pellin, M. J. *Thin Solid Films* **2006**, *515*, 1664–1673.
- (19) Hämäläinen, J.; Ritala, M.; Leskela, M. *Chem. Mat.* **2014**, *26*, 786–801.
- (20) Senkevich, J. J.; Tang, F.; Rogers, D.; Drotar, J. T.; Jezewski, C.; Lanford, W. A.; Wang, G.-C.; Lu, T.-M. *Chem. Vap. Depos.* **2003**, *9*, 258–264.
- (21) Christmann, K. *Surf. Sci. Rep.* **1988**, *9*, 1–163.

- (22) Stair, P. C. *J. Chem. Phys.* **2008**, *128*, 182507.
- (23) Goldstein, D. N.; George, S. M. *Appl. Phys. Lett.* **2009**, *95*, 143106.
- (24) Goldstein, D. N.; George, S. M. *Thin Solid Films* **2011**, *519*, 5339–5347.
- (25) Profijt, H. B.; Potts, S. E.; van de Sanden, M. C. M.; Kessels, W. M. M. *J. Vac. Sci. Technol. A Vacuum, Surfaces, Film.* **2011**, *29*, 050801.
- (26) Ten Eyck, G. A.; Senkevich, J. J.; Tang, F.; Liu, D.; Pimanpang, S.; Karaback, T.; Wang, G.-C.; Lu, T.-M.; Jezewski, C.; Lanford, W. A. *Chem. Vap. Depos.* **2005**, *11*, 60–66.
- (27) Ten Eyck, G. A.; Pimanpang, S.; Juneja, J. S.; Bakhru, H.; Lu, T.-M.; Wang, G.-C. *Chem. Vap. Depos.* **2007**, *13*, 307–311.
- (28) Mackus, A. J. M.; Garcia-alonso, D.; Knoops, H. C. M.; Bol, A. A.; Kessels, W. M. M. *Chem. Mater.* **2013**, *25*, 1769.
- (29) Hämaläinen, J.; Puukilainen, E.; Kemell, M.; Costelle, L.; Ritala, M.; Leskelä, M. *Chem. Mater.* **2009**, *21*, 4868–4872.
- (30) Langereis, E.; Knoops, H. C. M.; Mackus, A. J. M.; Roozeboom, F.; van de Sanden, M. C. M.; Kessels, W. M. M. *J. Appl. Phys.* **2007**, *102*, 083517.
- (31) Fujiwara, H. *Spectroscopic Ellipsometry, principles and Applications*; Wiley: Chichester, England, 2007.
- (32) Tompkins, H. G.; Irene, E. A. *Handbook of Ellipsometry*; William Andrews Inc.: New York, U.S.A., 2005.
- (33) Weber, J. W.; Hansen, T. A. R.; van de Sanden, M. C. M.; Engeln, R. *J. Appl. Phys.* **2009**, *106*, 123503.
- (34) Johs, B.; Hale, J. S. *Phys. Status Solidi* **2008**, *205*, 715–719.
- (35) Langereis, E.; Keijmel, J.; van de Sanden, M. C. M.; Kessels, W. M. M. *Appl. Phys. Lett.* **2008**, *92*, 231904.
- (36) Moniz, B. J. *Metallurgy*; 2nd ed.; American Technical: Homewood, U.S.A., 1994.
- (37) Maciejewski, M.; Baker, A. *Pure Appl. Chem.* **1995**, *67*, 1879–1884.

- (38) Huang, Y.; Zhou, X.; Liao, J.; Liu, C.; Lu, T.; Xing, W. *Electrochem. commun.* **2008**, *10*, 1155–1157.
- (39) Nigg, H. L. *The surface reaction mechanisms of beta-diketones on transition metal surfaces including applications to metal thermal chemical vapor etching and heterogeneous catalyst particle redispersion*; University of Illinois at Urbana-Champaign, 1999; p. 692.
- (40) Nigg, H. .; Masel, R. . *Surf. Sci.* **1998**, *409*, 428–434.
- (41) Prasad, R.; Kennedy, L. A.; Ruckenstein, E. *Catal. Rev. - Sci. Eng.* **1984**, *26*.
- (42) Bond, G. C. *Catalysis by Metals*; Academic press: New York, U.S.A., 1962; p. 519 pp.
- (43) Parmeter, J. E. *J. Phys. Chem.* **1993**, *97*, 11530–11541.
- (44) Lin, W.; Wiegand, B. C.; Nuzzo, R. G.; Girolami, G. S. *J. Am. Chem. Soc.* **1996**, *118*, 5977–5987.
- (45) Knoops, H. C. M.; Langereis, E.; van de Sanden, M. C. M.; Kessels, W. M. M. *JVSTA* **2012**, *30*, 01A101–1/10.
- (46) Lu, D.; Wu, Y.; Guo, J.; Lu, G.; Wang, Y.; Shen, J. *Mater. Sci. Eng. B* **2003**, *97*, 141–144.
- (47) Bernal Ramos, K.; Saly, M. J.; Chabal, Y. J. *Coord. Chem. Rev.* **2013**, *257*, 3271–3281.
- (48) Kessels, W. M. M.; Knoops, H. C. M.; Dielissen, S. A. F.; Mackus, A. J. M.; van de Sanden, M. C. M. *Appl. Phys. Lett.* **2009**, *95*, 013114.
- (49) Basova, T. V.; Kiselev, V. G.; Filatov, E. S.; Sheludyakova, L. a.; Igumenov, I. K. *Vib. Spectrosc.* **2012**, *61*, 219–225.
- (50) Condorelli, B. G. G.; Gennaro, S.; Fragalà, I. L. *Chem. Vap. Depos.* **2000**, *6*, 185–192.
- (51) Zheng, B.; Braeckelmann, G.; Kujawski, K.; Lou, I.; Lane, S.; Kaloyeros, A. E. *J. Electrochem. Soc.* **1995**, *142*, 3896–3903.
- (52) Mackus, A. J. M.; Verheijen, M. A.; Leick, N.; Bol, A. A.; Kessels, W. M. M. *Chem. Mater.* **2013**, *25*, 1905–1911.
- (53) Simonsen, S. B.; Chorkendorff, I.; Dahl, S.; Skoglundh, M.; Sehested, J.; Helveg, S. *J. Am. Chem. Soc.* **2010**, *132*, 7968–75.

- (54) Huang, S.-Y.; Huang, C.-D.; Chang, B.-T.; Yeh, C.-T. *J. Phys. Chem. B* **2006**, *110*, 21783–7.
- (55) Yamauchi, M.; Ikeda, R.; Kitagawa, H.; Takata, M. *J. Phys. Chem. C* **2008**, *112*, 3294–3299.
- (56) Meusel, I.; Hoffmann, J.; Hartmann, J.; Heemeier, M.; Bäumer, M.; Libuda, J.; Freund, H. *Catal. Letters* **2001**, *71*, 5–13.
- (57) McCarty, J. G. *Catal. Today* **1995**, *26*, 283–293.
- (58) Kan, H. H.; Shumbera, R. B.; Weaver, J. F. *Surf. Sci.* **2008**, *602*, 1337–1346.
- (59) Putkonen, M.; Szeghalmi, A.; Pippel, E.; Knez, M. *J. Mater. Chem.* **2011**, *21*, 14461.
- (60) Mackus, A. J. M.; Leick, N.; Baker, L.; Kessels, W. M. M. *Chem. Mater.* **2012**, *24*, 1752–1761.

Chapter 5

*Supported Core/Shell Bimetallic Nanoparticles Synthesis by Atomic Layer Deposition**

Abstract: A continuing goal in catalysis research is to engineer the composition and structure of noble metal nanomaterials in order to precisely tune their catalytic activity. Herein, we present proof-of-concept results on the synthesis of supported bimetallic core/shell nanoparticles entirely by atomic layer deposition (ALD). ALD is a novel and scalable method, which can be used to prepare noble-metal catalysts on high surface area support materials. Two properties of ALD of noble metals, namely the Volmer-Weber growth and surface-selectivity, are exploited to decouple primary island growth from subsequent selective shell growth. This concept is applied to synthesize highly dispersed Pd/Pt and Pt/Pd nanoparticles. In-depth characterization of the nanoparticles provides evidence for the core/shell morphology and for the narrow size distribution. The self-limiting nature of the ALD process allows for independent control of the core and shell dimensions, opening up unique possibilities for precise engineering of metallic nanoparticle properties.

*This work has been published as: M. J. Weber, A. J. M. Mackus, M. A. Verheijen, C. van der Marel, and W. M. M. Kessels, *Chemistry of Materials*, 24(15), 2973-2977 (2012).

5.1 Introduction

Noble metal nanoparticles (NPs) are known for being excellent materials for heterogeneous catalysis¹ in applications such as hydrogen storage,² sensing,³ automotive emissions catalytic conversion⁴ and fuel cells.⁵ The catalytic activity of these metallic NPs can be maximized when the size, structure and composition are optimized for a specific catalytic reaction.^{6,7} In this light, structured bimetallic core/shell NPs have attracted tremendous interest in the last few years.⁸⁻¹¹ The lattice strain created in these core/shell NPs, as well as the hetero-metallic bonding interactions, modify the surface electronic properties of the NPs.¹² Therefore, core/shell NPs often show improved catalytic properties compared to their alloyed counterparts or to mixtures of monometallic NPs.^{8,9} Pd core/Pt shell (Pd/Pt) NPs, for example, exhibit excellent catalytic performance for oxygen reduction and for methanol electro-oxidation, which are two key reactions in methanol fuel cells.^{5,13,14} Furthermore, placing expensive and scarce Pt material as a shell on top of a less expensive core material is economically favorable.

Various wet chemistry routes exist to produce supported metallic nanoparticles, such as impregnation, deposition-precipitation, galvanic displacements, colloidal synthesis and ion exchange processes.^{5,15} The synthesis of bimetallic core/shell structures is usually performed by reducing a second metal onto pre-formed cores but this method is challenging.^{8,15,16} Although these wet chemistry techniques offer satisfying NP size and shape control, there are often difficulties during purification and collection of the synthesized NPs since they tend to agglomerate. Furthermore, the separation of the NPs from the chemicals (e.g. stabilizers, solvents) used in certain processes requires additional post treatments.

Atomic Layer Deposition (ALD) has been used in many recent studies for the synthesis of supported metallic NPs.¹⁷⁻²¹ ALD is a thin film deposition technique based on sequential and self-limiting surface reactions, and is known for its atomic level thickness control.²² Many metals have however the tendency to form highly dispersed nanoparticles on oxide substrates during the initial stage of the ALD process,²³ because the interactions between the deposited metal atoms are stronger than those between the metal adatoms and the oxide substrate. This is mainly due to the difference in surface energies between the deposited metal and the oxide substrate.²⁴ This so-called Volmer-Weber (island) growth is therefore a natural and straightforward way to deposit supported metallic NPs. ALD is also a good alternative to wet chemistry techniques because it allows the deposition of the materials to occur on substrates with demanding 3D surface topologies as well as on materials with high surface-to-volume ratios. Moreover, since only volatile by-products are formed during ALD, the synthesized NPs can be used for heterogeneous catalysis applications without the need for post treat-

ment steps (reduction, cleaning). Previously, the nucleation stage of ALD of noble metals on oxides has been exploited to successfully prepare Pt,^{17,21} Pd,¹⁸ Ir,¹⁹ and Ru²⁰ supported monometallic NPs, mainly for catalysis applications. Bimetallic Pt-Ru alloyed NPs were synthesized by alternating between Ru ALD and Pt ALD cycles.²⁵ Recently, core/shell Pt/Ag NPs have been prepared by depositing Ag through wet chemistry on Pt cores prepared by ALD.²⁶

In this work, we present proof-of-concept results for the synthesis of core/shell structured bimetallic NPs entirely by ALD. To this end, an area-selective ALD process has been developed to deposit shells on metal cores also grown by ALD. We demonstrate the feasibility of this method through the synthesis of Pd/Pt core/shell NPs supported on Al₂O₃ substrates. The tailoring of the properties of such core/shell NPs in terms of particle sizes and compositions by changing the ALD process parameters is addressed. The versatility of the method is further demonstrated through the synthesis of Pt/Pd core/shell NPs.

5.2 Experimental section

All depositions have been carried out in an open-load ALD reactor equipped with a remote plasma source. The precursors, methylcyclopentadienyl(trimethyl)platinum (MeCpPtMe₃, 98%) and palladium hexafluoroacetylacetonate (Pd(hfac)₂, 99%), were obtained from Sigma-Aldrich and were used as received. They were contained in steel bubblers connected to the reactor. The precursor exposure time was 3 s for both Pt and Pd ALD cycles. The substrates used were Si wafers and Si₃N₄ Transmission Electron Microscopy (TEM) windows respectively covered by 50 and 3 nm Al₂O₃ deposited by ALD. The ALD processes were monitored by *in-situ* spectroscopic ellipsometry (SE) (J.A. Woollam, Inc) over a 0.75-5 eV photon energy range and thickness information was extracted from the data through B-spline and Drude-Lorentz oscillator parametrizations. High Angle Annular Dark Field (HAADF) STEM (Scanning Transmission Electron Microscopy) and Electron Energy Loss Spectroscopy (EELS) studies were performed using a FEI Tecnai F30ST, operated at 300 kV and a Cs probe-corrected JEOL ARM 200F, operated at 200 kV, respectively. X-Ray Photoelectron Spectroscopy (XPS) measurements were carried out in a Quantera SXMtm from Ulvac-PHI using a spot size of 1200×500 μm² (High Sensitivity Mode) and a take-off angle of the detected electrons of 45°. Rutherford Backscattering Spectrometry (RBS) measurements were performed with 2 MeV ⁴He⁺ ions and a spot size of 500×500 μm².

5.3 Results and discussion

First, the fact that ALD of noble metals starts with island growth was used to deposit the Pd cores. For ALD of Pd, the plasma-assisted process employing Pd(hfac)₂ and H₂ plasma at a substrate temperature of 100 °C as developed by Ten Eyck et al.²⁷ was used. The detailed parameters of this process are given (Table 5.1).

Table 5.1. Detailed process parameters of the different ALD processes used in this work *

	Pt ALD process		Pd ALD process	
	A	B	A	B
Precursor	MeCpPtMe ₃		Pd(hfac) ₂	
Precursor exposure time (s) **	3		3	
Ar purge time (s)	3		5	
Pump time (s)	4		5	
Co-reactant	O ₂ gas at 7.5 mTorr	O ₂ gas at 750 mTorr	H ₂ gas at 7.5 mTorr	H ₂ plasma at 7.5 mTorr
Co-reactant exposure time (s)	5		2.5	5
Pump time (s)	8			
Bubbler temperature (°C)	30		50	
Substrate temperature (°C)	300		100	
Reactor wall temperature (°C)	90			
Reactor base pressure (mTorr)	≤10 ⁻³			

* Conditions labeled “A” yield growth on noble metal surfaces but not on oxide surfaces, i.e., the growth is surface selective. Conditions labeled “B” yield also growth on oxide substrates.

** Ar was used as a carrier gas.

As can be seen in Figure 5.1a, this process leads to steady-state ALD growth of ~0.2 Å/cycle after a nucleation delay of ~100 cycles.

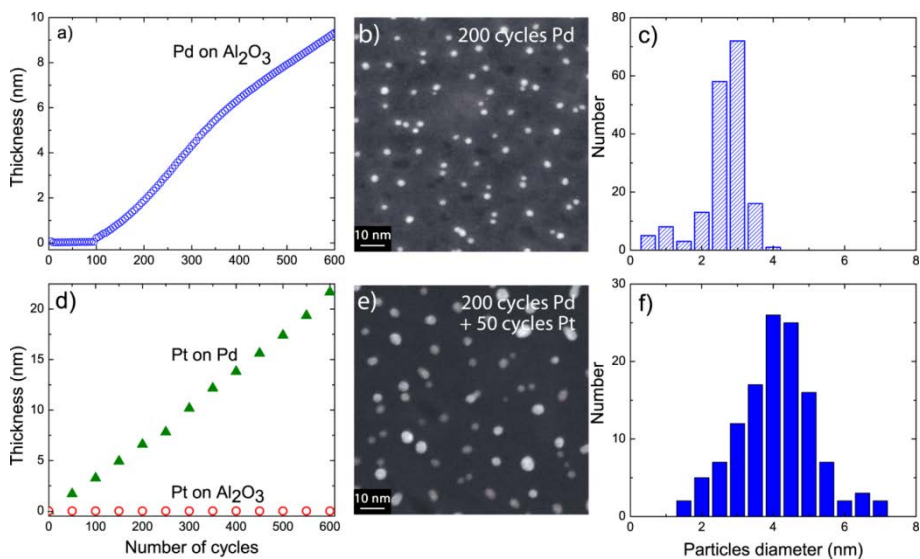


Figure 5.1. (a) Thickness evolution of Pd during ALD as obtained from *in-situ* spectroscopic ellipsometry (SE). Pd(hfac)₂ and a H₂ plasma at a pressure 7.5 mTorr were employed, and Al₂O₃ was used as the substrate material. It should be noted that the Pd ALD process results in Volmer-Weber growth in the first hundreds of cycles with film closure taking place around a film thickness of 10 nm. (b) HAADF-STEM image of Pd nanoparticles obtained by applying 200 cycles of plasma-assisted ALD of Pd on an Al₂O₃ covered Si₃N₄ TEM window. (c) Particle size distribution extracted from (b). (d) Thickness evolution of Pt during ALD from MeCpPtMe₃ and O₂ gas at a pressure of 7.5 mTorr. The data was obtained from *in-situ* SE. The Pt was deposited on Pd (green triangles) and Al₂O₃ (red circles) surfaces. The process allows for direct growth on Pd, whereas no growth could be observed on alumina even after 600 cycles. (e) HAADF-STEM image of Pd/Pt nanoparticles supported on an Al₂O₃ covered Si₃N₄ TEM window. The nanoparticles were obtained by applying 200 cycles of plasma-assisted ALD of Pd and subsequently 50 cycles of ALD of Pt. (f) Particle size distribution extracted from (e).

The use of H₂ plasma as co-reactant, which provides H atoms as reactant species, enables the Pd ALD process to initiate on oxides such as Al₂O₃.^{27,28} The nucleation delay observed is typical for Pd ALD, and is mainly due to surface poisoning by remaining precursor ligands.²⁹ To deposit Pd nanoparticles 200 ALD cycles were employed. The synthesized NPs were visualized by HAADF-STEM imaging. This technique enables high-contrast imaging of high-Z elements (such as Pt or Pd) against the lower-Z background (such as Al₂O₃), as can be seen in Figure 5.1b. Figure 5.1c shows the particle size distribution. The Pd NPs have an average diameter of 2.6 ± 0.5 nm and a density of 8.6×10^{11} NPs/cm².

To deposit the Pt shell, the Pt ALD process was tuned such that only selective growth on Pd NPs was obtained. The selective ALD process was based on Pt ALD from MeCpPtMe₃ and O₂ gas at 300 °C, as developed by Aaltonen et al. and Knoops et al.^{30,31} It has been shown that selective ALD growth of Pt can be obtained when using a low O₂ partial pressure during the O₂ pulse.^{31,32} Selective Pt ALD is based on the dissociative chemisorption of O₂ on the catalytic Pt group metals, which is a key step in the reaction mechanism of Pt ALD. This selective ALD growth process has been used previously for nanopatterning of Pt.^{32,33} For an O₂ pressure of 7.5 mTorr, no Pt growth could be observed on Al₂O₃, even after a long deposition of 1000 cycles. On the other hand, immediate growth occurred on a Pd substrate at a rate of 0.45 Å/cycle (Figure 5.1d). The Pt ALD process at 7.5 mTorr pressure can therefore be considered as selective towards Pd versus Al₂O₃. In order to synthesize the supported Pd/Pt NPs, 50 cycles of Pt ALD were applied to selectively cover the catalytic Pd cores, without breaking the vacuum between the two ALD processes. The resulting core/shell particles were characterized through STEM imaging as shown in Figure 5.1e. The diameter of these Pd/Pt NPs was 4.1±0.5 nm. Compared to the Pd NPs of Figure 5.1b, a shift in the distribution of NPs towards larger particles and broader size distribution was obtained after the deposition of the Pt shell as can be seen in Figure 5.1f. The density of the Pd/Pt NPs was 7.9×10¹¹ NPs/cm² which is virtually equal to the density of the Pd NPs. Furthermore, no particles with a diameter smaller than 1.5 nm can be distinguished. These observations suggest that the Pt ALD process only takes place on the Pd cores without creating new monometallic Pt NPs.

To study the geometry of the synthesized Pd/Pt NPs in more detail, the NPs were characterized using probe corrected STEM-HAADF imaging. The exceptional resolution of probe corrected STEM combined with the Z-contrast provides insight into the core/shell structure of these bimetallic NPs. In Figure 5.2a and 5.2b, the contrast between the Pd core and the Pt shell is well recognizable, proving the selective growth of Pt on the Pd core. The lattice fringes in the Pt shell do not continue in the Pd core (see Figure 5.2b), which can be attributed to the lattice mismatch between the two metals. For this sample, the STEM-HAADF images revealed an average shell thickness of ~0.8 nm for particles with a total diameter of ~5 nm.

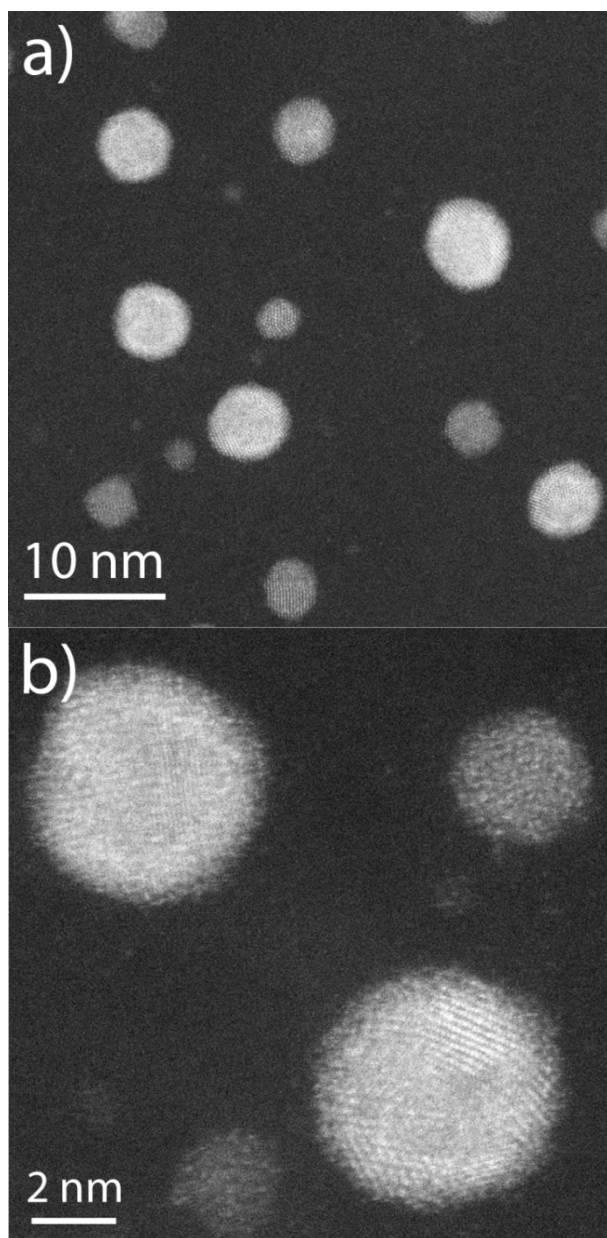


Figure 5.2. (a, b): High magnification HAADF-STEM images of Pd/Pt core/shell nanoparticles of the same sample as in Figure 1e. In (a), the core/shell structure is visible on most of the particles. Contrast differences result from the atomic number (Z) difference between Pd and Pt. In (b), the HAADF-STEM high resolution image displays lattice fringes of the Pt shells.

Electron Energy Loss Spectroscopy (EELS) was carried out to provide an independent proof of the core/shell geometry of the nanoparticles. Figure 5.3a displays an EELS line scan across a single particle of ~ 5.5 nm in diameter. Pd could be detected by EELS, whereas the Pt peak appeared to be too weak to be detected with this technique. The STEM-HAADF brightness plotted in Figure 5.3b displays the full diameter of the core/shell NP. Pd was detected only in the ~ 3.5 nm wide core of the particle in Figure 5.3a. This 3.5 nm core diameter corresponds well to the reduced HAADF brightness in the centre of the particle, reflecting the lower atomic number of Pd, as compared to the higher atomic number of the Pt shell.

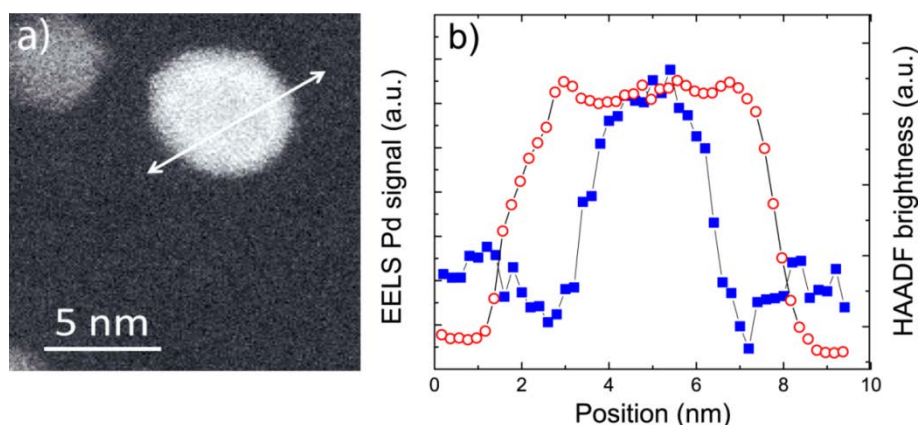


Figure 5.3. (a, b): Energy Electron Loss Spectroscopy (EELS) line scan across a single Pd/Pt nanoparticle. The position of the line scan is indicated in the HAADF-STEM image (a). Only Pd (blue squares) could be detected by EELS as the Pt signal appeared to be too weak. The HAADF brightness profile (red circles) displays the full diameter of the particle (~ 5.5 nm). The Pd signal was only detected in the core (~ 3.5 nm wide) of the particle.

The atomic composition of the NPs was determined by Rutherford Backscattering Spectrometry (RBS) using 2 MeV $^4\text{He}^+$ ions. The areal density of Pd and Pt present on the sample were $(1.2 \pm 0.1) \times 10^{15}$ atoms/cm 2 and $(0.55 \pm 0.05) \times 10^{15}$ atoms/cm 2 , respectively. This corresponds to an average Pd/Pt atomic ratio of 2.1 ± 0.2 . From the sum of Pd and Pt atoms present on the sample, a surface loading of $\sim 0.39 \pm 0.03$ $\mu\text{g}/\text{cm}^2$ was calculated. This is in good agreement with the 0.36 ± 0.04 $\mu\text{g}/\text{cm}^2$ loading calculated from the density and diameters of the NPs measured in the STEM images, assuming a semi-spherical core/shell geometry.

X-Ray Photoelectron Spectroscopy (XPS) measurements have been carried out to obtain information on the chemical state of the deposited atoms. The XPS spectrum is given in Figure 5.4.

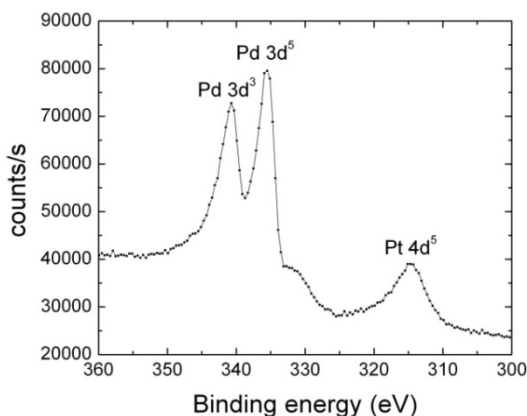


Figure 5.4. X-Ray Photoelectron Spectroscopy (XPS) spectrum of the Pd/Pt core/shell nanoparticles. Pd and Pt were in their metallic state (binding energies of Pd 3d⁵ and Pt 4d⁵ appear at 335.0±0.2 eV and 314.1±0.2 eV, respectively). The Pd 3d doublet partly overlaps with the Pt 4d doublet.

The XPS data revealed that both Pd and Pt were in their metallic state. This implies that the Pd/Pt NPs were not oxidized during processing, despite the use of O₂ gas in the Pt ALD process. Furthermore, a Pd/Pt atomic ratio of 2.0±0.2 was calculated from the XPS data assuming a semi-spherical core/shell geometry. This Pd/Pt ratio is in good agreement with the value calculated from the RBS data.

To demonstrate the versatility of the method, also Pt core/Pd shell NPs have been prepared. First, the Pt ALD process was carried out at 300 °C employing a high O₂ partial pressure (750 mTorr) in order to initiate Pt growth on the Al₂O₃ substrate. The deposition was limited to 5 cycles to deposit small nanoparticles. Subsequently, without breaking the vacuum, 150 cycles of Pd ALD were carried out at 100 °C. In this case, H₂ gas was used as the co-reactant,²⁷ such that Pd grows selectively on the Pt nanoparticles. In this thermal ALD process, H₂ dissociatively chemisorbs on the Pt and Pd and not on Al₂O₃. This leads to selective growth of Pd on Pt as demonstrated by the immediate and constant Pd growth of ~0.2 Å/cycle on a Pt substrate, and the absence of growth on Al₂O₃ (Figure 5.5).

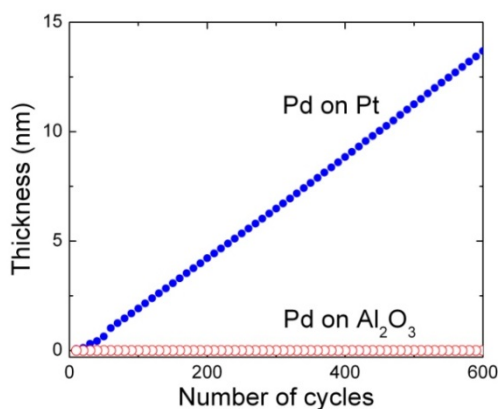


Figure 5.5. Pd ALD from Pd(hfac)₂ and H₂ gas at 7.5 mTorr pressure on Pt and Al₂O₃. The thickness evolution is obtained by *in-situ* spectroscopic ellipsometry. The ALD process allows for direct growth of Pd on the catalytic Pt substrate (blue circles), while no growth was observed on the Al₂O₃ substrate even after 600 cycles (red circles). The Pd ALD process from H₂ gas can therefore be considered as selective towards the Pt surface.

Using STEM-HAADF imaging, a comparison of the particle size before and after shell growth (for different samples) confirmed that Pd was deposited on the Pt nanoparticles. Because HAADF visualization of the lower atomic number shell of Pd around the Pt core is difficult, a simple oxidation treatment was applied to visualize the core/shell structures. The deposited Pt/Pd NPs were exposed to a gentle Ar-O₂ plasma for 3 min, which oxidized the Pd shell. As the intensity in HAADF images is roughly proportional to $Z_{av}^{1.7}$, with Z_{av} the average atomic number, oxidizing the shell will reduce the HAADF intensity of the oxidized shell, yielding a better Z-contrast. Figure 5.6 shows HAADF-STEM images of these Pt/PdO nanoparticles, displaying the core/shell structure even at a relatively low magnification.

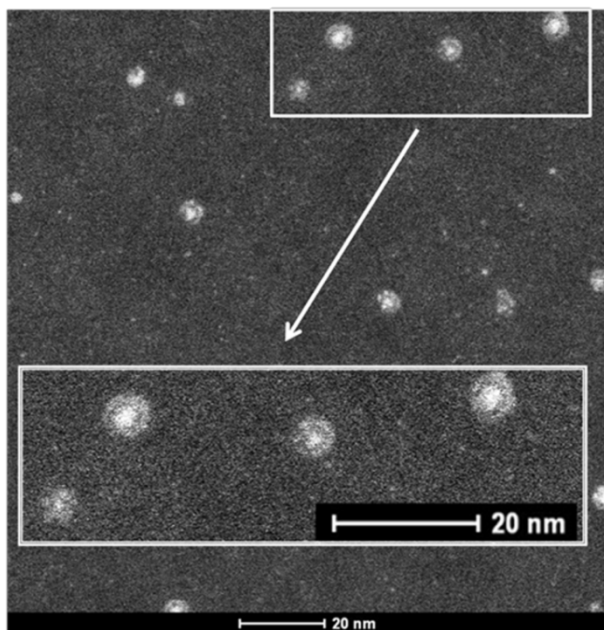


Figure 5.6. HAADF-STEM image of Pt/PdO core/shell nanoparticles supported on an Al_2O_3 covered Si_3N_4 TEM window. These structures were obtained by oxidizing the Pd shell by applying a gentle Ar- O_2 plasma to Pt/Pd nanoparticles. The increased Z-contrast enables the visualization of core/shell structures at relative low magnification.

The PdO shell thickness was $\sim 1.5 \pm 0.5$ nm for particles with a total diameter of $\sim 4.5 \pm 0.5$ nm. This PdO shell thickness is probably not identical to the initial Pd shell thickness. XPS measurements revealed that the Pt core remained metallic, while the Pd shell was fully oxidized to PdO³⁴ (Figure 5.7).

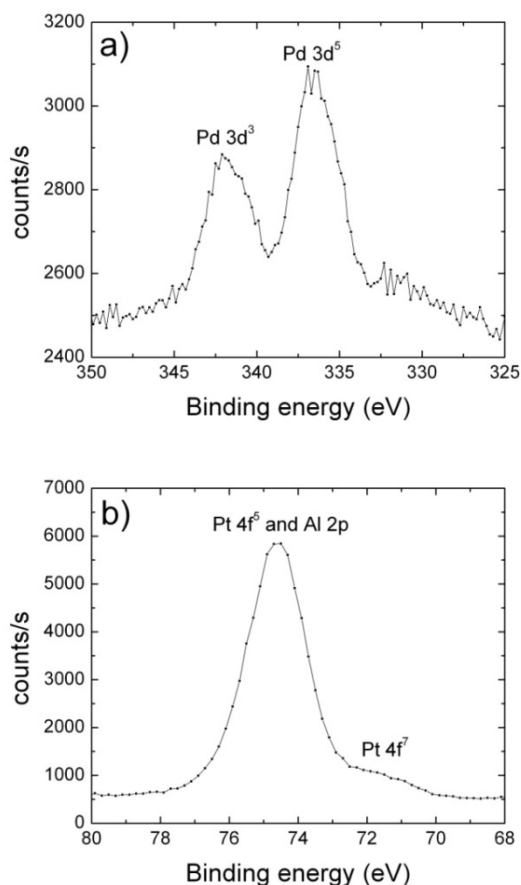


Figure 5.7. X-Ray Photoelectron Spectroscopy (XPS) spectra of the Pt/PdO nanoparticles. In a) the binding energies of the Pd 3d doublet are shown. The Pd 3d⁵ peak appears at 336.7 eV, revealing that Pd was oxidized (PdO). In b) the binding energies of the Pt 4f doublet are shown. The Pt is in its metallic state (binding energy of Pt 4f⁷ at 71.6 eV). The Pt 4f⁵ and Al 2p peaks are overlapping. The binding energy of Al 2p at 74.8 eV corresponds to Al₂O₃.

5.4 Conclusion

In summary, an innovative method enabling the synthesis of supported noble metal core/shell nanoparticles by ALD has been demonstrated. The new route exploits two distinct characteristics of noble metal ALD processes, i.e. Volmer-Weber growth on oxides and the selectivity that can be achieved on catalytic metal surfaces. The method to prepare core/shell NPs is versatile since it allows for independent tuning of the core and shell diameter by varying the number of

ALD cycles applied. The method can also be used to create core/shell/shell structures and other “designed” nanoparticles. Furthermore, the process is extendable to any substrate for which metal ALD results in Volmer-Weber (island) growth. By depositing the core/shell NPs on substrates with a high aspect-ratio (e.g., carbon nanotubes, semiconductor wires, etc.) the loading of the NPs can be increased. Furthermore, selective ALD growth is not limited to Pd and Pt, and therefore the choice for metals that can be used in the NPs can be extended. The versatility of the innovative approach presented in this work will therefore enable full control of the composition and dimensions of multimetallic core/shell nanostructures. As this is an ultimate goal in catalyst design, it is anticipated that many applications, including fuel cells and advanced sensors, can benefit from core/shell nanoparticles prepared by ALD.

Acknowledgments

We would like to thank E. Okunishi (JEOL) for performing the probe corrected STEM and EELS measurements. The skilful technical assistance of M.J.F. van de Sande, J.J.A. Zeebregts and J.J.L.M. Meulendijks was appreciated. This work was supported by the Marie Curie Project ENHANCE (European Research Training Network of “New materials: Innovative Concepts for their Fabrication, integration and Characterization”) within the European seventh framework programme.

References

- (1) Astruc, D., Nanoparticles and catalysis. Wiley-VCH, New York, USA, 2008.
- (2) Yamauchi, M.; Kobayashi, H. Kitagawa, H. *ChemPhysChem* **2009**, *10*, 2566-2576.
- (3) Lal, S.; Link, S.; Halas, N. J. *Nat. Photonics* **2007**, *1*, 641-648.
- (4) Kaspar, J.; Fornasiero, P.; Hickey, N. *Catal. Today* **2003**, *77*, 419-449.
- (5) Zhao, X.; Yin, M.; Ma, L.; Liang, L.; Liu, C.; Liao, J.; Lu, T.; Xing, W. *Energy Environ. Sci.* **2011**, *4*, 2736-2753.
- (6) Niu, W.; Xu, G. *Nano. Today* **2011**, *6*, 265-285.

- (7) Peng, Z.; Yang, H. *Nano. Today* **2009**, *4*, 143-164.
- (8) Serpell, C. J.; Cookson, J.; Ozkaya, D.; Beer, P. D. *Nat. Chem.* **2011**, *3*, 478-483.
- (9) Alayoglu, S.; Nilekar, A. U.; Mavrikakis, M.; Eichhorn, B. *Nat. Mater.* **2008**, *7*, 333-338.
- (10) Wang, F.; Sun, L.-D.; Feng, W.; Chen, H.; Yeung, M. H.; Wang, J.; Yan, C.-H. *Small* **2010**, *6*, 2566-2575.
- (11) Strasser, P.; Koh, S.; Anniyev, T.; Greeley, J.; More, K.; Yu, C.; Liu, Z.; Kaya, S.; Nordlund, D.; Ogasawara, H.; et al. *Nat. Chem.* **2010**, *2*, 454-460.
- (12) Tedsree, K.; Li, T.; Jones, S.; Chan, C. W. A.; Yu, K. M. K.; Bagot, P. A. J.; Marquis, E. A.; Smith, G. D. W.; Tsang, S. C. E. *Nat. Nanotechnol.* **2011**, *6*, 302-307.
- (13) Nilekar, A. U.; Xu, Y.; Zhang, J.; Vukmirovic, M. B.; Sasaki, K.; Adzic, R. R.; Mavrikakis, M. *Top. Catal.* **2007**, *46*, 276-284.
- (14) Zhang, H.; Yin, Y.; Hu, Y.; Li, C.; Wu, P.; Wei, S.; Cai, C. *J. Phys. Chem. B* **2010**, *114*, 11861-11867.
- (15) Yang, H. *Angew. Chem. Int. Ed.* **2011**, *50*, 2674-2676.
- (16) Lim, B.; Jiang, M.; Camargo, P. H. C.; Cho, E. C.; Tao, J.; Lu, X.; Zhu, Y.; Xia, Y. *Science* **2009**, *324*, 1302-1305.
- (17) Christensen, S. T.; Elam, J. W.; Rabuffetti, F. A.; Ma, Q.; Weigand, S. J.; Lee, B.; Seifert, S.; Stair, P. C.; Poepfelmeier, K. R.; Hersam, M. C.; et al. *Small* **2009**, *5*, 750-757.
- (18) Feng, H.; Libera, J. A.; Stair, P. C.; Miller, J. T.; Elam, J. W. *ACS Catal.* **2011**, *1*, 665-673.
- (19) Vuori, H.; Silvennoinen, R. J.; Lindblad, M.; Osterholm, H.; Krause, A. O. I. *Catal. Lett.* **2009**, *131*, 7-15.
- (20) Biener, J.; Baumann, T. F.; Wang, Y.; Nelson, E. J.; Kucheyev, S. O.; Hamza, A. V.; Kemell, M.; Ritala, M.; Leskela, M. *Nanotechnology* **2007**, *18*, 055303.
- (21) Baker, L.; Cavanagh, A. S.; Seghete, D.; George, S. M.; Mackus, A. J. M.; Kessels, W. M. M.; Liu, Z. Y.; Wagner, F. T. *J. Appl. Phys.* **2011**, *109*, 084333.

- (22) Ritala, M.; Leskela M. Handbook of Thin Film Materials, Nalvwa H.S., Ed. Academic Press, San Diego, CA, USA, **2002**; Vol. 1, p. 103.
- (23) Stair, P. C. *J. Chem. Phys.* **2008**, *128*, 182507.
- (24) Campbell, C. T. *Surf. Sci. Reports* **1997**, *27*, 1-111.
- (25) Christensen, S. T.; Feng, H.; Libera, J. L.; Guo, N.; Miller, J. T.; Stair, P. C.; Elam, J. W. *Nano Lett.* **2010**, *10*, 3047-3051.
- (26) Sivakov, V. A.; Hoflich, K.; Becker, M.; Berger, A.; Stelzner, T.; Elers, K.-E; Pore, V.; Ritala, M.; Christiansen, S. H. *ChemPhysChem* **2010**, *11*, 1995-2000.
- (27) Ten Eyck, G. A.; Senkevich, J. J.; Tang, F.; Liu, D.; Pimanpang, S.; Karaback, T.; Wang, G.-C.; Lu, T.-M.; Jezewski, C.; Lanford, W. A. *Chem. Vap. Depos.* **2005**, *11*, 60-66.
- (28) Profijt, H. B.; Potts, S. E.; van de Sanden, M. C. M.; Kessels, W. M. M. *J. Vac. Sci. Technol. A* **2011**, *29*, 050801.
- (29) Goldstein, D. N.; George, S. M. *Thin Solid Films* **2011**, *519*, 5339-5347.
- (30) Aaltonen, T.; Ritala, M.; Sajavaara, T.; Keinonen, J.; Leskela, M. *Chem. Mater.* **2003**, *15*, 1924-1928.
- (31) Mackus, A. J. M.; Dielissen S. A. F., Mulders, J. J. L.; Kessels, W. M. M. *Nanoscale* **2012**, *4*, 4477-4480.
- (32) Mackus, A. J. M.; Mulders, J. J. L.; van de Sanden, M. C. M.; Kessels, W. M. M. *J. Appl. Phys.* **2010**, *107*, 116102.
- (33) Mackus, A. J. M.; Kessels, W. M. M.; Mulders, J. J. L. *Microscopy and Analysis* **2011**, *25*, 6-8.
- (34) Moulder, J. F.; Chastain, J. Handbook of X-ray Photoelectron Spectroscopy: A Reference Book of Standard Spectra for Identification and Interpretation of XPS Data. Physical Electronics Division, Perkin-Elmer Corporation, 1992, 262 p.

Chapter 6

*Nanotailored Pd/Pt Core/Shell Nanoparticles prepared by Atomic Layer Deposition**

Abstract: Pd/Pt core/shell nanoparticles (NPs) have been prepared on Al₂O₃ substrates by atomic layer deposition (ALD). Subnanometer control of the core and the shell dimensions, as studied by Z-contrast scanning transmission electron microscopy, has been demonstrated for NPs ranging from 2 to 7 nm in diameter. From the results it is derived that the main conditions for the synthesis of nanotailored core/shell metallic NPs by ALD are: (i) a difference in surface energy between the deposited core metal and the substrate to obtain island growth; (ii) a process yielding linear growth of the NP cores with ALD cycles to obtain monodispersed NPs with a narrow size distribution; (iii) a selective ALD process for the shell metal yielding a linearly increasing thickness to obtain controllable shell growth on the cores only. For Pd/Pt core/shell NPs it is found that a minimum core diameter of 1 nm exists above which the NP cores are able to catalytically dissociate the precursor molecules for shell growth. The knowledge acquired is vital for the design and control of bimetallic NPs by ALD. The precise nanotailoring of core and shell dimensions opens up prospects for heterogeneous catalysis research.

*This work will be submitted as: M. J. Weber, M. A. Verheijen, A. A. Bol, and W. M. M. Kessels in *Chemistry of Materials*.

6.1 Introduction

Bimetallic nanomaterials are the subject of intense research because they have potential applications in a large number of technologies in the fields of electronics^{1,2} and catalysis.¹⁻³ The ability to precisely control the size, composition and structure of metallic nanoparticles (NPs) is of high importance in order to synthesize efficient nanocatalysts.^{4,5} In this light, structured bimetallic core/shell NPs have attracted significant interest in the last few years.^{6,7} When compared to their alloyed counterparts or to mixtures of monometallic NPs, core/shell NPs often show improved catalytic properties.^{6,8} For example, Pd core/Pt shell (Pd/Pt) NPs of 3-6 nm in diameter synthesized by wet chemistry are known to exhibit excellent catalytic performance for oxygen reduction and for methanol electro-oxidation, which are two key reactions in methanol fuel cells.⁹⁻¹² The ability to nanotailor the core and the shell dimensions would further extend the control over the NP design, opening new opportunities for technologies involving nanocatalysts.¹³⁻¹⁵ For example, the core diameter is known to affect the nanocatalyst durability,¹⁶ whereas the shell thickness has a strong influence on the overall performance of the nanocatalyst.¹⁷ Furthermore, placing expensive and scarce materials as an (ultra)thin shell on top of a less expensive core material can lead to a more efficient and hence a more economic use of scarce materials.¹¹

Atomic layer deposition (ALD) is a thin film deposition technique based on the cycle-wise and alternate pulsing of precursor and reactant gases to a reactive surface. During the first half-cycle, the surface is exposed to the precursor molecules that adsorb on the surface through self-limiting chemical reactions. The surface becomes saturated with precursor molecules typically after a few seconds exposure. Subsequently, the excessive amount of precursor and the reaction products generated in the half-cycle are purged out of the reactor. The second half-cycle consists of the introduction of the co-reactant which reacts with the surface species generated in the first half-cycle. This occurs again in a self-limiting way and after the second half-cycle the initial surface conditions before the first half-cycle are re-established. The last step is again a purge step to remove the excess of co-reactant and the reaction products. One full cycle results in the deposition of a submonolayer of material and the targeted film thickness can be reached by repeating the cycles. Consequently, ALD is known for providing an ultimate control of thin film growth of many materials.^{18,19} Moreover, the self-limiting surface chemistry allows for an excellent uniformity and conformality. In the initial stage of film growth, however, the deposition of metals by ALD on certain surfaces is known to start with the formation of islands, mainly because of the difference in surface energies between the deposited metal and the support.²⁰ Hence, turning this drawback into an opportunity, ALD can also be con-

sidered as a new route for the synthesis of metallic NPs.²¹ It allows for the deposition of highly dispersed NPs on high-aspect ratio substrates,^{22,23} which is very relevant for heterogeneous catalysis applications such as fuel cells for example.^{22,24,25} Various highly dispersed NPs of platinum group metals such as Ru,²⁶ Ir,²⁷ Pt²³ and Pd²⁸ have been synthesized by ALD recently, and it has been demonstrated that their diameter can be controlled at the nanometer-level by simply tuning the number of cycles applied.

Bimetallic Pt–Ru alloyed NPs were synthesized by alternating between Ru ALD and Pt ALD cycles.^{29,30} By placing alloyed Pd–Pt NPs in a reductive environment, segregation could be established, leading to Pt/Pd core/shell NPs.³¹ The core/shell structure has been obtained by dealloying because a Pd-rich shell is thermodynamically favored in this reductive environment. As a proof for their catalytical performance, these core/shell NPs have been used for propene dehydrogenation.³¹

De-alloying is an indirect method for preparing core/shell NPs, where the sub-set of combinations that can be realized is governed by thermodynamics. To gain full freedom in the selection of core and shell metals, we presented a proof-of-concept method that allows for the deposition of supported bimetallic NPs with a controlled core/shell structure entirely by ALD.³² This innovative method is a two-step process that makes use of the island growth during the initial stage of metal ALD in order to deposit the core material, and of a selective ALD process to cover these cores with a shell of another metal. We presented and reported this general strategy by synthesizing supported Pt/Pd and Pd/Pt core/shell NPs on metal oxides surfaces.³² Lu *et al.* recently extended this promising route by preparing core/shell NPs with different combinations of noble metals including Pd, Pt and Ru supported on metal oxides.³³ The area selectivity of an ALD process towards specific materials such as noble metals can be achieved by tuning the process parameters, e.g. the temperature,³⁴ the pressure³⁵ or the nature of the co-reactant.^{32,33} Figure 6.1a schematically illustrates the concept with the Pd/Pt core/shell system. Figure 6.1b is an atomic resolution scanning transmission electron microscopy (STEM) image, clearly displaying the core/shell morphology of the NPs. Figure 6.1c presents energy-dispersive X-ray spectroscopy (EDS) mapping of an ensemble of Pd/Pt core/shell structured NPs synthesized using this approach. The EDS mapping shows that Pd (in green) is confined to the centre of the NPs, while Pt (in red) is best visible at the NPs edge in this 2-D projection of the particles. More details about this two-step process for core/shell NPs synthesis can be found in Reference.³²

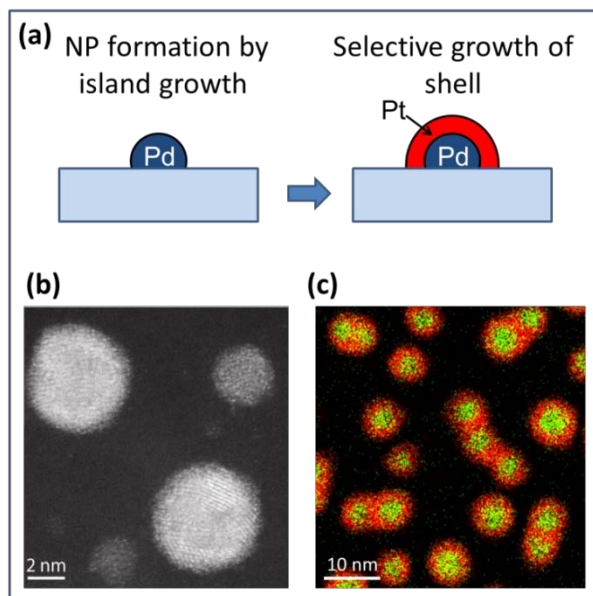


Figure 6.1. (a) Illustration of the two-step ALD process to deposit core/shell NPs of Pd/Pt. (b) HAADF-STEM image and (c) EDS mapping of Pd/Pt core/shell NPs (150 cycles Pd; 50 cycles Pt) on an Al_2O_3 covered Si_3N_4 TEM window.

This route for core/shell NPs synthesis has been demonstrated for the synthesis of Pd/Pt and Pt/Pd core/shell NPs on oxide substrates,³² but the method can be extended to other metals as well. The formation of the NPs (core) on oxide substrates is relatively well established and understood.^{21,36,37} This is however less the case for the selective ALD process used for shell growth.

Key for the selective ALD processes of noble metals such as Pt and Pd is their catalytic activity. The selectivity stems from the dissociative chemisorption of co-reactant molecules on their surface which does not occur on the surface of the support material.^{35,38} For example, during Pt ALD, oxygen atoms are created on the Pt surface from the dissociation of O_2 gas which is used as a co-reactant. These oxygen atoms can decompose incoming MeCpPtMe_3 molecules during the precursor half-cycle (and subsequently remove the resulting organic ligands from the surface).³⁹ The fact that dissociative chemisorption of O_2 does take place on all platinum group metals but not on oxide support material is exploited to obtain area-selective deposition. For example, Pt can deposit selectively on Pd because Pd does dissociate O_2 while an Al_2O_3 support does not. Another important aspect for selective ALD of Pt is the fact that the nucleation of Pt on oxides is ruled by the O_2 exposure.^{35,38} This O_2 dependence of the Pt nucleation has been explained by the enhanced diffusion of Pt species in the presence of oxygen and the resulting faster aggregation of Pt atoms in metal clusters that catalyze the

surface reactions of ALD growth. This means that nucleation effects resulting from adsorption of Pt precursors on surface (defects) sites on the support can be suppressed when applying a low O₂ partial pressure during the O₂ co-reactant pulse.^{32,35,38} Using an O₂ pressure of 7.5 mTorr, no Pt growth was observed on Al₂O₃, even after a long deposition run of 1000 ALD cycles. On the other hand, immediate growth of Pt occurred on a Pd film substrate at a rate of 0.45 Å/cycle under these conditions.³² The same selective process was shown for Pt on Pt surfaces with respect to Al₂O₃.^{35,38} The Pt ALD process at 7.5 mTorr pressure can therefore be considered as selective towards Pd and Pt versus Al₂O₃.

In this work, the innovative route for synthesis of core/shell NPs is further investigated and explored in order to better understand the Pt shell growth on Pd NPs and to demonstrate the possibility to synthesize Pd/Pt core/shell NPs with tailored core and shell diameters. The work has been focused on Pd/Pt core/shell NPs, because the narrow size distribution obtained using this arrangement allows for the accurate investigation of the effect of the core dimension on the shell growth. Two series of experiments have been carried out. First, we fixed the Pd core diameter and varied the shell thickness in order to study the shell growth. Next, a series of samples with various Pd core sizes and constant Pt shell radius has been prepared in order to study the effect of Pd core diameter on the shell growth properties. Z-contrast scanning transmission electron microscopy (STEM) analysis, as well as surface science and catalysis literature reports allowed us to gain more insight into the selective ALD process for shell growth. This understanding allowed us to establish the conditions for the controllable synthesis of core/shell NPs.

6.2 Experimental section

The NPs have been prepared in an open-load ALD reactor equipped with a remote plasma source, described in detail elsewhere.⁴⁰ The precursors, methylcyclopentadienyl-(trimethyl)platinum (MeCpPtMe₃, 98%) and palladium hexafluoroacetylacetonate (Pd(hfac)₂, 99%), were obtained from Sigma-Aldrich and were used as received. The substrates used were Si₃N₄ TEM windows covered by 3 nm Al₂O₃ prepared by ALD.

To deposit the Pd cores, a plasma-assisted ALD process employing Pd(hfac)₂ dosing with subsequent H₂ plasma and O₂ plasma exposure at 100 °C has been used (ABC process, see Chapter 4 for more details). The ALD precursor step consisted of 3 s of Pd(hfac)₂ dosing with Ar as a carrier gas, followed by a 5 s pump step. Subsequently, H₂ gas at a pressure of 7.5 mTorr was dosed for 2.5 s, followed by a H₂ plasma of 5 s at 100 W. This was followed by O₂ gas exposure for

1 s at a pressure of 7.5 mTorr before a O₂ plasma was applied for 1 s at 100 W. This O₂ step was separated from the H₂ step by a pump step of 6 s. Finally the reactor chamber was pumped down for 8 s to complete the ALD cycle.

To deposit the Pt shell, the Pt ALD process was tuned such that selective growth of Pt on Pd NPs was obtained without any growth on the oxide surface. The ALD process was based on MeCpPtMe₃ and O₂ gas dosing at 300 °C, as developed by Aaltonen *et al.* and Knoops *et al.*^{41,42} The precursor step consisted of 3 s of MeCpPtMe₃ dosing with Ar as a carrier gas followed by a 3 s pump step. Selectivity of the ALD process of Pt was achieved by using an O₂ partial pressure of 7.5 mTorr during the 5 s O₂ pulse.³⁵ The reactor chamber was pumped down for 5 s to complete the Pt ALD cycle.

High Angle Annular Dark Field (HAADF) STEM studies were performed using a FEI Tecnai F30ST, operated at 300 kV and a Cs probe-corrected JEOL ARM 200F operated at 200 kV. The latter system was also used for EDS mapping which was executed by a summation of 225 maps with 0.1 ms/pixel acquisition time using a 0.5 nm probe size. During EDS mapping, HAADF images were acquired regularly to allow for drift correction. This series of images was monitored continuously to make sure the original shape remained unaltered during EDS acquisition. The number of NPs and their size distribution were determined over an area of 100×100 nm² using the iTEM software and manual counting of the NPs. It has to be noted that only separated NPs were used in the analysis and no merged NPs or agglomerates.

6.3 Results and discussion

6.3.1. Shell growth by selective ALD

First, a series of core/shell NPs with different shell thicknesses has been synthesized in order to study the growth of the Pt shell. For all the samples, the initial step consisted of depositing the Pd cores, exploiting the island growth mode taking place during the initial stage of Pd ALD. The ALD process ensures a reproducible and controllable deposition of pure Pd NPs during the nucleation stage. This has been underlined by a comparison of two series of samples in which Pd NPs were deposited in the same ALD reactor with the interval of one year. It has been observed that the NPs had a very similar density and size distribution and that in both cases the average diameter of the Pd NPs increased linearly as a function of the number of cycles with a growth in diameter of 0.02 nm/cycle (see Figure 6.2). This demonstrates the reproducibility and robustness of the Pd ALD process for NP synthesis.

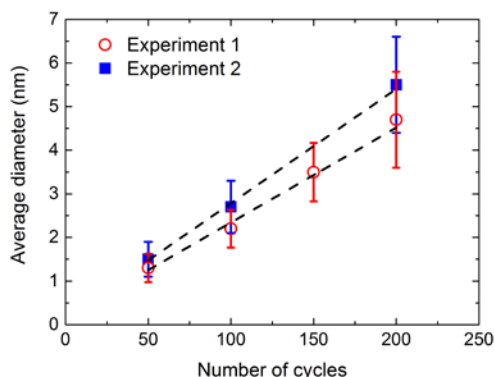


Figure 6.2. Average diameter of Pd NPs deposited by ALD with one year interval Experiment 1 and Experiment 2 correspond to experiments carried out in 2012 and 2013, respectively. The error bars correspond to the standard deviations extracted from the NP size distributions. The linear fits lead to an increase of the diameter of 0.022 ± 0.02 nm/cycle 0.026 ± 0.01 nm/cycle for the NPs in Experiment 1 and Experiment 2, respectively.

Figure 6.3a shows Pd NPs that were prepared on Al_2O_3 substrates by applying 100 Pd ALD cycles. HAADF-STEM was used to visualize the NPs as it enables high-contrast imaging of high-Z elements such as Pd or Pt against the lower-Z background of oxides such as Al_2O_3 . The NPs are highly dispersed with a narrow size distribution and they are round in shape. After 100 ALD cycles, the Pd NPs have an average diameter of 2.2 ± 0.4 nm and their surface density is $(1.0\pm 0.1)\times 10^{12}$ NPs/ cm^2 .

Using the Pd NPs obtained after 100 ALD cycles as cores, subsequently Pt shells of different thicknesses were deposited by selective ALD employing 25, 50 and 75 cycles of Pt ALD. The Z-contrast STEM images in Figures 6.3b, 6.3c and 6.3d yield insight into the core/shell structure of these bimetallic NPs. There is a clear contrast between the Pd core and the Pt shell, confirming the formation of core/shell NPs through selective growth of Pt on the Pd cores while not depositing on the oxide surface. The TEM images clearly demonstrate the increase of the shell thickness.

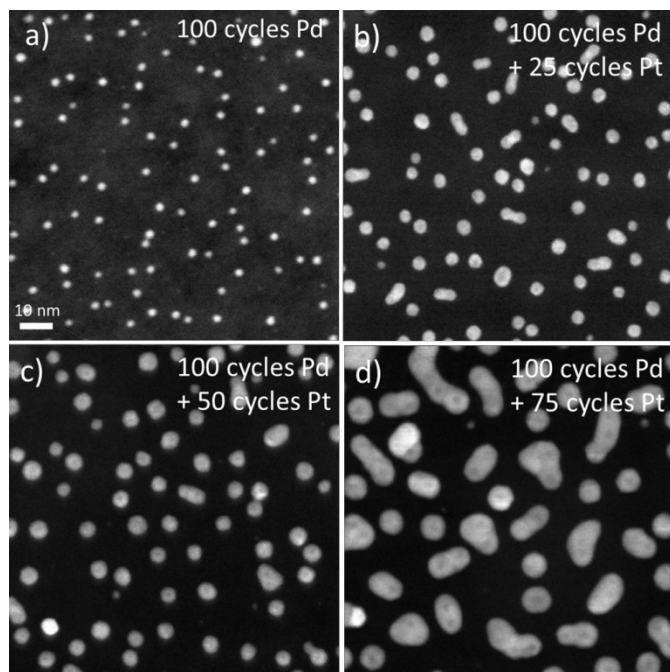


Figure 6.3. HAADF-STEM images of (a) Pd NPs obtained after 100 Pd ALD cycles. Pd/Pt NPs with increasing shell thicknesses obtained by (b) 25, (c) 50 and (d) 75 cycles of Pt ALD on Pd cores obtained by 100 Pd ALD cycles. The substrates were Si_3N_4 TEM windows covered by 3 nm Al_2O_3 prepared by ALD. The scale bar, shown in (a), applies also for (b) – (d).

Figure 6.4a presents the NPs size distribution, as extracted from the TEM images presented in Figure 6.3, as a function of the number of Pt ALD cycles applied. The figure shows that the size distributions are unimodal and stay narrow for all the samples studied, which is of particular interest for many catalysis applications, since a precise definition of the NP size allows for optimum control of the catalytic activity and/or selectivity.^{43,44} A reduction of the density of core/shell NPs can be observed which can be attributed to the merging of NPs. However the density Pd cores density stays constant in the whole series with values of $(0.9 \pm 0.2) \times 10^{12}$ NPs/cm². This corroborates the good reproducibility of the Pd ALD process and it also illustrates the successful application of selective ALD, i.e., no new NPs have been formed on the oxide during shell growth.

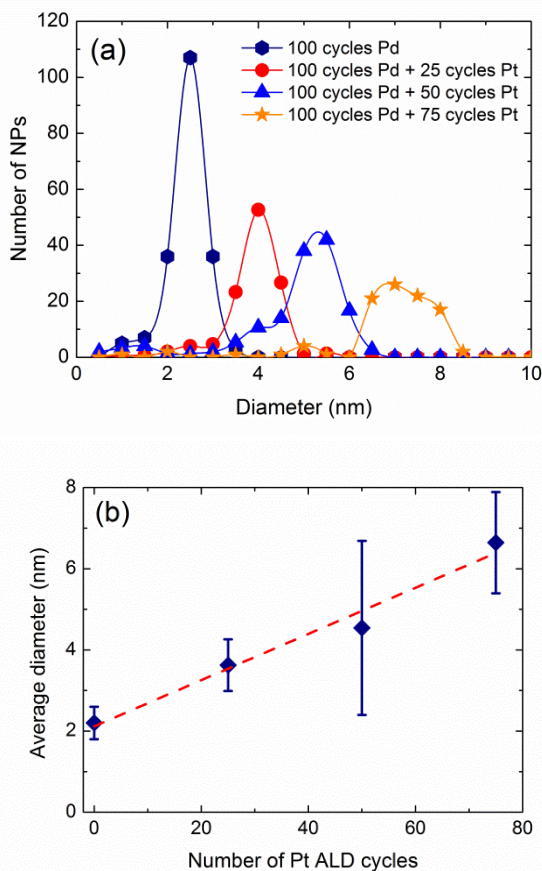


Figure 6.4. (a) Size distribution and (b) average diameter of the NPs determined from the TEM images presented in Figure 6.3, over a surface of $100 \times 100 \text{ nm}^2$. The error bars correspond to the standard deviations extracted from the NPs size distributions. The dashed line is a linear fit of the data.

Figure 6.4b shows the evolution of NP diameter as a function of the number of Pt ALD cycles applied. The average diameter of the NPs increases linearly with the number of Pt ALD cycles, implying that the Pt shell thickness grows at a constant rate. This behavior provides additional information on the surface processes active during shell growth. If Pt atoms would be also deposited on the oxide surface, their diffusion to the NPs could contribute to the growth of the NPs. Obviously, this contribution would decrease as a function of the number of ALD cycles, as the fraction of oxide surface area decreases upon island growth. Thus, the linear increase in shell thickness is a further proof for the high selectivity of

the ALD growth process where this increase only depends on the availability of catalytically active surface sites. As these sites are only present at the NPs surface, these NPs grow at a constant rate. The diameter of the NPs increases with 0.06 ± 0.02 nm/cycle which corresponds to an increase of the shell thickness of 0.03 ± 0.01 nm/cycle. This thickness increase of the shell can be compared to the growth-per-cycle of 0.045 nm/cycle typically observed for ALD of planar Pt films.^{35,45} It shows that the Pt shell can be tailored with a control of the thickness through the choice of the number of ALD cycles and with a thickness precision of 0.03 nm. Moreover, the linearly increasing shell thickness indicates that the Pd core acts as a good catalyst for O₂ dissociation. This O₂ dissociation is required for Pt ALD growth and there is no indication for a delay of growth on the initial surface of the Pd core.

The size distribution and the shape of the NPs observed before and after the shell growth yield more insight into surface mechanisms taking place during growth. The size distribution remains narrow and similar in shape with the increase of the shell thickness. This trend, combined with observation that the NP core density remains constant indicates the absence of significant Ostwald ripening, i.e. the process of net diffusion of atoms from small NPs to larger NPs. This mechanism would lead to an enhanced growth of larger NPs at the expense of smaller NPs. We thus believe that the surface diffusion of metal atoms over the Al₂O₃ surface has a limited role during the selective ALD growth of the shell. This allows for an optimal control of the diameter of the NPs.

The round shape of the core/shell NPs can reflect the selective growth of the Pt shell on the Pd cores which are round in shape but it can also imply fast diffusion of Pt atoms along the NP edge. The latter leads to a round and compact shape of the NPs by the minimization of the total free energy of each NP as driving force.⁴⁶ A close examination in Figure 6.3d of particles that have merged through shell growth reveals that atomic diffusion along the particle edges does play a significant role. If two NPs merge, a double-core/shell structure is created and a concave curvature results at the position where they merge. However, as is clear from Figure 6.3d, for several merged core/shell structures with a small distance between their cores, the concave parts of the edge have been eliminated. This is a sign of atoms diffusing along the NPs edges enabling a reduction in surface energy. However, this process also reduces the (catalytic) surface area. Consequently, in catalytic systems, in which a high NPs density – and more importantly a large effective surface – is desired, a minimum distance between the core/shell NPs is essential to optimize this effective surface.

6.3.2. Influence of the core size on the shell growth

In a second series of samples, the effect of the diameter of the Pd core on the shell growth by selective ALD was studied. The Pd core diameter was varied by varying the number of Pd ALD cycles while the number of Pt cycles was kept constant. The number of Pd ALD cycles was 50, 100, 125, and 175 and the number of cycles applied for the Pt shell was 50 cycles. Figure 6.5 presents the HAADF-STEM images of the resulting Pd/Pt core/shell NPs with various core diameters.

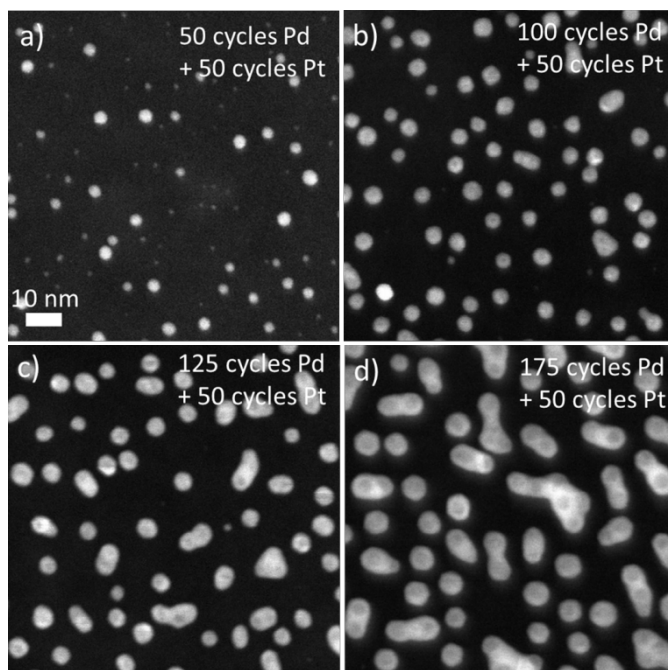


Figure 6.5. HAADF-STEM images of Pd/Pt core/shell NPs with increasing core diameters. (a) 50, (b) 100, (c) 125, and (d) 175 ALD cycles were applied for the synthesis of the Pd cores. The number of cycles applied for the Pt shell deposition was kept constant at 50 cycles. The substrates were Si_3N_4 TEM windows covered by 3 nm Al_2O_3 prepared by ALD. The scale bar, shown in (a), applies also for (b) – (d).

From the Z-contrast imaging the Pd cores can again well be distinguished from the Pt shells. Similarly as for the samples presented in Figure 6.3, the Pd/Pt core/shell NPs are round in shape when not merged. Merged NPs with multiple cores are observed in Figure 6.5c and 6.5d. No signs of asymmetrical shell development can be observed which could have been to the result of mismatch between the Pd and Pt crystal lattices or of a high interfacial energy between Pd

and Pt. The fact that the Pt shells are compactly formed around the Pd cores reveals that the minimization of surface energy of the NPs plays a major role in the Pt ALD process.

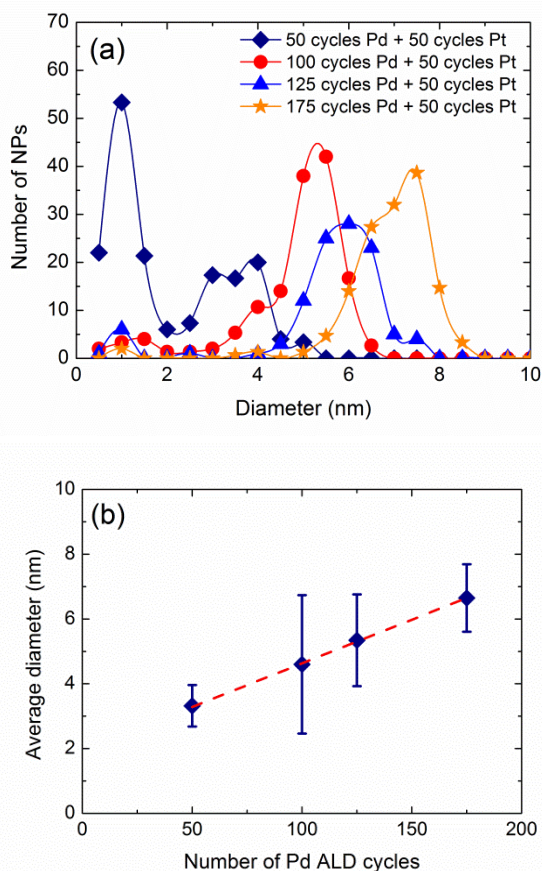


Figure 6.6. (a) Size distribution and (b) average diameter of the NPs determined from the TEM images presented in Figure 6.5, over a surface of $100 \times 100 \text{ nm}^2$. The horizontal axis in (b) corresponds to the number of Pd ALD cycles for the synthesis of the Pd core. The error bars correspond to the standard deviations extracted from the NP size distributions. The dashed line is a linear fit of the data.

Figure 6.6a presents the size distribution of the core/shell NPs with various core diameters, as extracted from the TEM images in Figure 6.5. As can be seen in Figure 6.6a, the core/shell NPs with Pd cores prepared by applying 100, 125 and 175 Pd ALD cycles (shown in Figure 6.5b, 6.5c and 6.5d) present unimodal size distributions. However, a bimodal size distribution can be observed for the sample in Figure 6.5a with the smallest Pd cores prepared by applying only 50 cycles of Pd ALD. For the specific surface area imaged in Figure 6.5a, it

can be extracted that 57% of the NPs present have a small diameter of 1.0 ± 0.5 nm whereas 38% have a larger diameter of 3.5 ± 1.0 nm (the other NPs have an intermediate size). The bimodal size distribution observed suggests that the NPs with a diameter of 1 nm are not covered by a Pt shell and thus do not form core/shell NPs. This hypothesis is supported by further interpretation of the bimodal size distribution. From earlier studies we know that the average diameter of Pd NPs prepared on an Al_2O_3 support is 1.3 ± 0.7 nm after 50 cycles of Pd ALD (see Figure 6.2). From the linear increase in shell thickness (0.03 ± 0.01 nm/cycle) calculated earlier, the expected diameter of the core/shell NPs in this sample can be determined. Adding a shell thickness of 1.5 ± 0.5 nm after 50 cycles of Pt ALD to a Pd core diameter of 1.3 ± 0.7 nm results in a total diameter of 4.3 ± 1.7 nm for the core/shell NPs. This value is in good agreement with the largest diameters obtained for the NPs in Figure 6.5a (3.5 ± 1.0 nm). A possible explanation for the absence of a shell for a fraction of the Pd cores can be found in the fact that the smallest Pd cores (those at the lower side of the distribution) do not act as good nucleation centers for the Pt shell growth because of their reduced catalytic activity. It can be hypothesized that Pt shell growth by the selective ALD process requires a critical Pd core diameter of 1 nm diameter in order to take place.

This hypothesis is corroborated by ALD and catalysis literature. ALD of Pt using MeCpPtMe_3 precursor dosing in combination with O_2 dosing involves surface reactions which are comparable to hydrocarbon combustion processes, i.e. the precursor ligands are removed through combustion-like processes with oxygen atoms created at the catalytic Pt surface. It is known that the combustion of hydrocarbons on oxide supported Pd and Pt nanocatalysts is sensitive to the size of the NPs.^{47,48} In fact, the catalytic activity of Pd NPs smaller than 1 nm is drastically reduced in most chemical reactions, whereas a size between 1 and 10 nm is often optimal.⁴⁸ We therefore believe that the Pt shell does not grow on the smallest Pd NPs because of their reduced catalytic activity. As the highest catalytic activity of noble metal NPs is usually achieved for diameters in between 2 and 10 nm,⁴⁷⁻⁴⁹ we note that the minimum Pd core diameter requirement is not a real drawback for the application of these core/shell NPs in catalysis. We demonstrated that our process allows for accurate tuning of the diameter in the 2-10 nm range. Consequently, even if the process may lead to the presence of a small fraction of smaller Pd NPs, these NPs will not significantly contribute to the catalytic reactions and thus do not have a major impact. Considering the specific case of oxygen reduction reactions for example, the highest catalytic activity of Pd/Pt core/shell NPs is obtained when the diameter is between 2 and 6 nm.^{12,49} The ALD-based approach presented here is therefore very promising for the synthesis of nanocatalysts for fuel cells applications, among others.

Closer inspection of the samples prepared with larger Pd cores (Figure 6.5b, 6.5c and 6.5d) reveals that these have actually also a very small fraction (<5%) of NPs with a diameter 1 nm NPs. This was not expected, because the Pd process normally results in NPs with a unimodal and narrow size distribution and the shell grows selectively on these Pd cores. One hypothesis is that surface diffusion could have taken place during the temperature increase applied between the deposition of the Pd cores (at 100°C) and the Pt shells (at 300°C). This higher temperature increases considerably the diffusion and ripening mechanisms of Pd atoms and clusters, and could have led to the formation of new Pd NPs. These small particles are probably not covered by the Pt shell due to the low probability for catalytic decomposition and thus have kept their original size.

Figure 6.6b shows the average diameter of the NPs as a function of the number of Pd cycles. Concerning the NPs formed by applying 50 cycles of Pd ALD for the cores, only the larger NPs (3.5 ± 1.0 nm) of the bimodal size distribution (the ones covered with a shell) were considered. The average diameter increases linearly showing that for the Pd/Pt NPs the Pt shell growth is independent of the Pd core size (once that the diameter is larger than 1 nm). From the linear fit it can be deduced that the core/shell NPs grow with a rate of 0.02 nm per Pd ALD cycle. This implies that the diameter of the Pd core increases 0.02 nm per Pd ALD cycle. This agrees well with the data for ALD of Pd NPs as shown in Figure 6.2 highlighting the good reproducibility of the process.

As discussed previously, the catalytic activity of Pd NPs below 1 nm is drastically reduced, but the catalytic performance of larger and active NPs towards carbonaceous species combustion depends on their size as well.⁴⁷ Therefore, at first sight the same shell growth rate on Pd cores presenting different diameters is surprising. This result implies that the dissociation of O₂ and the combustion of precursor ligands are not the limiting steps anymore, which means that these surface reactions can occur for the amount of precursor molecules (which is rather limited) that undergo the self-limiting reactions during one ALD cycle. Thus, we believe that the same shell thickness obtained does not depend on the predeposited NPs size, but is due to the fact that the growth takes place under ALD conditions in which a small and fixed amount of precursor molecules is deposited each cycle.

6.4 Conclusion

A detailed study of the preparation of Pd/Pt core/shell NPs entirely by ALD has been presented. It has been shown that this novel route allows for a precise and independent control of the core diameter and the shell thickness, both at the subnanometer level. The Pd cores supported on Al₂O₃ are round in shape and

and their diameter increases at a rate of 0.02 nm per Pd ALD cycle. The core size can therefore be precisely tuned by simply defining the number of ALD cycles to be applied. The Pt shell thickness can also easily be varied since Pt growth takes place at a rate of 0.03 nm per cycle on the Pd cores. This Pt growth is selective which means that it takes only place on the Pd NPs and not on the support material. Furthermore, it has been found that the shell growth is independent of Pd core size when the Pd core diameter is larger than 1 nm.

The controllable synthesis of core/shell NPs by ALD has been obtained using a robust Pd ALD process for the preparation of the core and a selective Pt ALD process for the shell. From the results the following main general conditions for the synthesis of nanotailored core/shell metallic NPs by ALD can be derived. First, initial wetting difficulties are required to obtain island growth. Then, an ALD process presenting a linear growth rate to deposit monodispersed NP cores with a narrow size distribution and a predefined diameter is desired. Third, a selective ALD process presenting a linear growth rate for the shell metal is required, in order to obtain controllable shell growth on the cores only. As the highest catalytic activity of noble metal NPs is achieved for NP diameters between 2 and 10 nm, this ALD-based approach is a promising route for the preparation of efficient nanocatalysts. The ease and precision of the nanotailoring of core/shell NPs by ALD as demonstrated in this work opens new prospects for nanocatalyst design and synthesis.

Acknowledgments

The skilful technical assistance of M.J.F. van de Sande, J.J.A. Zeebregts and J.J.L.M. Meulendijks is acknowledged. This work was supported by the Marie Curie Project ENHANCE (European Research Training Network of “New materials: Innovative Concepts for their Fabrication, integration and Characterization”) within the European seventh framework programme. W.M.M.K. acknowledges that this work was financially supported by the Technology Foundation STW, applied science division of the Netherlands Organisation for Scientific Research (VICI-programme, 10817).

References

- (1) Wang, D.; Li, Y. *Adv. Mater.* **2011**, *23*, 1044–60.
- (2) Ferrando, R.; Jellinek, J.; Johnston, R. L. *Chem. Rev.* **2008**, *108*, 845–910.
- (3) Markovic, N. M.; Schmidt, T. J.; Stamenkovic, V.; Ross, P. N. *Fuel cells* **2001**, *1*, 105–116.
- (4) Niu, W.; Xu, G. *Nano Today* **2011**, *6*, 265–285.
- (5) Peng, Z.; Yang, H. *Nano Today* **2009**, *4*, 143–164.
- (6) Serpell, C. J.; Cookson, J.; Ozkaya, D.; Beer, P. D. *Nat. Chem.* **2011**, *3*, 478–83.
- (7) Alayoglu, S.; Eichhorn, B. *J. Am. Chem. Soc.* **2008**, *130*, 17479–86.
- (8) Alayoglu, S.; Zavalij, P.; Eichhorn, B.; Wang, Q.; Frenkel, A. I.; Chupas, P. *ACS Nano* **2009**, *3*, 3127–3137.
- (9) Nilekar, A. U.; Alayoglu, S.; Eichhorn, B.; Mavrikakis, M. *J. Am. Chem. Soc.* **2010**, *132*, 7418–28.
- (10) Wu, B.; Kuang, Y.; Zhang, X.; Chen, J. *Nano Today* **2011**, *6*, 75–90.
- (11) Sasaki, K.; Wang, J. X.; Naohara, H.; Marinkovic, N.; More, K.; Inada, H.; Adzic, R. R. *Electrochim. Acta* **2010**, *55*, 2645–2652.
- (12) Wang, J. X.; Inada, H.; Wu, L.; Zhu, Y.; Choi, Y.; Liu, P.; Zhou, W.-P.; Adzic, R. R. *J. Am. Chem. Soc.* **2009**, *131*, 17298–302.
- (13) Zhang, J.; Tang, Y.; Lee, K.; Ouyang, M. *Science (80-.)*. **2010**, *327*, 1634–8.
- (14) Ghosh, Y.; Mangum, B. D.; Casson, J. L.; Williams, D. J.; Htoon, H.; Hollingsworth, J. a *J. Am. Chem. Soc.* **2012**, *134*, 9634–43.
- (15) Habas, S. E.; Lee, H.; Radmilovic, V.; Somorjai, G. a; Yang, P. *Nat. Mater.* **2007**, *6*, 692–7.
- (16) Inaba, M.; Ito, H.; Tsuji, H.; Wada, T.; Banno, M.; Yamada, H.; Saito, M.; Tasaka, A. *ECS Trans.* **2010**, *33*, 231–238.

- (17) Chen, T.-Y.; Lin, T.-L.; Luo, T.-J. M.; Choi, Y.; Lee, J.-F. *Chemphyschem* **2010**, *11*, 2383–92.
- (18) Leskelä, M.; Ritala, M. *Angew. Chem. Int. Ed. Engl.* **2003**, *42*, 5548–54.
- (19) George, S. M. *Chem. Rev.* **2010**, *110*, 111–31.
- (20) Campbell, C. T. *Surf. Sci. Rep.* **1997**, *27*, 1–111.
- (21) Stair, P. C. *J. Chem. Phys.* **2008**, *128*, 182507.
- (22) Liu, C.; Wang, C.-C.; Kei, C.-C.; Hsueh, Y.-C.; Perng, T.-P. *Small* **2009**, *5*, 1535–8.
- (23) Xie, J.; Yang, X.; Han, B.; Shao-Horn, Y.; Wang, D. *ACS Nano* **2013**, *7*, 6337–6345.
- (24) Osaka, T.; Iida, H.; Tominaka, S.; Hachisu, T. *Isr. J. Chem.* **2008**, *48*, 333–347.
- (25) Yu, Y.; Xin, H. L.; Hovden, R.; Wang, D.; Rus, E. D.; Mundy, J. A.; Muller, D. A.; Abruña, H. D. *Nano Lett.* **2012**, *12*, 4417–4423.
- (26) Yim, S.-S.; Lee, D.-J.; Kim, K.-S.; Lee, M.-S.; Kim, S.-H.; Kim, K.-B. *Electrochem. Solid-State Lett.* **2008**, *11*, K89.
- (27) Vuori, H.; Pasanen, A.; Lindblad, M.; Valden, M.; Niemelä, M. V.; Krause, A. O. I. *Appl. Surf. Sci.* **2011**, *257*, 4204–4210.
- (28) Liang, X.; Lyon, L. B.; Jiang, Y.-B.; Weimer, A. W. *J. Nanoparticle Res.* **2012**, *14*.
- (29) Christensen, S. T.; Feng, H.; Libera, J. L.; Guo, N.; Miller, J. T.; Stair, P. C.; Elam, J. W. *Nano Lett.* **2010**, *10*, 3047–51.
- (30) Johansson, A.-C.; Larsen, J. V.; Verheijen, M. A.; Haugshøj, K. B.; F. Clausen, H.; Kessels, W. M. M.; H. Christensen, L.; Thomsen, E. V. *J. Catal.* **2014**, *311*, 481–486.
- (31) Lei, Y.; Liu, B.; Lu, J.; Lobo-Lapidus, R. J.; Wu, T.; Feng, H.; Xia, X.; Mane, A. U.; Libera, J. A.; Greeley, J. P.; Miller, J. T.; Elam, J. W. *Chem. Mater.* **2012**, *24*, 3525–3533.
- (32) Weber, M. J.; Mackus, A. J. M.; Verheijen, M. A.; van der Marel, C.; Kessels, W. M. M. *Chem. Mater.* **2012**, *24*, 2973–2977.
- (33) Lu, J.; Low, K.-B.; Lei, Y.; Libera, J. A.; Nicholls, A.; Stair, P. C.; Elam, J. W. *Nat. Commun.* **2014**, *5*, 1–9.

- (34) Färm, E.; Kemell, M.; Ritala, M.; Leskelä, M. *Thin Solid Films* **2008**, *517*, 972–975.
- (35) Mackus, A. J. M.; Mulders, J. J. L.; van de Sanden, M. C. M.; Kessels, W. M. M. *J. Appl. Phys.* **2010**, *107*, 116102.
- (36) Feng, H.; Libera, J. A.; Stair, P. C.; Miller, J. T.; Elam, J. W. *ACS Catal.* **2011**, *1*, 665–673.
- (37) Kaganer, V.; Jenichen, B.; Shayduk, R.; Braun, W.; Riechert, H. *Phys. Rev. Lett.* **2009**, *102*, 016103.
- (38) Mackus, A. J. M.; Dielissen, S. A. F.; Mulders, J. J. L.; Kessels, W. M. M. *Nanoscale* **2012**, *4*, 4477–4480.
- (39) Kessels, W. M. M.; Knoops, H. C. M.; Dielissen, S. A. F.; Mackus, A. J. M.; van de Sanden, M. C. M. *Appl. Phys. Lett.* **2009**, *95*, 013114.
- (40) Langereis, E.; Knoops, H. C. M.; Mackus, A. J. M.; Roozeboom, F.; van de Sanden, M. C. M.; Kessels, W. M. M. *J. Appl. Phys.* **2007**, *102*, 083517.
- (41) Aaltonen, T.; Ritala, M.; Sajavaara, T.; Keinonen, J. *Chem. Mater.* **2003**, *15*, 1924–1928.
- (42) Knoops, H. C. M.; Mackus, A. J. M.; Donders, M. E.; van de Sanden, M. C. M.; Notten, P. H. L.; Kessels, W. M. M. *Electrochem. Solid-State Lett.* **2009**, *12*, G34.
- (43) Astruc, D. *Nanoparticles and Catalysis*; Wiley-VCH Verlag GmbH: Weinheim, Germany, 2008.
- (44) Schauermaun, S.; Nilius, N.; Shaikhutdinov, S.; Freund, H.-J. *Acc. Chem. Res.* **2013**, *46*, 1673–1681.
- (45) Mackus, A. J. M.; Verheijen, M. A.; Leick, N.; Bol, A. A.; Kessels, W. M. M. *Chem. Mater.* **2013**, *25*, 1905–1911.
- (46) Chen, P.; Wang, T. Y.; Luo, M. F. *J. Chem. Phys.* **2007**, *127*, 144714.
- (47) Bukhtiyarov, V. I.; Moroz, B. L.; Bekk, N. E.; Prosvirin, I. P. *Catal. Ind.* **2009**, *1*, 17–28.
- (48) Stakheev, A. Y.; Mashkovskii, I. S.; Baeva, G. N.; Telegina, N. S. *Russ. J. Gen. Chem.* **2010**, *80*, 618–629.
- (49) Shao, M.; Peles, A.; Shoemaker, K. *Nano Lett.* **2011**, *11*, 3714–3719.

Chapter 7

General conclusions and outlook

This doctoral thesis focused on the controlled synthesis of high purity Pd and Pt NPs with tuneable properties, through the in-depth understanding of the reaction mechanisms taking place during noble metal ALD nucleation and growth. The following general conclusions can be drawn from this work:

- ALD offers more opportunities for nanoengineering than conventional methods for the preparation of NPs of noble metals, and many achievements have already been achieved by the ALD community in this upcoming field. In addition to the precise diameter control and the possibility to deposit NPs in various high aspect ratio substrates, another major benefit is that the preparation of NPs by ALD does not require any post-treatment. This promising route can find its applications in emerging devices such as micro-reactors or micro fuel cells in particular.
- The nucleation stage of Pd and Pt ALD processes results in supported crystalline particles between 1 and 10 nm. The surface density of both Pd and Pt NPs present maximum values of $\sim 10^{12}$ NPs/cm², which is in line with maximum density values obtained with other vapor phase techniques such as PVD. The Pd NPs obtained present a unimodal and very narrow size distribution when compared to Pt NPs. The growth mechanism of the NPs includes the adsorption of precursor molecules at the substrate surface followed by the diffusion of metal adatoms to form clusters or to join growing NPs. In addition, Ostwald and Smoluchowski ripening processes are also likely to take place and to participate in the growth of the NPs and in their resulting properties. The island growth mode obtained through metal ALD nucleation on oxide surfaces results from the difference in surface energies between the noble metals and the oxide substrate, but also from specific reaction mechanisms taking place during the ALD processes. For example, the catalytic activity of the noble metal surfaces enables the decomposition of entering precursor molecules and the dissociation of the co-reactant gas, which leads to an enhanced 3D island growth. The focus was on the materials Pt and Pd, but many of the described mechanisms are expected to occur during the ALD of other noble metals as well.
- A new palladium ALD process has been developed, which was derived from the insights obtained from *in situ* studies of the surface chemistry in combination with the surface science literature. The process uses Pd(hfac)₂ as precursor and employs two consecutively applied plasmas – a H₂ plasma and an O₂ plasma – as co-reactant step. The H₂ plasma step

is employed to remove the hfac ligands in order to obtain the deposition of the single-element palladium. It has been found that the additional O₂ plasma pulse is required to combust the carbon contaminants that remain after the H₂ plasma step, as shown by *in-situ* Fourier transform infrared (FT-IR) spectroscopy studies. The new ABC-type Pd ALD process allows for the preparation of high quality Pd thin films at relatively low temperatures. The fact that the films prepared were virtually 100% pure was demonstrated and benchmarked against the much lower purity of the films prepared by an ALD process based on Pd(hfac)₂ and H₂ plasma. The study of initial film growth on Al₂O₃ surfaces investigated by scanning transmission electron microscopy showed that nucleation takes place in the so-called island growth mode. Therefore, this process can be used for the preparation of high purity supported NPs of Pd. As this new route allows for the deposition of palladium with good material properties in the 100-200°C range, these results open up prospects for various existing and emerging applications of Pd thin films and NPs in microelectronics, catalysis and advanced sensing.

- A new route enabling the synthesis of supported bimetallic core/shell nanoparticles entirely by ALD has been developed. Because ALD depends critically on surface chemistry, it is possible to achieve selective deposition of a shell material on pre-deposited NPs, and thus to enable the synthesis of core/shell NPs. The method to prepare core/shell NPs is versatile since it allows for independent control of the core and the shell dimensions, as shown by Z-contrast scanning transmission electron microscopy studies. The design of the core and shell can be controlled at the (sub)nanometer-level by simply tuning the number of ALD cycles applied. It is anticipated that many applications, including fuel cells and advanced sensors, can benefit from core/shell nano-particles prepared by ALD.

Based on the work presented in this thesis, further research could be carried out in fields described below:

- For the further understanding of NPs growth, more characterization studies should be carried out. The NPs resulting from the initial ALD cycles should be monitored carefully in term of atoms deposited, for example by carrying out RBS measurements after each cycle. Furthermore, a better control of the ligand poisoning observed at the initial stage of

ALD could be achieved through the exact understanding of the surface reactions taking place. For this purpose, surface FT-IR spectroscopy analysis of the substrate surface after the first few cycles could unravel many reaction mechanisms. The influence of precursor and co-reactant exposures (in term of time and pressure) on the amount of material deposited and the NP properties would also be an interesting field of study. In particular, the saturation behaviour of the initial ALD stage should be checked, for example by studying the diameter of NPs (using TEM) formed after different (long) precursor exposure times during only a few cycles.

Because NPs can undergo structural and chemical variations during their growth and in response to different environments, a better understanding of the NPs formation and properties could be achieved using *in-situ* TEM. The combination of ALD and *in-situ* TEM would reveal exceptional details about ALD growth. There is also a growing interest in the understanding of the NPs properties evolution (e.g. restructuring) during the catalytic conditions in which the NPs are aimed to be used. For this purpose as well, the use of *in-situ* TEM could unravel many mechanisms taking place under “close-to-real” conditions.

- The final aim of these NPs is to catalyse chemical reactions taking place in devices such as sensors, micro fuel cells or micro reactors in general. Therefore, the actual testing of the catalytic performances of the NPs prepared by ALD would be a good way to pursue this research. For example, testing the Pd/Pt core/shell NPs for oxygen reduction or for methanol electro-oxidation would be of particular interest, since these are two key reactions in methanol fuel cells. These studies would have to be compared to NPs prepared with other methods under same loading. If this research brings promising results, applying these NPs in real micro devices would be the next step. In case of an industrialisation aim, the ALD reactors should also be optimally designed in order to save precursor consumption.
- Concerning the synthesis of core/shell NPs, other metals than Pd and Pt could be tried as well in order to enlarge the possibilities in terms of NP composition. For this purpose, the selective growth conditions of the new materials must be identified first in order to achieve the selective deposition of the shell on the pre-deposited cores. This research, if successful, could lead to a large number of possible compositions and ar-

rangements for core/shell NPs, which would open prospects for catalytic applications.

ALD of noble metals is a fascinating field of research, and the atomic understanding of the surface reactions taking place during the processes allowed us to establish new approaches. In this work, new routes such as the ABC-type ALD process and the selective growth process have been developed, enabling the synthesis of pure palladium films at low temperature and of core/shell structured NPs. ALD offers many nano-engineering possibilities and I believe we are still far from having unlocked all the opportunities this technique has to offer. Many more new processes could be developed beyond the “classical” AB-type process. Furthermore, on the basis of the acquired understanding, many promising and broader research routes can be opened.

- For example, ABC-type processes, which make use of more than one co-reactant, could be applied to many other elements and thus potentially lead to the ALD of new materials and/or at lower temperatures. Furthermore, the control of the composition of a material and thus the tailoring of its properties at the nanoscale, can be achieved using ALD supercycles (e.g. $(AB)_n(CD)_m$ -type process).
- The catalytic activity of noble metal NPs can allow for a local chemistry to take place and this has been used in this work for the synthesis of core/shell NPs. However, many more opportunities exist and should be investigated. The catalytic activity of noble metals could be used to etch a material locally and at the nanoscale. In fact, by applying specific process parameters, the etching of a supporting material could take place only under noble metal nanostructures. The created nano holes or nano trenches could find their applications in nanofiltration or photonics. Furthermore, by successively using such an etching process and a selective growth process of a metal, it would be possible to “fill” these nano holes or trenches with a conductive material. These created nanoelectrodes could have important applications in the semiconductor and solar cells industries. The deep understanding of the surface reactions taking place during ALD could also lead to the development of a new type of process, *i.e.* atomic layer etching. Self-limiting etching reactions during atomic layer etching could allow for the etching of films at the sub(nanometer) scale in high aspect ratio structures. The combination of ALD and atomic layer etching could therefore allow for the deposi-

tion of closed metal films of unparalleled small thicknesses, which opens many prospects in the fuel cells, solar cells and semiconductor industries.

Summary

Atomic Layer Deposition of Noble Metal Nanoparticles

Noble metal nanoparticles (NPs) supported on oxide and carbon materials form the basis for many catalysts and have important applications such as in chemical industry, fuel cell technology and pollution prevention. Atomic layer deposition (ALD), a well-established and scalable vapor phase technology for the preparation of thin films, is currently gaining interest in the R&D community for the synthesis of noble metal NPs. ALD is a cyclic deposition technique in which precursors and reactants are injected into the reactor chamber alternately and in which the reactions are driven by self-limiting surface chemistry. This deposition technique allows for a sub-nanometer growth control of high quality materials as well as for an excellent uniformity and conformality on demanding surface topologies.

In this thesis, the nano-engineering capabilities of ALD were explored in order to achieve the controlled synthesis of high purity Pd and Pt NPs with tuneable properties. In order to gain better control of the NP properties, their formation has been studied in-depth. It has been demonstrated and discussed that the use of ALD for preparation of NPs brings additional opportunities to nano-engineering compared to conventional synthesis methods, and that this approach can be a benefit for and contribute to the field of heterogeneous catalysis.

The first part of the work described in this dissertation involved studies to obtain accurate information about the properties of metal NPs as well as to gain a higher level of understanding of the main physical mechanisms and processes taking place during metal ALD nucleation. The experimental aspects of the preparation of NPs by ALD, their analysis by TEM, and the underlying physical mechanisms that play a role during the preparation of the NPs have been addressed. Phenomena such as surface diffusion processes influencing the ALD NPs properties have been elucidated from physical theories, literature studies and experimental results from this work. The focus was on the materials Pt and Pd, but many of the described mechanisms are expected to occur during the ALD of other noble metals as well.

In order to obtain metals with high purities, part of the research focused on the development of an innovative plasma-assisted ALD process for Pd. For the synthesis of high-purity palladium films, detailed understanding of the surface reactions turned out to be crucial. Palladium with low contamination lev-

els has been deposited on Al₂O₃ substrates at low temperature using Pd(hfac)₂ dosing and exposure to subsequently a H₂ plasma and an O₂ plasma. The film growth, the material properties, and the reaction mechanisms have been investigated. In-depth understanding of the ALD surface chemistry revealed that the O₂ plasma pulse was required to combust carbon contaminants that remained after the H₂ plasma reduction step. Furthermore, the nucleation of the Pd NPs during the initial stage of this novel ALD process has been studied using Transmission Electron Microscopy (TEM).

Furthermore, a proof-of-concept method enabling the synthesis of bimetallic core/shell NPs entirely by ALD has been developed. This novel route was demonstrated for the synthesis of Pd/Pt and Pt/Pd core/shell nanostructures on Al₂O₃ substrates. The versatility of this approach has been addressed and it has been shown that this new strategy allows for nano-tailoring of the core and shell diameters of the NPs at a sub-nanometer level. This suggests that the catalytic properties of the NPs can be tuned for specific applications. The acquired knowledge is crucial for designing new high performance nanocatalysts by ALD and it could lead to improved and also novel promising applications.

In conclusion, through this project it has been demonstrated that ALD is a powerful approach for the controlled synthesis of noble metal NPs. The opportunities that ALD provides for nano-engineering can lead to many novel materials and applications. Moreover, this work contributed an atomic level understanding of Pd and Pt NP formation by ALD, and therefore will advance the science and technology of metal ALD.



Acknowledgments

Here we are. The acknowledgments. The most read part of a PhD thesis. No experimental results, no new science, just a lot of “thank you”, and still, most of you will read this part first! But all right, fair enough, hopefully you will enjoy the reading and find your name in this “chapter”!

During the last 4 years, I learned a lot and acquired many new skills. Hereby, I would like to thank several people who contributed to this project. This doctoral work was a team effort and the achievements presented in this thesis would not have been possible without the support and guidance of many people.

First of all, I would like to thank **Erwin**, my promotor, for giving me the chance to do this project in the PMP (Plasma & Materials Processing) research group. The results obtained during this PhD would not have been possible without the fruitful discussions we had during constructive and motivating meetings. Thank you for your guidance during the PhD and for sharing your knowledge. I am very grateful for that. Your passion for ALD and science in general, as well as your extreme criticism for the choice of words enabled me to strengthen my scientific and writing skills enormously. Your help was also very useful for the improvement of my presentation skills. Thank you. Finally, I also would like to express my gratitude to you for giving me the chance to participate to the yearly scientific conferences in the U.S.A. These conferences were opportunities to present my research, to get inspiration, and to meet the main specialists of the ALD field. These scientific meetings were fantastic experiences.

I would like to thank **Ageeth**, my co-promotor, for the re-reading of the chapters and for her guidance. Thanks as well for the nice discussions we had and for your support on different levels. I am also extremely grateful to **Marcel**, my second co-promotor, for many different things. Marcel, thank you for the beautiful TEM images, but also for the close scientific guidance, for the fruitful discussions we had during (almost weekly) meetings, and for the countless iterations we had with some chapters! Your smart scientific advices, your interest and involvement in my project, your continuous and enormous support, as well as your good mood over these years really helped a lot. Thank you.

I then would like to thank former PMP members that considerably helped me during my PhD, especially at the beginning. **Adrie** (Stanford Univ.), I want to thank you first. You basically introduced me to the science of metal ALD and taught me how to use the ALD-I set-up. Your passion for ALD, smartness, pedagogic skills and scientific guidance were extremely useful, especially during my first year here. Thank you. **Harald** (ASM), I would like to thank you for your availability and help with the electrical system and the labview program of the ALD-I. Your expertise with this system saved us a lot of time.

I also want to thank the PMP technicians, who helped us so many times to fix the ALD-I set-up. I especially want to thank **Ries, Joris, Christian, Wytze** and **Janneke**. Your expertise and availability were extremely useful for my project.

This PhD project was a Marie Curie project called “Enhance”. It is a European collaborative project, and thus I had the opportunity to participate to many workshops

all over Europe where I met other PhDs and post-docs working in the same scientific field. Big thanks to **Tim** and **Yohann** from Helsinki, **Bruno** from Aachen, **Anne-charlotte** from Copenhagen, **Marco** from Vienna and **Daniella** from Padova for the good times we had all together. The scientific knowledge and skills, as well as the friendships we developed over the years during these regular meetings were fantastic experiences. I also want to mention the many international culinary benefits (that we drastically needed when living in NL) of this Marie Curie program: From the first Chateaubriand steaks in Bochum (Germany), the reindeer and steaks tartare in Helsinki (Finland), to the nice Italian pizze in Padova (Italy) and tartes flambées (flammkuchen) in Strasbourg (France), this “Enhance” project was a real delight!

Valentino, as we were both part of this “Enhance” project, you represent a perfect link between “Enhance” and PMP. Thanks for having been such a good colleague and friend over these 4 years. From the first BBQ at your first flat, to the nice gardening in your latest flat, we lived many other fun adventures, in many different countries. I will always cherish the good enhance times all over Europe as well as the DR experience. For all these good memories, thank you.

Back to PMP: Many people I want to thank for the nice times we had together over these 4 years: First, my office mates **Gijs**, **Rene**, **Roger**, and of course **Diana** (thanks for your constant Spanish accent and positive mood, I love it)! **Claire** (Dr. in GoT ☺), **Valerio** and **Ben**, smily **Yizhi**, but also **Roy**, **Ilker**, **Floran** and **Florian**, thanks for the lunch and the coffee breaks, the parties, you guys are great! **Harm** and **Nick**, thank you for your assistance at the ALD-I and for your smart support. **Ivo**, thanks for your jokes, and for your good taste in music and clubs, I think we will always share our love for Berlin city! And of course I cannot forget to mention **Alberto**: Thanks for your friendship over these 2 last years, a special thanks to you for the delicious bread baking and the constant support, man you are awesome and you helped me a lot!

Living in Eindhoven you realize that the international community is huge - smart people come all over the world to this “brainport” city - and therefore I had the chance to meet many exceptional people also outside of my direct working environment over these 4 years in NL. All of you guys filled my stay here with great and unforgettable moments. Thank you so much! I would love to be able to write a list of all the people that counted for me and with whom I enjoyed my life here, but please forgive me if your name is not in the list.

Florence (my first encounter in NL!) and **Benjamin**: Thanks for all the good times we shared, the travelling all over Europe (especially the summer in the Balkans) and the countless number of beers! **Camille D.**: thanks for your amazing positive and playful mood; the “Fort, O’sheas and buurvrouw group” (let’s call it like that) composed of many great italians and/or chemists such as **Maurizio**, **Maria**, **Danielle**, **Camille C.**, **Gokhan**, **Raph** and **Isabelle**! Thanks as well to **Enrico** and **Dominik** for the nice successive apéros, Dr. Ink and Kitsch times; **Domenico** for your impressive play of The game, **Marloes** and **Stephanie**, thanks for the great times we shared. **Christophe**, thanks for the regular and countless Zywiec evenings. Thanks for the Kruisstraat times with my flat-mates **Penny** and **Sami**, and of course **Maté**! **Olivia** and **Gabriel**, your stay with us was always great, I am really glad I had the chance to meet you!

Ece, thanks for the nice dinners and good times we had 4 years ago in Pastoor Peterstraat! **Olivier**, my dear friend from 67, thanks for your good mood and our shared Alsatian culture! I wish you both all the best in Tarragona!

Rocío, I want to thank you for many things: First, thank you for introducing me to your beautiful culture and life! Thanks as well for your positive and enthusiastic mood (95% of the time ☺), and thank you for all the amazing and unforgettable moments we shared in Eindhoven and Wageningen, as well as in many other places. Gracias. I wish you all the best with your new permaculture designer career and for your life in general.

Other great persons I had the chance to meet here and that I would like to thank: **Sabrye** and **Hans** (for the climbing sessions at Monk!), **Gosia**, **Ivelina** (you nasty girl ☺), **Mindaugas** (lets go to Kitsch again? ☺), **Lucia** (thanks for the nice lunch breaks, I always enjoyed your sweet and positive philosophy), **Carolina** and **Sylvester**, and thank you **Sylvia**, for the good times we had together. Of course I will remember **Marine**, and obviously I also cannot forget the **R7 people**: especially big thank you to **So-young** and **Martin**, you guys are awesome and I will never forget the funny moments we had at R7 and at Kitsch! Thanks also to **Mélanie**, **Guus**, **Ewoud**, **Blanca** and **Jaime**, you guys are perfect R7 hosts! **Flo**, thanks for the nice Xmas brunches and parties in Amsterdam! **Antoine**, thanks for your friendship and for all the good times we had this last year, the monday series, the regular apéros and of course the parties in Stratum! ☺

Finally, I would like to thank my family for their unconditional love and support. **Maman**, **Papa**, **Fanny** (et **Nicolas**), votre support et votre compréhension m'ont également beaucoup aidé tout au long de ces années d'études! Merci!

Curriculum Vitae



Matthieu Weber was born on August 6th 1984 in Obernai, France.

After finishing his high school studies by obtaining his scientific baccalaureate (with honors) in 2002 at Lycée Schuman in Haguenau, he started his technical studies with a two-year degree course on chemistry (D.U.T.) at the University Institute of Technology Strasbourg-Sud. After this first chemistry degree, he obtained a Bachelor of Applied Science in Environmental Engineering from the University Louis Pasteur (Strasbourg) in 2005.

He then moved to the Université de Technologie de Troyes (U.T.T.), a leading French engineering school, to strengthen his scientific knowledge. There, his education mainly focused on material science engineering and nanotechnologies, but also on project management and intellectual property. During his studies, Matthieu spent six months as an exchange student in the Czech Technical University in Prague (Czech Republic) and subsequently spent another half-year in the IMS lab (Laboratoire de l'Intégration du Matériau au Système) in Bordeaux (France) to work on the research and development of organic thin film solar cells (P3HT/PCBM system). To complete his degree, Matthieu spent six months in the Helmholtz-Zentrum Berlin für Materialien und Energie GmbH (Berlin, Germany) to carry out his Master project. There, he developed and characterized inorganic thin film solar cells based on the $\text{CuInS}_2/\text{Zn(S,O)}/\text{ZnO}$ technology. He obtained his Master of Science degrees in Materials Science Engineering and in Nanotechnologies in 2009. In 2010, he started his PhD project at the Eindhoven University of Technology in the "Plasma & Materials Processing" group under the supervision of Prof. W.M.M. Kessels. His PhD research covers the field of atomic layer deposition (ALD) of noble metal nanoparticles and thin films. The research was carried out in the frame of a collaborative European project of the Marie Curie Actions and the 7th Framework Programme, and the most important results are presented in this dissertation.